7.11 The Core–Mantle Boundary Region

JW Hernlund, Tokyo Institute of Technology, Tokyo, Japan
AK McNamara, Arizona State University, Tempe, AZ, USA

7.11.1 Introduction

The Earth was formed by the accretion of both differentiated and undifferentiated parent bodies, and the large density difference between metallic and ionic components gave rise to internal gravity-driven segregation into the primary regions of our planet: a central metallic core and a rocky oxide mantle. At the current pressure (136 GPa) and temperature ($\approx$4000 K) conditions of the Earth's core–mantle boundary (CMB), the material in the core exhibits a density of 9900 kg m^{-3}, while the density of the mantle is around 5500 kg m^{-3} (Dziewonski and Anderson, 1981), yielding a greater density contrast than that of the Earth's surface. Besides density, the outermost core and lowermost mantle also exhibit strong differences in transport properties such as viscosity (the outer core is liquid, while the mantle is mostly solid), thermal and electrical conductivity, and atomic diffusivity, all of which strongly influence the contrasting dynamics of the core and mantle regions. The strong differences between the mantle and core are reflected in the structure and dynamics of the CMB, where the two major regions of the Earth exchange both heat and matter.

Studying the CMB region is key to building a complete Earth model that integrates the dynamics, structure, and evolution of both major regions of the Earth's interior. By understanding how the myriad dynamics in one region are coupled to those in the other, a broader range of constraints can be brought to bear by linking together major hypotheses related to the evolution of Earth's interior through geologic time. Thus, a major discovery in the deep mantle can carry important implications for the core, and vice versa. However, CMB studies are challenging because of the extreme pressure–temperature (P–T) conditions, which strongly affect material properties and have historically been difficult to mimic in laboratory experiments. Direct observations are also hampered by the difficulty of obtaining reliable seismological and electromagnetic observations that are obscured by heterogeneous structure in the shallower mantle. Nevertheless, the adoption of new technologies for obtaining CMB P–T conditions in the laboratory, the improvement in the reliability of ab initio methods for calculating material behavior at extreme conditions, and the proliferation of digital seismograph networks and methods to process large data sets have ushered in a new era in CMB research that is beginning to shed light on this critically important but enigmatic region of the Earth's deep interior. Geodynamics research is also increasingly playing a key role in integrating the available constraints into models of greater scope and predictive capacity, which is essential for the incorporation of constraints from other geologic sciences (e.g., geochemistry).

CMB research is presently in a period of rapid change, and a single paradigmatic view has yet to become firmly established. This chapter presents the evolution in thought regarding the dynamics of the CMB region and the excitement of new discoveries and models currently under way while also surveying some of the current debates and uncertainties. We begin with an overview followed by an exploration of the primary observed features of the CMB region, including the D'' discontinuities, the large low-shear-wave-velocity provinces (LLSVPs) beneath the Pacific and Africa, the relatively thin ultralow-velocity zones (ULVZs) and other thin basal layers at the CMB itself, and the proposition of an outermost core stratified layer just underneath the CMB, which could play an important role in core–mantle chemical interactions. We then examine the exchange of heat and matter across the CMB, a key area of CMB research that aims to connect the core and mantle systems.

7.11.2 Overview of the CMB Region

Before proceeding with our in-depth discussion, we present a summary of CMB region structures and terminology in order to help orient readers. Indeed, there are numerous acronyms, in addition to varying names for features, which are sometimes connected to specific hypotheses. We thus give a brief history for these features and a discussion on the evolution of their descriptive terminology. Finally, we settle upon the accepted modern usage, although we are sure that the nomenclature will continue to evolve in the future. For visual reference in the following discussion, Figure 1 gives an illustration of the basic seismic observations of the primary features of the CMB region, while Figure 2 shows a typical interpretation of these

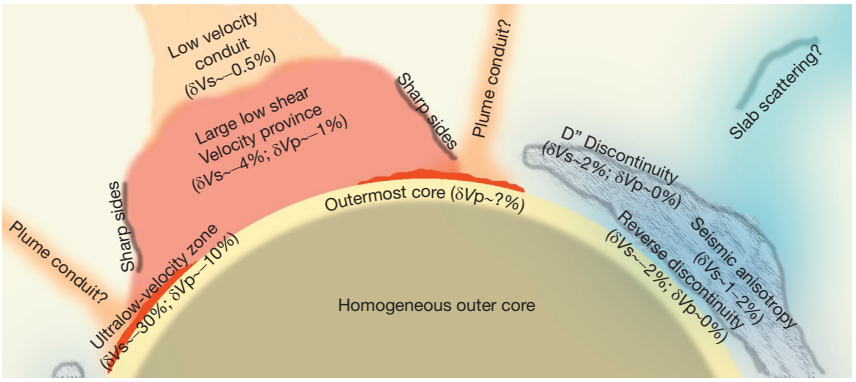

Figure 1 Schematic illustration of some major features of the CMB region proposed by seismological observations. Refer to the text for a more detailed discussion.

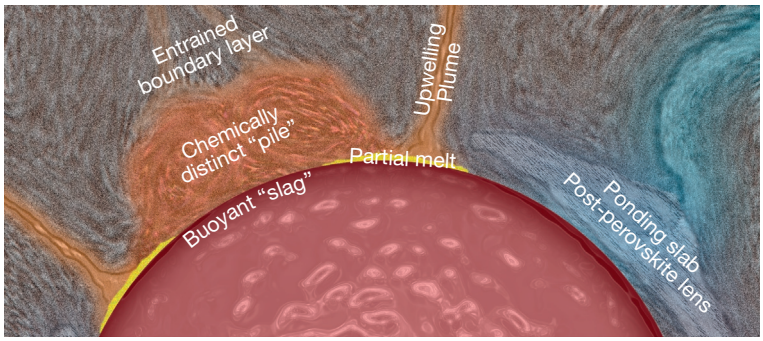

Figure 2 Schematic illustration of a possible interpretation of structures in the CMB region.

features. In each subsection in the succeeding text, the basic observations and the common interpretations listed in Figures 1 and 2 are briefly explained.

7.11.2.1 *D″* Discontinuity

It is important to note from the beginning that the term *D″* has its origin in the alphabetic description of regions in Earth's interior used in the early days of seismology and was meant to describe the anomalous region in the lowermost several hundred kilometers of the mantle (e.g., Bullen, 1949). As such, *D″* is a layer of the Earth's mantle, comprising the lower boundary layer of the mantle side of the CMB transition. The *D″* discontinuity, on the other hand, was originally discovered as a sudden increase in shear-wave velocity occurring several hundred kilometers above the CMB many years later (Lay and Helmberger, 1983). Further work has found that the discontinuity may not be globally ubiquitous or may have significant depth variations that make it difficult to detect in some regions (see reviews by Lay et al. (2004) and Wysession et al. (1998)). Therefore, the *D″* layer should not be thought of as a region that is simply defined by a seismic discontinuity, in the same manner as shallower regions of Earth's mantle are separated by clear global seismic-wave speed jumps. Where it exists, the *D″* discontinuity is revealed by a triplication in the arrival times of S-waves turning in the lowermost several hundred kilometers of the Earth's mantle, clearly producing reflected, refracted, and penetrating branches in the travel-time curve. In some cases, *P*-wave discontinuities have also been reported, although it is not clear if they are correlated with the same *S* discontinuities, and they also exhibit greater variations in both the strength and sign of the velocity jump (Wysession et al., 1998).

The cause of the *D″* discontinuity was a mystery for more than two decades; however, recent mineral physics discoveries appear to have resolved many questions relating to its origin, although numerous details remain to be ironed out. In fact, the present explanation for the *D″* discontinuity as the result of a solid–solid phase change was predicted in advance of its discovery (Sidorin et al., 1998), based on the simple reasoning that the only mechanism that could elevate the discontinuity in seismically fast regions (i.e., beneath cool downwellings) is a strongly exothermic phase transition with a Clapeyron slope of >6 MPa K^{-1} (compositional or thermal frontiers would instead be depressed in such a context). The discovery of a phase change from $MgSiO_3$ perovskite (Pv) to postperovskite (PPv) (Murakami et al., 2004) at the appropriate pressures and with a suitably large transition Clapeyron slope (Oganov and Ono, 2004; Tsuchiya et al., 2004) fits very well with the predictions and remains the most commonly invoked explanation for the *D″* discontinuity at the present time. The PPv phase exhibits a significant degree of elastic anisotropy and should also help to explain observations of seismic anisotropy in these regions (Oganov et al., 2005; Stackhouse et al., 2005). The Pv–PPv phase change may also explain deeper seismic discontinuities in *D″* and suggests that PPv occurs in lens-shape structures rather than a global layer, as a consequence

of the 'double-crossing,' with important implications for characterizing thermal gradients at the base of the mantle (Hernlund et al., 2005).

7.11.2.2 Large Low-Shear-Wave-Velocity Provinces

Since the dawn of seismic tomography, it has been known that the lowermost 1000 km of the mantle contains large-scale 'degree-2' anomalies in seismic-wave speed that are correlated with similar variations in the geoid and that might be simply explained by the presence of abnormally dense matter beneath the Pacific and Africa (Dziewonski et al., 1977). Others have interpreted these features as being large thermal plumes, in which case the terminology is usually 'superplumes' (particularly in a geologic context, e.g., Larson (1991)), but sometimes, the term 'megaplumes' is used in reference to dynamical models (e.g., Matyska et al., 1994; Thompson and Tackley, 1998). It has also been suggested that these regions could be a collection of small plumes, in which case the term used to describe these features is 'plume clusters' (e.g., Schubert et al., 2004). Many lines of evidence suggest that these regions are compositionally distinct from the surrounding mantle, usually based upon evidence such as distinct *S*- and *P*-wave speed variations (e.g., Bolton and Masters, 2001; Hernlund and Houser, 2008; Houser et al., 2008; Lekic et al., 2012; Romanowicz, 2003), sharp gradients and/or reflections of seismic waves from the edges of these features (e.g., Ford et al., 2006b; Luo et al., 2001; Sun et al., 2007a; Wang and Wen, 2004; Wen, 2001), and corresponding variations in both seismic-wave speeds and gravity (e.g., Ishii and Tromp, 1999; Simmons et al., 2006; Trampert et al., 2004). Under the presumption of a compositionally distinct origin, these features have been described by terms such as 'cryptocontinents' (Stacey, 1992), 'domes' (e.g., Davaille, 1999), and 'piles' (e.g., McNamara and Zhong, 2004), some of these terms having further implied meaning with regard to their dynamical manifestation. In reference to the high bulk modulus that can account for their distinct *S*- and *P*-wave speed characteristics, dynamical models attributing chemically distinct dense structures with a corresponding anomalous compressibility also refer to them as 'high-bulk modulus structures' (HBMS) (Tan et al., 2011). In order to establish a purely descriptive term based on seismic observations, while avoiding explicit reference to a particular origin hypothesis, Thorne Lay suggested the terminology LLSVPs (Lay, 2007), which appears to have become more commonly used in recent years than previous terminology. Thus, we adopt the acronym LLSVPs to refer to these large laterally discontinuous regions exhibiting low seismic-wave speeds residing beneath the Pacific and Africa.

Whatever their name, it is clear that LLSVPs are of central importance in deciphering the dynamics of the CMB region. Many active hot spots attributed to deep-seated plumes appear to be located near the edges of LLSVPs (Thorne et al., 2004), and plate motion reconstructions seem to place many of the large igneous provinces (LIPs) in the vicinity of the LLSVPs when they originally erupted in the past 200 My (Torsvik et al., 2006). On the basis of seismic tomography models, it has also been proposed that the LLSVPs channel significant volumes of warm material upward into the shallow mantle in a manner that does not manifest as straightforward hot spots (e.g., Romanowicz and Gung, 2002). Geochemically, the LLSVPs have become a popularly invoked repository for putative 'primitive reservoirs' (e.g., Tolstikhin and Hofmann, 2005) or 'slab graveyards' (e.g., Christensen and Hofmann, 1994), and deciphering their true origin is of utmost importance for models of Earth's chemical and isotopic composition. These features have also been proposed to influence geomagnetic variations and reversals (e.g., Clement, 1991; Costin and Buffett, 2004; Laj et al., 1991) or occasionally produce increased volcanic activity at the surface with significant impacts upon the Earth's paleoclimate (e.g., Caldeira and Rampino, 1991; Condie, 2001), perhaps even playing a major role in mass extinction events (e.g., Courtillot et al., 1996; Keller, 2005; Zhou et al., 2002). Indeed, Courtillot and Olson (2007) suggested a correlation between all of these phenomena, highlighting the central role LLSVPs may play in our planet's evolution, from its surface to the center.

It is also noteworthy that, despite the variety and volume of evidence – both direct and indirect – indicating that LLSVPs are composed of compositionally distinct material with a high bulk modulus, there are still some who argue that these features may be explained solely by temperature variations alone. Usually, these perspectives refer to only a single kind of seismic-wave speed variation in the deep mantle (e.g., Schubert et al., 2004), thus limiting their a priori constraints in a way that would allow for multiple interpretations. On the other hand, recently, the interpretation of distinct *S*- and *P*-wave behaviors inside these regions has itself been challenged as an artifact of certain kinds of travel-time determinations combined with finite frequency propagation effects (Schuberth et al., 2012). This particular interpretation also represents a challenge to the LLSVP nomenclature itself: if the *P*-wave speed anomaly is just as strong as that for *S*-wave speeds, then we could simply have called them low-velocity provinces (LVPs).

7.11.2.3 Ultralow-Velocity Zones

Unlike the LLSVPs described in the preceding text, which are 1000 km scale features of the lowermost mantle, there also exist anomalous patchy 10 km layers at the CMB that exhibit more extreme velocity variations: 10% for *P*-waves and 10–30% for *S*-waves (Garnero and Helmberger, 1996). Similar to the other structures discussed in the preceding text, ULVZs are also not globally ubiquitous but rather seem to be present as distinct patches (Thorne and Garnero, 2004). It is also possible that the usual ULVZs are the much thicker manifestation of a layer that is much thinner ($\sim$1 km or less) in other locations (Ross et al., 2004). In some particular regions, it has been possible to employ the *ScP* seismic phase to obtain constraints on ULVZ density, suggesting an $\approx$10% increase relative to the overlying mantle (Rost et al., 2006). Thus, the variations in velocity and density in ULVZ of order 10% are large, comparable with the variations across the Mohorivičić discontinuity at the base of the Earth's similarly thin and variable crust. However, these anomalies are still relatively small in comparison with the density and velocity changes across the CMB itself.

As the veneer separating the Earth's core and mantle, ULVZs are undoubtedly important for understanding the chemical disequilibrium between the mantle and core and the possibility of mass exchange between Earth's major interior regions.

The sharpness of the upper boundary of ULVZs, geographic correlation with mantle upwellings (Williams et al., 1998), and relatively larger *S*-wave velocity reduction relative to *P* motivate a partial melt hypothesis for their origin (Berryman, 2000; Hier-Majumder, 2008; Williams and Garnero, 1996). However, other mechanisms for producing ULVZ have also been considered, such as subduction and gravitational settling of banded-iron formations (Dobson and Brodholt, 2005), sediments floating to the top of an alloy-saturated core (Buffett et al., 2000; Manga and Jeanloz, 1996), strong iron enrichment in PPv (Mao et al., 2004) or magnesiowüstite (Mw) (Wicks et al., 2010), and upward entrainment of iron by morphological instabilities (Otsuka and Karato, 2012) or even poroelastic mechanisms (Petford et al., 2005). However, given the association of all these mechanisms with an enrichment in iron, which is thought to lower the melting temperature and the inevitability of significantly higher CMB temperatures in the Earth's past, these model spaces probably contain significant overlap and may anyways be partially molten at the present or past conditions of the CMB. Recent models that incorporate energy constraints for the geodynamo and corresponding secular cooling of the CMB suggest that ULVZs are the residue of a much larger magma body in the Earth's past, called the 'basal magma ocean' or BMO, which might also help to explain the relationship between ULVZ and LLSVP (Labrosse et al., 2007; Nomura et al., 2011).

7.11.2.4 Outermost Core Stratification

On the underside of the CMB lies the outermost molten metallic core, a region of dramatically different physical and chemical properties relative to the overlying mantle. Outer-core convection is generally thought to produce the Earth's geomagnetic field via dynamo action in electrically conducting metallic fluid (e.g., Braginsky and Roberts, 1995; see also Volume 8), and indeed, most of the Earth's outer core is well fit by an isentropic compression profile consistent with vigorous convection (e.g., PREM; Dziewonski and Anderson, 1981). The presence of convective motions of order 10^{-4} m s^{-1} atop the core can be inferred from geomagnetic secular variations, providing important constraints on the dynamical regime of the core (e.g., Bloxham and Jackson, 1991). However, it is not clear that coherent radial convective motions penetrate all the way up from the bulk of the outer core to the CMB, and it has long been suspected that the outermost ~100 km of the core may be gravitationally stratified owing to excess accumulation of light alloying elements (e.g., Fearn and Loper, 1981) and/or a subadiabatic thermal gradient (e.g., Labrosse et al., 1997). The enrichment of incompatible light elements at depth owing to inner-core growth either could contribute to formation of such a stratified layer (Fearn and Loper, 1981) or could work to disrupt its accumulation (e.g., Loper, 1978). On the basis of improved models for core–mantle chemical equilibria (e.g., Asahara et al., 2007; Frost et al., 2010; Ozawa et al., 2008), it has also been proposed that such a layer could form as a consequence of core–mantle reactions that cause excessive accumulation of oxygen atop the core (Buffett and Seagle, 2010). Given the low viscosity of the outer core (e.g., de Wijs et al., 1998) and inefficiency of viscous entrainment, the only processes capable of mixing such a stratified layer downward involve turbulent entrainment and/or thermal diffusion. Departures in density sufficiently large to be seismically detectable are more than sufficient to stabilize such a layer over geologic timescales (Buffett and Seagle, 2010).

While some features of the geomagnetic secular evolution may be consistent with a stratified layer atop the core (Whaler, 1980), so long as it is not much thicker than ~100 km (Gubbins, 2007), these interpretations are inherently nonunique, and therefore, we must also rely upon seismological verification of the stratification hypothesis. Unfortunately, the only seismic phases capable of probing the outermost core for such a stratified layer (i.e., *SmKS*) are very sensitive to the strong heterogeneity at the base of the mantle (Garnero et al., 1993a). Many seismological models have proposed a velocity decrease in the uppermost core relative to PREM (Eaton and Kendall, 2006; Helffrich and Kaneshima, 2010; Tanaka, 2004, 2007); however, the models exhibit significant differences, and some authors have since argued for a lack of evidence for stratification (Alexandrakis and Eaton, 2010). Nevertheless, it is clear that the presence of any stratified layer has important connections to dynamics in the CMB region, owing to the sensitivity of such structures to heat flow and potential chemical reactions. Furthermore, the presence of a stratified layer may render some core–mantle chemical exchange mechanisms implausible, such as the upward transport of fractionated osmium isotopes (Brandon and Walker, 2005) or material exhibiting excess Fe/Mn (Humayun et al., 2004), since transport across such a layer would be limited to diffusion alone.

7.11.2.5 Plumes, Slab Ponds and Graveyards, and Other Features

There is presently little doubt that at least some subducted lithosphere sinks to the very bottom of the mantle, consistent with basic observations such as the geoid above subduction regions (Hager, 1984) and seismological imaging that reveals high-seismic-wave speed features extending to the bottom of the mantle in portions of the circum-Pacific region (e.g., Grand, 1994, 2002). There is also a good correlation between the expected locations of subducted slabs and regions of high seismic-wave speed in the D'' layer (Lithgow-Bertelloni and Richards, 1998; Ricard et al., 1993). The presence of slabs may also be essential for stabilizing postperovskite in the deep mantle consistent with seismological observations (e.g., Hernlund and Labrosse, 2007). For these reasons, among others, the focus of dynamical studies has turned to questions regarding what happens to subducted lithosphere when it reaches the D'' layer, its relation to some of the key features of the CMB region discussed in the preceding text, and the possibility of 'slab graveyards' where ancient crust is sequestered for over relatively long residence times.

There also exist a variety of other features in the D'' region that are key to dynamical interpretations. Morgan (1971) proposed that LIPs and long-lived hot spots at the Earth's surface are caused by plumes rising from the deep mantle and assume the form of large plume heads followed by trailing conduits of hot buoyant rock. Additionally, ocean island basalts (OIBs) produced by hot spots carry unique isotopic and compositional signatures that are distinct from the mid-ocean ridge basalts (MORBs) that sample large swaths of the upper mantle,

suggesting a deeper origin for OIBs (Hofmann, 1997). Some seismological analyses claim to have sufficient resolving power to image these plumes, in support of this hypothesis (e.g., Montelli et al., 2004). Hotspots exhibit topographic 'swells' that can be related to the flux of buoyant material from below (Davies, 1988; Sleep, 1990), and when assigned a temperature contrast consistent with petrologic inferences (e.g., Takahashi et al., 1993), these account for a minimum heat flow of 2–4 TW, slightly less than 10% of the total surface heat flow. Note that this number is sometimes mistakenly adopted as the CMB heat flow, but many studies indicate that the CMB heat flow should be much larger than plume heat flow measured in the upper mantle, although the precise reasons are still debated (Labrosse, 2002; Mittelstaedt and Tackley, 2005; Zhong, 2006). When corrected for these effects, in addition to adiabatic heating/cooling upon compression/decompression, dynamical models suggest that the implied heat flow carried by plumes from the deepest mantle consistent with hot spot swell topography exceeds 10 TW, consistent with more recent inferences of CMB heat flow that will be discussed in detail in later sections.

7.11.3 D'' Discontinuities

One of the most prominent features of the D'' layer is discontinuous variations in elastic-wave speeds, which can be detected by the analysis of variations in seismic waves that pass through the deep Earth. The most well-known and characterized discontinuity is an increase in the propagation speed of shear (S) waves near the top of the D'' layer, 200–400 km above the CMB (see Wysession et al. (1998) for a review). This particular discontinuity has typically been referred to as *the* D'' discontinuity; however, in recent years, other kinds of discontinuities have also been reported, which, although less well characterized, may be very important for revealing further details and dynamics of the mantle side of the CMB region. Additionally, a discontinuity near the top of D'' is not observed everywhere and may be either difficult to detect or genuinely absent in some portions of the deepest mantle. Thus, the D'' layer is not itself defined by the presence of such a discontinuity.

In this section, we will discuss the main types and features of the known D'' discontinuities, recent interpretations of the cause of discontinuities as a consequence of a perovskit to postperovskite phase transition, and the important dynamical implications of these various scenarios. Relative to other main features of the CMB region, many features of the D'' discontinuities are known with a fair degree of accuracy, and a simple interpretation for producing most of these has already become widely accepted. However, it is less clear that all discontinuities can be produced by the same mechanism, thus indicating the need for other mechanisms to explain all of these features. In relation with the D'' discontinuity, we also discuss the strong anisotropy that is often associated with these kinds of discontinuities, which should provide important constraints on the dynamics of the lowermost mantle.

7.11.3.1 Seismic Observations and Inferences

In this section, we summarize some of the primary seismic observations regarding D'' discontinuities. Because much of this subject has already been well reviewed elsewhere (e.g., Lay, 2007; Lay et al., 1998, 2004; Wysession et al., 1998), we give only a basic summary of the observations while emphasizing those that have an important bearing upon the dynamics of the CMB region.

7.11.3.1.1 Discontinuities near the top the D″ layer

It is important to understand why the discontinuity in S-wave speed near the top of D'' is a well-established feature of some regions in the deep mantle. A rapid increase in seismic velocity with depth can be detected unambiguously by the analysis of seismic travel times for waves turning above and below the depth of its occurrence. The basic scenario is described in **Figure 3**, showing ray paths that turn above the discontinuity, waves that turn within the gradient region (diffraction waves), and waves that turn below the discontinuity. Observation of such a triplication is usually regarded as an unambiguous indication of a seismic-wave speed increase with depth. Lay and Helmberger (1983) established the occurrence of such a wave field triplication for horizontally polarized shear waves turning above the CMB, corresponding to a 2–3% increase in velocity about ~280 km above the CMB. This S discontinuity, where it is observed, may have a gradient thickness of up to ~75 km (Wysession et al., 1998).

Many attempts have been made to correlate the S discontinuity with other features of the deep mantle. Observations of P-wave discontinuities have also been reported near the top of D'' (Wright et al., 1985); however, they are not clearly correlated with – and are more variable than – the S-wave discontinuities (Lay et al., 1998; Wysession et al., 1998). Another main feature of D'' seismic structure is the presence of variable anisotropy (Mitchell and Helmberger, 1973). S discontinuities

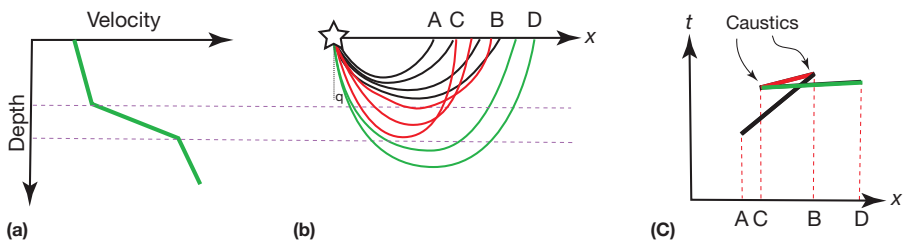

Figure 3 Illustration of how a seismic velocity increase with depth (a) causes ray paths for waves turning above, at, and below the increase (b) to produce a 'triplication' pattern in the travel-time curve. In this figure, x is the distance from the source (star) and t is the travel time of the seismic wave. Base image courtesy of Edward J. Garnero.

near the top of D'' are spatially correlated with the onset of seismic anisotropy in the circum-Pacific (Lay et al., 1998), a region lacking P discontinuities and exhibiting higher-than-average seismic velocities (Figure 4). The anisotropy revealed by techniques such as splitting of S-waves suggests that horizontally polarized S-waves may travel up to several percent faster than vertically polarized S-waves (Lay et al., 1998), a pattern that also appears in more recent global inversions for S anisotropy (Panning and Romanowicz, 2006). Because the anisotropy exhibits similar strength as the S discontinuity atop D'', much or perhaps all of the S-wave speed variations in these regions may be characterized as a discontinuity in horizontally polarized shear waves and only a weak or absent discontinuity for vertically polarized waves. The correlation between strong anisotropy and the D'' discontinuity should provide important clues for assessing the origin of both features.

Note that while D'' discontinuities are typically found in seismically fast regions of the lowermost mantle, there are also some observations of S discontinuities in slow regions, such as the Pacific LLSVP (e.g., Avants et al., 2006; Garnero et al., 1993b). However, in these cases, there is no clear association with the kind of shear-wave anisotropy like that observed in the circum-Pacific region; thus, it has been suggested that slow region D'' discontinuities have an origin distinct from those in fast regions (Lay et al., 1998). Also, the association with P-wave anomalies appears to be different in some regions (Cobden and Thomas, 2013). In addition to these semihorizontal features, nearly vertical discontinuities with gradient thickness less than 100 km have also been detected around the edges of some LLSVPs (Ford et al., 2006b; Luo et al., 2001; Sun et al., 2007a; Wang and Wen, 2004; Wen, 2001), perhaps demarcating the edge of these features, as will be discussed in later sections. It has also been proposed that D'' discontinuities may manifest as a transition from weak to strong scattering atop the D'' layer (Cormier, 2000). The variety of observations and interpretations are therefore not always as simple as a simple S increase discontinuity and weak or absent P discontinuity, suggesting that the features in the deep mantle derive from a variety of origins (Figure 5).

7.11.3.1.2 Velocity decrease discontinuities

In addition to velocity increase discontinuities, there also exists evidence for velocity decrease discontinuities deeper inside the D'' layer. Using techniques similar to those employed in exploration seismology, Thomas and coworkers proposed S velocity decrease discontinuities beneath the more well-established increase discontinuities under Eurasia (Thomas et al., 2004b) and the Caribbean (Thomas et al., 2004a), mostly confined to the lowermost ~100 km of the mantle. However, unlike

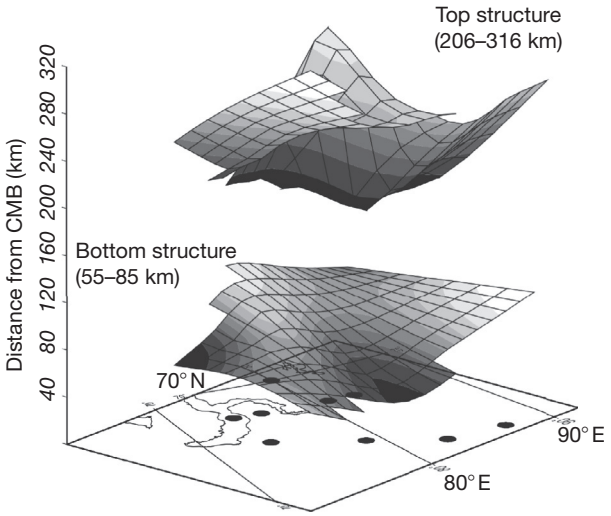

Figure 5 Variation in the depth of an S velocity decrease discontinuity situated beneath the usual S velocity increase discontinuity in the D'' layer under Eurasia. Reproduced from Thomas C, Kendall J, and Lowman J (2004). Lower-mantle seismic discontinuities and the thermal morphology of subducted slabs. *Earth and Planetary Science Letters*, 225: 105–113.

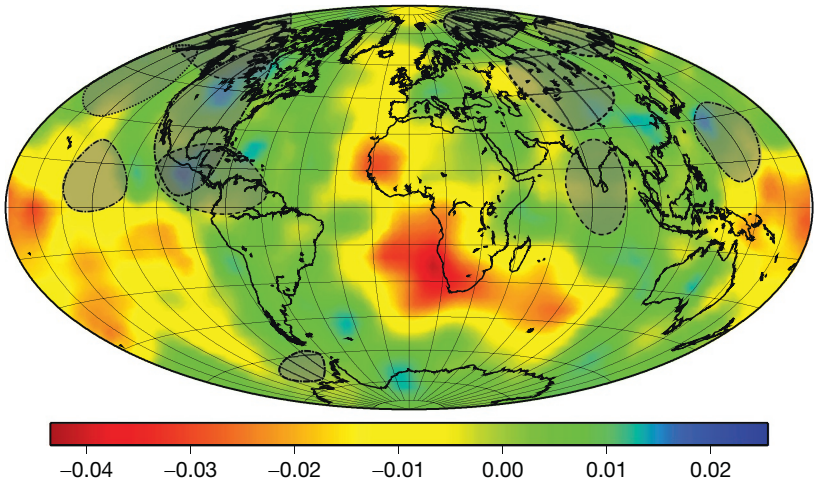

Figure 4 Map showing regions where an S discontinuity near the top of D'' (dot-dashed lines), strong S-wave anisotropy (dotted lines), or both (dashed lines) have been detected (see review by Lay, 2007) along with an addition discontinuity detection under North America (van der Hilst et al., 2007) overlain on an S-wave tomography model at 2800 km depth (Houser et al., 2008). Note that lack of detection does not imply absence, as some regions are not sufficiently covered to provide unambiguous evidence for S discontinuities and/or strong anisotropy.

triplications in the case of velocity increase discontinuities, velocity decrease discontinuities do not yield unambiguous signatures and are more difficult to detect (Flores and Lay, 2005).

The presence of *S* velocity decrease discontinuities beneath *S* velocity increase discontinuities has since been reported using different techniques in a variety of locations, such as waveform inversion of long-period data beneath the Caribbean (Kawai et al., 2007b) and Arctic (Kawai et al., 2007a), waveform modeling beneath the Cocos Plate (Sun et al., 2006), seismic imaging using the 'generalized Radon transform' beneath North America (van der Hilst et al., 2007), and dense array stacking and reflection profiling beneath the central Pacific (Lay et al., 2006) and central America (Hutko et al., 2008).

7.11.3.2 Models and Mechanisms

We now consider proposed mechanisms to explain the presence of discontinuities near the top and within the D'' layer. Prior to 2004, the cause of the *S* discontinuity near the top of D'' was attributed to variations in phase, temperature, and/or composition (Wysession et al., 1998), but the discovery of a perovskite (Pv) to postperovskite (PPv) phase change in $MgSiO_3$ now provides the most plausible explanation (Murakami et al., 2004). The discovery of the Pv–PPv phase change reinvigorated research efforts and may reveal important details about the D'' thermal boundary layer that were previously not well known.

7.11.3.2.1 Geodynamical predictions

Sidorin et al. (1998) predicted a phase change origin for the *S* discontinuity atop D'' 6 years prior to the discovery of a Pv–PPv phase change in $MgSiO_3$, with remarkably similar characteristics. They used thermochemical convection models of deep mantle convection interacting with a phase change to generate synthetic seismograms to test for consistency with observed data. Sidorin et al. first found that thermal gradients were not steep enough to account for the sharpness of observed seismic discontinuities. Compositional frontiers were depressed beneath downwellings and elevated beneath upwellings, which contradicted the observation of discontinuities several hundred kilometers above the CMB in the seismically fast (presumably cool) circum-Pacific region. Only a phase change exhibiting a strongly positive Clapeyron slope was able to elevate the discontinuity in cold regions in a manner consistent with the geography and observed sharpness of D'' discontinuities. They predicted a Clapeyron slope of ~6 MPa K^{-1}, an *S*-wave velocity change of ~1%, and a very weak *P*-wave velocity change. Although no suitable phase change was known at the time, this seminal prediction laid the foundation for the later discovery of the Pv–PPv phase change and facilitated more rapid acceptance of a Pv–PPv origin for the D'' discontinuity.

In the absence of known phase changes, modeling efforts were also undertaken in order to better understand how lower-mantle mineral assemblages could produce the kinds of anisotropy observed in the D'' region, particularly given the association between strong anisotropy and discontinuities in the circum-Pacific. Using a composite rheology, McNamara et al. (2001) used numerical models of mantle convection to investigate the possibility that a transition from diffusion creep to dislocation creep might occur in the lowermost mantle boundary layer and suggested that dislocation creep could become dominant beneath downwelling, while upwellings tend to remain in the diffusion creep regime. If dislocation creep could give rise to lattice-preferred orientation (LPO) beneath downwellings, it may provide an explanation for the occurrence of strong anisotropy in the circum-Pacific (McNamara et al., 2003), a region that is expected to be influenced by subducted oceanic lithosphere, consistent with its higher-than-average seismic velocity and historical locations of subduction zones (Lithgow-Bertelloni and Richards, 1998; Ricard et al., 1993). If the onset of LPO were relatively rapid, then such a mechanism might also produce a D'' discontinuity, in which case it would represent the frontier between diffusion- and dislocation-dominant creeps. However, such mechanisms depend on many complexities involved in rock rheology, which are currently debated. While it is presently thought that deformation and/or transformation textures in PPv dominate lower-mantle anisotropy, it has recently been proposed that PPv may inherit textures from Pv, and vice versa, emphasizing the importance of understanding anisotropy development in both Pv- and PPv-bearing phase assemblages (Dobson et al., 2013). The localization of high stresses at the base of downwelling subducted lithospheric slabs is also relevant for more recent interpretations regarding a PPv-related origin for anisotropy, as will be discussed in the succeeding text.

7.11.3.2.2 Postperovskite phase transition

Given the Fe + Mg/Si ratio of the silicate Earth and the stable crystalline phases over the relevant *P*–*T* range, the phase $(Mg,Fe)SiO_3$ Pv is thought to comprise ~80% of the lower mantle, and therefore, changes from Pv to another solid phase have long been considered as a primary candidate for the D'' discontinuity. Early attention focused on the possibility that Pv could dissociate into component oxides SiO_2 and (Mg,Fe)O (e.g., Meade et al., 1995; Saxena et al., 1996); however, experimental reports of such a phase change were controversial and not faithfully reproduced in later experiments. The discovery of the Pv–PPv transition in $MgSiO_3$ at a pressure and temperature similar to those expected atop the D'' layer, with a Clapeyron slope of 7–9 MPa K^{-1} (Murakami et al., 2004; Oganov and Ono, 2004; Tsuchiya et al., 2004) fits very well with the predictions of Sidorin et al. discussed in the preceding text and was accepted relatively quickly in comparison with the earlier-proposed mechanisms for the D'' discontinuity.

Additionally, the PPv phase is composed of a layered crystal structure with an elastic anisotropy (Oganov et al., 2005; Stackhouse et al., 2005) that may be consistent with correlations between the *S* velocity increase discontinuities atop D'' and the onset of strong anisotropy. Unfortunately, the precise mechanism(s) for generating anisotropy via mantle flow and transformation of Pv to PPv has been controversial (Hernlund, 2013). However, many complexities such as the use of analogue materials and distinction between transformation and deformation fabrics are presently being elucidated (e.g., Miyagi et al., 2011). However, other important behaviors are being discovered, such as inheritance of textures between Pv and PPv during phase changes (Dobson et al., 2013). The analysis of the lowermost mantle anisotropy is still a very active field and

should be important for establishing the connection between deformation and seismic anisotropy in the D'' region.

Recently, much attention has turned to the effects of soluble components in Pv and PPv such as $FeSiO_3$ and Al_2O_3 upon the phase change. Akber-Knutson et al. (2005) predicted that Al_2O_3 would cause a significant broadening of the two-phase coexistence region between Pv and PPv, consistent with later experimental inferences (e.g., Andrault et al., 2010; Catalli et al., 2009; Grocholski et al., 2012). The influence of an expected $FeSiO_3$ component has been somewhat controversial. Early results suggested that the addition of a $FeSiO_3$ component helps to stabilize the PPv structure at lower pressures (e.g., Mao et al., 2004; Ono and Oganov, 2005; Spera et al., 2006; Stackhouse et al., 2006). However, later experiments indicated that $FeSiO_3$ should destabilize PPv and shift the transition to higher pressures (Hirose et al., 2006; Tateno et al., 2007). Also, a high-spin to low-spin (e.g., Badro et al., 2004; Stackhouse et al., 2006) or intermediate-spin (e.g., McCammon et al., 2008) electronic transition in iron hosted in Pv and/or PPv may complicate matters, and its role in the phase relations is not completely understood. Partitioning of FeO between Pv–PPv and ferropericlase will also affect the phase diagram and sharpness of any Pv–PPv discontinuity; however, once again, contradictory results have been reported in the literature (e.g., Auzende et al., 2008; Sinmyo et al., 2008). We will return to a discussion regarding the effects of a broad two-phase region in the Pv–PPv transition for seismic observations and models of the D'' in the following sections.

7.11.3.2.3 Postperovskite double-crossing

At the time of discovery of the Pv–PPv phase change in $MgSiO_3$, the range of estimates for the CMB temperature were roughly 4000 ± 500 K, overlapping with the range of estimates of the temperature for the Pv–PPv phase change at CMB pressure. For a constant Grüneisen parameter of 1.5 along a liquid iron isentrope in the outer core (Vočadlo et al., 2003), a CMB temperature of 4000 K corresponds to an inner-core boundary temperature of ~5200 K. If the CMB temperature is greater than that of the Pv–PPv transition, then Pv would be stable at the very bottom of the mantle and PPv could only occur as a layer above the CMB. The PPv-bearing layer would then be bounded above and below by a 'double-crossing' of the phase boundary by the geotherm. Such a scenario is facilitated by the expected curvature of the geotherm in a boundary layer setting, accounting for the gradual transition from advection- to conduction-dominant radial heat transport with depth as one approaches the CMB. For a relatively cool CMB, on the other hand, PPv would be stable all the way to the CMB and only a single-crossing of the geotherm and the phase boundary would be produced. It is important to recognize that the CMB is itself an isothermal surface, exhibiting lateral temperature fluctuations of order 10^{-4} K or smaller and that larger lateral temperature changes would drive core flows (akin to thermal winds) too strong to be compatible with the observed geomagnetic secular variation (Braginsky and Roberts, 1995; Stevenson, 1987). Thus, in the context of processes in the Earth's mantle, which involve lateral temperature changes of order 10^3 K, the CMB is practically isothermal. The temperature of the Pv–PPv transition at CMB pressure, on the other hand, is sensitive to composition variations; thus, lateral variations in the latter could cause the scenario to shift from single-crossing to double-crossing in different compositional settings (Tackley et al., 2007).

The double-crossing predicts a pair of seismic discontinuities at both depths of intersection between the geotherm and Pv–PPv phase boundary where every PPv becomes stable in the D'' layer, one of which is the classical shallower S-wave speed increase discontinuity, in addition to a deeper reversion to Pv, which should induce seismic velocity variations of opposite polarity. A single-crossing, on the other hand, predicts only a single S-wave speed increase discontinuity. The double-crossing can easily explain the absence of D'' discontinuities in some regions, as a consequence of mantle material that is too warm to cross the Pv–PPv phase boundary (Hernlund et al., 2005), whereas the single-crossing model encounters difficulties in 'hiding' the discontinuity in regions where it is not observed, since it predicts a global layer of PPv. Detections of S velocity decrease discontinuities discussed in previous sections (Hutko et al., 2008; Kawai et al., 2007a; Lay et al., 2006; Sun et al., 2006; Thomas et al., 2004a,b; van der Hilst et al., 2007), underlying the shallower S velocity increase discontinuities, support the double-crossing scenario and motivated the original proposal of the double-crossing hypothesis (Hernlund et al., 2005). Integrated geotherm and mineral physics models also show a good agreement between the kind of structures predicted by a double-crossing and both the S- and P-wave characteristics of regions such as the circum-Pacific (Wookey et al., 2005), including very weak negative P discontinuities associated with larger S discontinuities (Cobden and Thomas, 2013; Hutko et al., 2008).

Some of the particular settings where a double-crossing was originally proposed are subject to different interpretations. For example, the imaging of a double-crossing-like structure in the mid-Pacific LLSVP (Lay et al., 2006) may require heat flux in excess of what would be expected in a chemically distinct 'pile' (e.g., Nakagawa and Tackley, 2008). Further illumination of this region by seismic data from USArray reveals that the reflectivity structure is considerably more complex than it initially appeared (Thorne et al., 2013b) and may be better explained by ingestion of MORB crust into piles (Li et al., 2014). There is also evidence for complexity in some other regions of the Pacific that may not be straightforwardly explained by the double-crossing (e.g., Kawai and Tsuchiya, 2009). Thus, while the double-crossing may be a viable model for some regions, such as the circum-Pacific, it does not serve to explain all of the complex structures observed in other regions of the deep mantle.

7.11.3.2.4 Complexities in the postperovskite phase change

The Pv–PPv mechanism for producing a seismic discontinuity structures has been questioned because the transition may become too thick to account for the <75 km gradient thickness consistent with seismic observations (e.g., Andrault et al., 2010; Catalli et al., 2009; Grocholski et al., 2012). However, the two-phase coexistence region width (i.e., the experimentally determined pressure increment) is only strictly an upper bound on the gradient thickness of a discontinuity produced by a phase change. While some authors draw linear trends in phase abundance through the Pv–PPv coexistence region (e.g., Andrault et al., 2010), the actual phase abundance given by the

'lever rule' law of molar species conservation can be highly nonlinear, with important consequences for interpreting these kinds of results. In particular, it has been demonstrated that the effective gradient thickness compatible with seismic observations may be significantly smaller than the two-phase coexistence pressure increment (e.g., Stixrude, 1997). Numerical calculations of a D'' boundary layer geotherm and a divariant Pv–PPv phase diagram with variable pressure increments found that a broadening of the two-phase region could in fact sharpen the gradients in phase abundance at the top and bottom of a PPv lens, opposite to the intuitive picture obtained by distributing the phase change linearly across the two-phase region (Hernlund, 2010). Thus, a broadening of the Pv–PPv coexistence region in P–T space alone does not necessarily present any problems for explaining the observed discontinuities and surprisingly may even help to enhance the sharpness of the discontinuities. However, the extent of this asymmetrical sharpening inside the two-phase region depends on the details of the phase diagram itself, which are still poorly constrained. Additionally, the seismic velocity jump across the sharp portion of the phase change will be smaller than the total velocity jump, perhaps explaining some of the scatter in observed strength of the D'' discontinuity.

Another issue related to the sharpness of a D'' discontinuity is the bulk composition of the rock in which the transition takes place, with the pressure increment observed in diamond-anvil cell experiments being relatively sharp (~3 GPa) for natural olivine, broadening to ~8 GPa for MORB and increasing to as much as ~14 GPa for a 'pyrolite' composition, owing mostly to increasing concentrations of Al_2O_3 (e.g., Andrault et al., 2010; Grocholski et al., 2012). As will be discussed in the next section on LLSVP, there are a variety of evidences to indicate that large-scale chemical heterogeneity exists in D''; thus, the behavior of the Pv–PPv transition could change substantially from one location to another depending on the prevailing bulk chemistry of the rocks. The circum-Pacific context is perhaps the simplest case, given the association of this region with long-lived subduction zones and high seismic-wave velocities. Thus, in the circum-Pacific, D'' discontinuities and strong anisotropy are proposed to arise from a Pv–PPv phase change in ponded subducted lithosphere originally composed of ~5 km thick MORB crust and ~80 km thick depleted harzburgitic mantle lithosphere. Owing to the small (~5%) volume fraction of basalt veneers in subducted slabs and the olivine-dominant lithology of harzburgite, sharp phase transitions in this context are therefore compatible with experimental results. The lack of discontinuities in other settings could be due to a broadening of the discontinuity in more Al_2O_3-rich compositions or due to a thinning of the PPv lens in warmer mantle or perhaps a combination of both mechanisms.

Some studies have argued that the Pv–PPv phase change occurs at pressure ranges that traverse the CMB, at least for iron- and/or aluminum-rich compositions (Andrault et al., 2010; Grocholski et al., 2012). However, these different diamond-anvil cell (DAC) studies also yield different P–T conditions and Clapeyron slopes for the Pv–PPv phase transition itself, with reported Clapeyron slopes varying by more than a factor of 2. This can be partly attributed to the choice of different pressure standards and scales, as opposed to experimental error. In particular, some studies (e.g., Catalli et al., 2009; Grocholski et al., 2012; Mao et al., 2006) use the gold pressure scale of Tsuchiya (2003) that yields relatively small Clapeyron slopes (~5 MPa K^{-1}). Other studies use no high-P–T standard but instead rely upon extrapolations of thermal pressure from proposed equations of state for the sample itself (Andrault et al., 2010). Experiments performed simultaneously with both gold and MgO using the pressure scale of Speziale et al. (2001) imply a significantly larger Clapeyron slope (~12 MPa K^{-1}). Aside from the important differences in the Clapeyron slope, absolute pressure differences between these different standards and approaches exceed 10%, yet each of these studies claims much smaller errors. While the MgO pressure scale is sometimes called 'geophysically consistent' because it yields postspinel transition pressures that better agree with the depth of the 670 km discontinuity, MgO reacts with samples having geologic relevant compositions, and gold is therefore preferred in these kinds of experiments. Nevertheless, P–T inferences obtained using the gold scale can be transformed to the MgO scale, after which the Clapeyron slope inferences from a large variety of studies are in better agreement (Hirose et al., 2006). However, the correct choice of pressure scales at CMB conditions is still not completely resolved, and unfortunately, this uncertainty trades off with models of the CMB region and gives rise to large uncertainties in P–T determinations. For example, the PPv double-crossing fits nicely with the Clapeyron slope given by the Speziale MgO scale but is implausible if the Tsuchiya Au scale is more representative of the deep Earth (Hernlund and Labrosse, 2007).

A mechanism involving PPv plasticity and development of anisotropic fabric may also help to produce and/or sharpen the seismic velocity discontinuities associated with a Pv–PPv phase change. Additionally, the change in wave speeds across a Pv–PPv transition may be too small to account for seismic observations if the mixture is isotropic before and after the transition; thus, the development of anisotropic fabric may be required to explain the basic amplitude of the D'' discontinuity (Murakami et al., 2007). It has been suggested that, once the volume fraction of PPv becomes sufficiently large in the two-phase region, deformation of the host matrix will become controlled by PPv rheology. Experiments on analogue materials suggest that PPv is significantly weaker than Pv (perhaps by as much as an order of magnitude) and therefore may undergo rapid deformation at a critical fraction of PPv, causing a rapid onset of deformation and production of anisotropic fabric (e.g., Hunt et al., 2009; Thomas et al., 2011). This kind of mechanism is also consistent with the large stresses expected at the core of cool downwellings (McNamara et al., 2001) where PPv is expected to form in the circum-Pacific context, and if the LPO-inducing deformation mechanism is appropriate, there will be a corresponding sharp increase in the wave speed for horizontally polarized S-waves (V_{SH}) on top of a weaker and broader increase in isotropic S-wave speed (v_{SH}).

The aforementioned combined mechanisms and effects are illustrated in **Figure 6**, which shows a double-crossing (Hernlund et al., 2005), the effect of asymmetrical phase abundance in a 5 GPa thickness two-phase region calculated self-consistently by the lever rule in the model of Hernlund (2010), the associated isotropic S-wave speed structure it generates (Murakami et al., 2007), and the possible enhancement in V_{SH} at the onset of a rheologically critical fraction of PPv

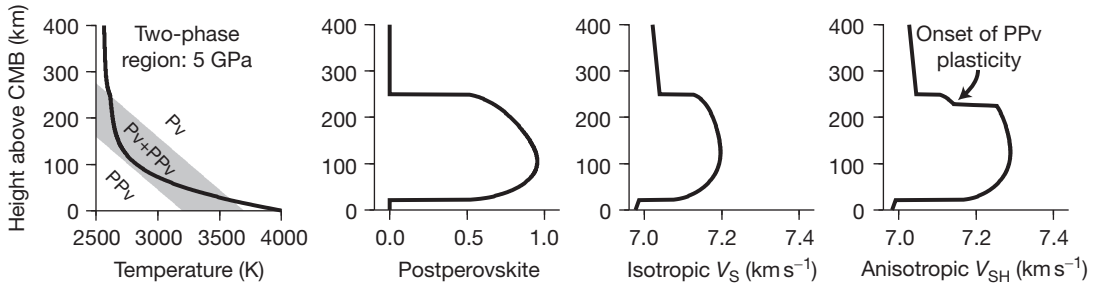

Figure 6 Deep mantle profiles illustrating a potential synthesis of current ideas regarding the occurrence of a Pv–PPv transition and double-crossing inside D'' in a way that could account for broadening of the two-phase region, the sharpness of the discontinuity, a weak change in isotropic S-wave speed (V_S), and the onset of strong seismic anisotropy. The left frame shows the geotherm calculated for interaction with a broad (5 GPa) mixed phase region (gray area), and the second frame from the left shows the resulting postperovskite fraction variation with depth. The profiles are calculated self-consistently using the method of Hernlund (2010). The corresponding isotropic and anisotropic S velocity profiles are shown on the right, in which a sudden onset of PPv plasticity and development of LPO fabric is invoked to explain a sharpening of the upper discontinuity as experienced by SH waves. Note that the transformation from Pv to PPv is never complete in this scenario; there is always a nonzero fraction of Pv phase present throughout the entire depth range. However, structures that are compatible with the PPv double-crossing are nevertheless produced by nonlinear variations in PPv abundance inside the two-phase region.

owing to its weak strength and strong anisotropy (Hunt et al., 2009). The details of this picture may change significantly in the future as the mechanisms are further constrained and/or new mechanisms are considered, and further illumination of D'' by seismic station proliferation will open new windows and perspectives into the complex structure of the CMB region.

7.11.3.3 D'' Discontinuity Summary

Discovery of a Pv–PPv phase transition in $MgSiO_3$ at conditions of the D'' layer revolutionized deep-Earth geophysics and heralded the onset of a new era in which experiments could be routinely performed at the relevant P–T conditions. A Pv–PPv phase change offers the best explanation for the basic first-order features of D'' discontinuities, in addition to their correlation with other features such as strong seismic anisotropy. However, different pressure scales are still applied to DAC experiments at D'' conditions, yielding significant differences in the inferred P–T conditions. And while it is probable that the transition in some bulk compositions occurs over a broad P range, it is also clear that such a measure represents only an upper bound on the gradients in seismic velocity, the latter of which could be very sharp even for very broad transitions.

The relevance of the Pv–PPv phase change for explaining deep mantle structures is probably limited to certain regional and dynamical settings in the lowermost mantle. A Pv–PPv origin for D'' discontinuities is most consistent with the circum-Pacific setting, in which cold ponding slabs are expected to elevate the height of the discontinuity and induce stresses large enough to give rise to anisotropic fabric; positive S discontinuities are associated with weak negative P anomalies; the harzburgite-dominant composition expected for subducted slabs should yield relatively sharp phase transitions; and double-crossing-like structures have been reported by a handful of seismology research groups using a variety of techniques. The mid-Pacific or sub-African lowermost mantle, on the other hand, may be too hot or exhibit thermal gradients too small to be compatible with a Pv–PPv phase change. These LLSVP regions exhibit many features that are probably better explained by variations in bulk composition, and after further examination, structures that once appeared compatible with Pv–PPv origin in the mid-Pacific seem to be more complex and random. However, the phase diagram for Pv–PPv is still constrained poorly enough to permit a variety of exceptional scenarios, and further work should help to limit the number of available options or expand upon the possible range of behavior. Some other regions, such as Eurasia, appear to exhibit a variety of complex behavior, and new kinds of anomalies are still being discovered, thus illustrating that some regions have no straightforward explanation for structures and motivating further work to better characterize them and develop mechanisms compatible with these observations. Increased seismic coverage, particularly in the southern hemisphere, would also help to test hypotheses in a broader array of settings and diversify the underlying observations that motivate research in D''.

One area of research that is very important for interpreting D'' discontinuities, which may yield surprises in the near future, is the development and transformation of anisotropic fabric in the deep mantle. In fact, it may be possible to explain some of the major observations of the D'' layer with fabric changes alone, although most of these must work in concert with a Pv–PPv phase change; thus, the contributions of a variety of factors may yield a variety of possible mechanisms and behaviors to provide a larger tool box for explaining D'' structure. Sorting out the appropriate slip systems for dislocation creep in PPv has proved very difficult, with many groups reporting significantly different results and debates regarding whether some experiments are observing textures due to transformation or deformation (Miyagi et al., 2011). It will ultimately be necessary to integrate these models with dynamical flow models in the D'' region (Nowacki et al., 2013; Walker et al., 2011); however, a consensus view has yet to emerge from all models.

Before concluding the discussion on D'' discontinuities, it is important to note that the Pv–PPv phase change is highly sensitive to variations in temperature, owing to the large Clapeyron slope. Pv–PPv-induced discontinuity depth variations of up to 200 km would correspond to pressure variations of 11 GPa or 850–1400 K lateral temperature variations for a Clapeyron slope of 8–13 MPa K^{-1}. It is difficult to explain such

large lateral temperature anomalies without considering the presence of subducted lithosphere in D'', and therefore, the interpretations of the D'' discontinuity in terms of Pv–PPv are consistent with, and also depend upon, the occurrence of whole mantle convection.

7.11.4 Large Low-Shear-Wave-Velocity Provinces (LLSVPs)

7.11.4.1 Seismic Observations

7.11.4.1.1 Seismic tomography

Over the past two decades, advances in seismic tomography have greatly improved our view of lower-mantle structure (e.g., Antolik et al., 2003; Dziewonski et al., 1977, 2010; Engdahl et al., 1995; Fukao et al., 1992; Grand, 2002; Grand et al., 1997; Gu et al., 2001; Ishii and Tromp, 1999, 2004a; Kuo et al., 2000; Lekic et al., 2012; Li and Romanowicz, 1996; Li et al., 2008; Masters et al., 1996; Megnin and Romanowicz, 2000; Panning and Romanowicz, 2006; Ritsema and van Heijst, 2002; Ritsema et al., 1999, 2004, 2011; Romanowicz and Gung, 2002; Su and Dziewonski, 1997; Takeuchi, 2007; van der Hilst et al., 1997; Zhao, 2004).

Figure 7 displays the seismic tomography model S20RTS (Ritsema and van Heijst, 2002; Ritsema et al., 2004). Higher-than-average seismic velocities are observed beneath the circum-Pacific and Western Asia. Because these faster regions are located beneath zones of ancient subduction, they are generally considered to be caused by thermal anomalies resulting from remnants of subducted lithosphere (e.g., Grand et al., 1997; van der Hilst et al., 1997). This idea is supported by geodynamical models that include the Earth's plate history over the past 120 million years as surface boundary conditions. To the first order, these geodynamical models predict the existence of relatively cool, previously subducted lithosphere descending in the mantle in the same regions that higher-than-average seismic-wave speeds are observed in seismic tomography (Bull et al., 2009, 2010; Bunge et al., 1998; Lithgow-Bertelloni and Richards, 1998; McNamara and Zhong, 2005; Richards and Engebretson, 1992; Ritsema et al., 2007; Schuberth et al., 2009). In most regions, particularly along the Pacific margin of the Americas, seismic tomography reveals subducted lithosphere extending into the

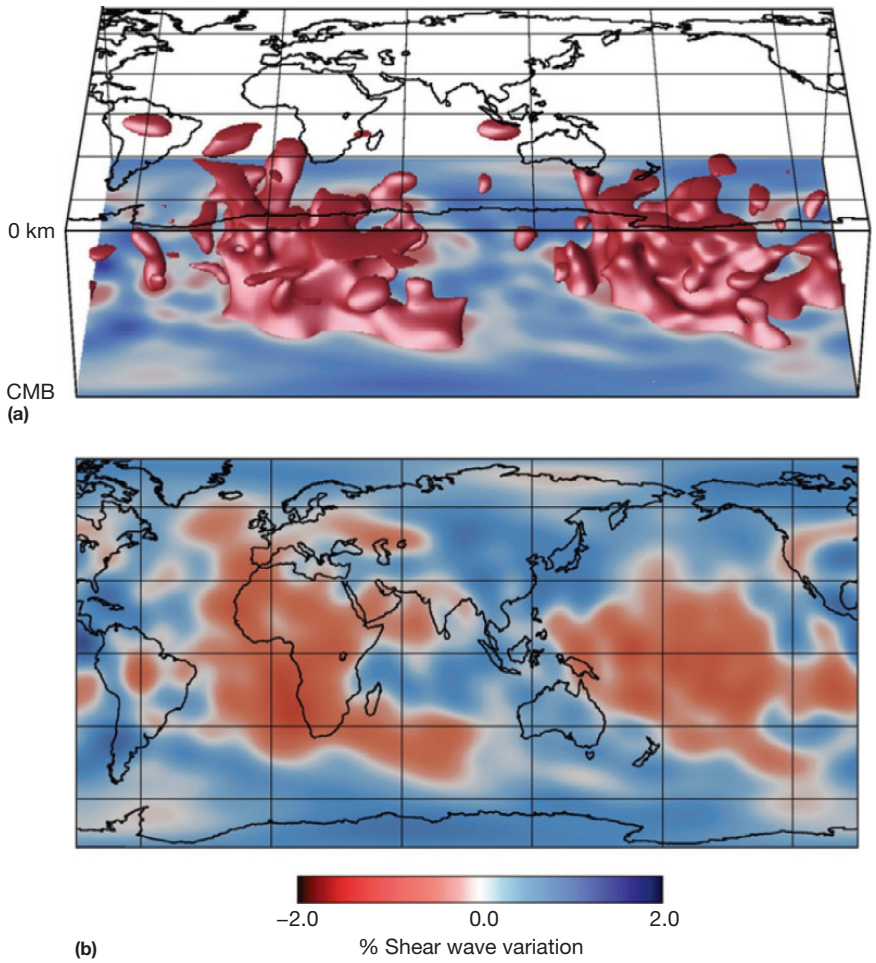

Figure 7 Seismic tomography model S20RTS (Ritsema et al., 1999, 2004). (a) Isosurface representing −0.6% shear-wave velocity anomaly that highlights the presence of large low-shear-wave-velocity provinces (LLSVPs) beneath Africa and the Pacific. (b) Map view of shear-wave velocity variation, slightly above the core–mantle boundary (at 2750 km depth). Reproduced from Bull AL, McNamara AK, and Ritsema J (2009) Synthetic tomography of plume clusters and thermochemical piles. *Earth and Planetary Science Letters* 278(3–4): 152–162.

lower mantle (e.g., Grand et al., 1997; Li et al., 2008; van der Hilst et al., 1997), providing strong evidence against a layered mantle, as hypothesized earlier from geochemical observations (e.g., Carlson, 1994; Hofmann, 1997).

The lowermost mantle beneath Africa and the Pacific is characterized by lower-than-average seismic-wave velocities (**Figure 7**). Classically, these slow regions have been called 'superplumes' (e.g., Ni et al., 2002; Romanowicz and Gung, 2002), which has sometimes caused confusion because the name connotes a dynamical dimension to the seismic observation. In recent years, the community has moved toward naming these regions the LLSVPs in order to more carefully separate the observation from the different hypotheses related to their origin. While the name LLSVP refers to shear-wave tomography, these features are also observed in *P*-wave tomography (e.g., Li et al., 2008; Ritsema and van Heijst, 2002; Zhao, 2004). *P*-wave speed anomalies in these features appear to be weaker than for *S* (e.g., see *P* velocity map in **Figure 21** versus the corresponding *S* velocity map in **Figure 4**); however, most *S* models have significantly better resolution than *P* models. In map view of the lowermost mantle, the African LLSVP is a relatively linear feature striking northwest–southeast, and it extends from the southern Indian Ocean, across Africa and the eastern Atlantic, to northwestern Europe. Lekic et al. (2012), using cluster analysis of multiple tomographic models, argued for the existence of a miniature LLSVP in the lowermost mantle beneath Eastern Europe, which they name the 'Perm Anomaly.' It is unclear how this anomaly is related to the larger African LLSVP, but they claim that it is a distinct feature because it is bounded by strong seismic velocity gradients. It is possible that it could be a recently detached portion of the African structure, thus not necessarily distinct in origin. In contrast to the African LLSVP, the Pacific LLSVP appears relatively more rounded in map view and is centered beneath the southwestern portion of the Pacific Ocean. As imaged by seismic tomography, lower-than-average seismic velocities from both LLSVPs extend from the base of the mantle and reach to the upper mantle (e.g., Romanowicz and Gung, 2002). The African LLSVP appears vertically tilted toward the northeast (e.g., Ritsema et al., 1999), whereas the Pacific LLSVP appears to be vertical.

7.11.4.1.2 Negative correlation between shear-wave and bulk sound velocities

Both shear-wave and bulk sound velocities can be computed by joint tomographic inversions for both *P*-wave and *S*-wave data. Bulk sound velocity is a synthetic velocity (computed from both *P*-wave and *S*-wave velocities) that has the practical advantage that it is only sensitive to bulk modulus and density. For a homogenous system of Earth minerals, both shear-wave and bulk sound velocities are expected to systematically vary together as a function of temperature and pressure (e.g., Masters et al., 2000). However, joint tomography studies typically agree that there is a negative correlation between shear-wave and bulk sound velocities in the lowermost mantle, particularly in the lowermost 500 km (e.g., Antolik et al., 2003; Masters et al., 2000; Ritsema and van Heijst, 2002; Su and Dziewonski, 1997; van der Hilst and Karason, 1999). The negative correlation observed in the lowermost mantle is an indication of compositional heterogeneity. Tomography using normal modes (i.e., free oscillations) provides a means to infer density structure. In addition to finding a negative correlation between shear-wave and bulk sound velocities in the lowermost mantle, normal-mode tomography determines that the lowermost mantle regions beneath Africa and the Pacific are characterized by increased relative density (e.g., Ishii and Tromp, 1999, 2001, 2004b). However, the relative density component of normal-mode studies is likely the least constrained (e.g., Lay and Garnero, 2011; Resovsky and Ritzwoller, 1999).

Hernlund and Houser (2008) examined the statistical distribution of areal distribution of *P*- and *S*-wave anomalies as a function of depth in various seismic tomography models. While both *P*-wave and *S*-wave distributions appear Gaussian-like at each depth range, the *S*-wave distributions form a thickened tail on the lower-than-average side of the distribution in the lowermost 700 km of the mantle. They argue that this provides evidence for compositional heterogeneity and/or phase change heterogeneity in the lowermost mantle.

By relating *P*- and *S*-wave velocity and density to changes in temperature and composition (e.g., perovskite and magnesiowüstite content), several probabilistic tomography studies have inferred that tomographic data are better explained with a heterogeneous compositional component in the lowermost mantle (e.g., Deschamps and Trampert, 2003; Trampert et al., 2001, 2004). Deschamps et al. (2012) found that the LLSVPs are better explained by iron and perovskite enrichment than the accumulation of oceanic crust (MORB).

7.11.4.1.3 Sharp gradients along LLSVP margins

Due to the spatially nonuniform distribution of both earthquake sources and seismograph stations, seismic tomography produces an incomplete and blurred view of the Earth's interior. Therefore, the LLSVPs may not accurately represent the true shape of the temperature and/or compositional anomalies that cause them (e.g., Ritsema et al., 2007). Additional seismic studies that rely upon travel-time analysis and waveform modeling have complemented seismic tomography in order to better elucidate the shape of the African and Pacific structures that cause the LLSVPs (e.g., Breger and Romanowicz, 1998; Ford et al., 2006a; He and Wen, 2009, 2012; He et al., 2006; Ni and Helmberger, 2003a,b,c; Ni et al., 2002, 2005; Ritsema et al., 1997; Sun et al., 2007a,b, 2009; To et al., 2005; Wang and Wen, 2004, 2007; Wen, 2001, 2002; Wen et al., 2001). Such studies have found sharp gradients in seismic-wave velocity near the margins of the LLSVPs. These sharp gradients cause a distortion (usually a broadening) of the waveform that appears on a seismogram. By comparing seismic waveforms along an array of seismic stations that are wide enough to include both seismic waves that pass through an anomaly and those that do not, travel-time analysis and waveform modeling can be used to constrain the position of the edges of the anomalies.

Figure 8 provides a summary of recent work that constrains the shape of the anomalies that cause the LLSVPs. Examining the African structure, it is evident that individual studies do not necessarily agree, likely the result of initial assumptions of the seismic model. One must first pose a trial model for the shape and refine it accordingly to find the best fit for the data. The northern extent of the African structure remains

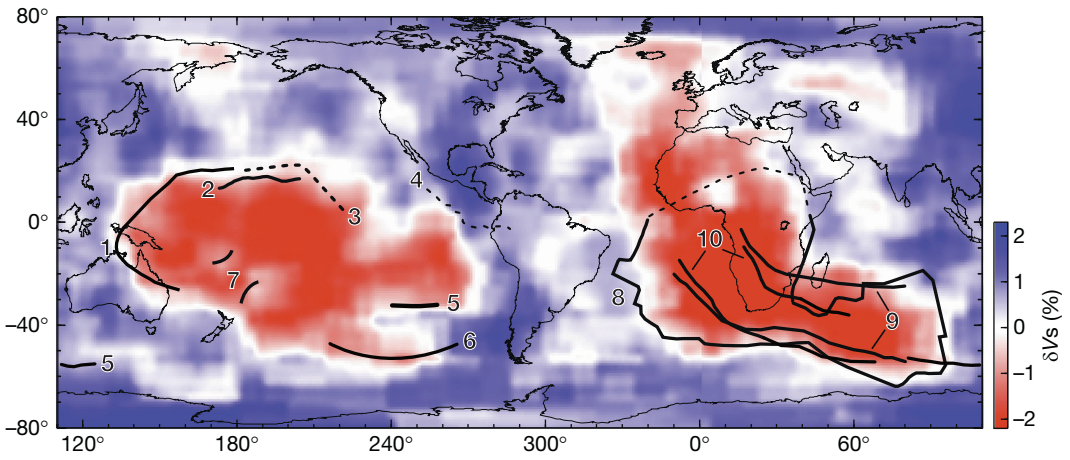

Figure 8 Map showing sharp edges of the large low-shear-wave-velocity provinces as inferred from travel-time and waveform seismic studies. The background map shows shear-wave tomography model TXBW (Grand, 2002). Sharp edges are represented as thick black lines, with dashed lines representing edges inferred from travel times. Numbers indicate the particular seismic studies (1. He et al. (2006); 2. Luo et al. (2001); 3. Breger and Romanowicz (1998); 4. Sun et al. (2007b); 5. To et al. (2005); 6. Ford et al. (2006a); 7. He and Wen (2009); 8. Wang and Wen (2004); 9. Sun et al. (2007b), Sun et al. (2009); and 10. Ni and Helmberger (2003c), Ni and Helmberger (2003a), and Ni and Helmberger (2003b)). This figure was provided by Ed Garnero and Chunpeng Zhao.

unconstrained, and geodynamical models (discussed later) predict that it should extend into Europe and perhaps wrap back down into Eastern Europe (e.g., the 'Perm' anomaly discussed earlier). Much of the Pacific LLSVP margin remains to be mapped. The sharp edges inferred in the middle of the Pacific LLSVP are particularly intriguing and could indicate that multiple anomalies contribute toward creating the LLSVP observed in tomography. He and Wen (2009, 2012) proposed two Pacific anomalies that they name the western Pacific Anomaly and the northern Pacific anomaly. The idea that the Pacific LLSVP is composed of distinct subregions is further supported by the seismic work of Thorne et al. (2013b). As will be discussed later, this is consistent with some geodynamical interpretations.

7.11.4.1.4 Summary of seismic observations

In summary, seismic tomography has revealed a pattern of higher-than-average velocities beneath the circum-Pacific and Asia and large regions of lower-than-average velocity beneath Africa and the Pacific. While the faster regions may be explained as subducted lithosphere extending into the lower mantle, the slower regions beneath Africa and the Pacific are more enigmatic. Joint tomography studies that invert for both *P*-wave and *S*-wave data find that the slower regions are difficult to explain by thermal effects alone and are likely characterized by compositional heterogeneity. Seismic tomography provides an incomplete, blurred view of the interior, so additional seismic methods need to be applied to constrain the shape of the anomalies that cause the LLSVPs. Waveform modeling studies infer sharp velocity gradients near the margins of the LLSVPs, and the anomalies are increasingly being mapped out in better detail. Furthermore, the strong velocity gradients along LLSVP margins are suggestive of sharp thermal and compositional boundaries.

7.11.4.2 Hypotheses Regarding the Cause of LLSVPs

7.11.4.2.1 Introduction

Numerous geodynamical studies have been performed that are geared toward understanding the cause of the LLSVPs and the dynamics associated with them. The various hypotheses that have emerged can be loosely categorized into three groups: thermal, active thermochemical, and passive thermochemical.

The simplest interpretation of the LLSVPs is that they are caused by large thermal anomalies, either as 'megaplumes' (e.g., Tackley, 2000a; Thompson and Tackley, 1998) or as groups of smaller plumes, 'plume clusters' (e.g., Schubert et al., 2004). This interpretation does not necessarily discount the presence of compositional heterogeneity, as inferred from the seismic studies, but it proposes that the dynamics are largely controlled by thermal convection.

Alternatively, other hypotheses propose that lower-mantle dynamics are controlled by a combination of thermal and compositional buoyancy. Mantle convection driven by thermal and compositional buoyancy is typically referred to as 'thermochemical convection'. Thermochemical mantle models include two or more compositional components, each of which is characterized by having a different intrinsic density. The intrinsic density is the density at a particular reference temperature. Thermal variations further modify the density by thermal expansion and contraction. Therefore, the net effective density of mantle material in these models is usually a linear combination of the material's intrinsic density and the density change due to temperature. Thermochemical convection systems that consist of multiple components in which the difference in intrinsic density between components is much greater than the variations in density due to temperature variations tend to develop stratified configurations, which are layered according to intrinsic density. An example of this would be the stratified core–mantle system, in which the

intrinsic density difference between the core and mantle is much greater than density differences due to temperature variation, leading to a layered configuration of the core and mantle. If the Earth's mantle consists of multiple internal compositional components, it is expected that the intrinsic density differences between each component are similar in magnitude to the density differences due to temperature, except for material with very large density anomalies that accumulate at the upper or lower boundaries. Such a system results in a rich variety of possible thermochemical convection behavior (e.g., Tackley, 2007, 2012).

Active thermochemical hypotheses propose that the LLSVPs are caused by compositional anomalies that have an effective density that varies in time such that it fluctuates between being more dense and less dense than the surrounding, background mantle. This type of hypothesis postulates that the LLSVPs are caused by thermochemical structures that cause buoyancy-driven vertical flow. Such structures are typically referred to as 'thermochemical superplumes' (e.g., Davaille, 1999). On the other hand, passive thermochemical hypotheses propose that the LLSVPs are caused by compositional structures that, on average through time, maintain a slightly heavier to near-neutral effective density with respect to the background mantle. Such structures tend to remain at the base of the mantle over geologic time and are passively swept around along the CMB by changing subduction patterns. They do not contribute significant driving force to large-scale mantle convection. Such structures are typically referred to as 'thermochemical piles'.

7.11.4.2.2 Significance of understanding the cause of LLSVPs

Discovering which, if any, of the broadly categorized hypotheses explain the cause of the LLSVPs is a fundamentally important endeavor because each of the conceptual models broadly listed in the preceding text has significantly different consequences toward our understanding of Earth's thermal evolution, temperature structure, chemical evolution, and the driving forces associated with plate tectonics. If the LLSVPs are caused by compositional reservoirs in the lower mantle, these reservoirs will also act as thermal reservoirs, causing the mantle to have a drastically different temperature structure and thermal evolution than that expected for a purely thermally driven mantle (e.g., McNamara and van Keken, 2000; Zhong, 2006). The fundamental ideas associated with the mantle plume hypothesis also hinge upon which of these LLSVP hypotheses may be occurring within the Earth. In particular, geodynamical models consistently reveal that plumes are swept toward upwelling areas governed by the global distribution of subduction (e.g., Zhong et al., 2000). In purely thermal models of mantle convection, plumes are predicted to arise from a thermal boundary layer along the CMB in these regions. In passive thermochemical models however, compositional reservoirs are also driven toward these upwelling regions with mantle plumes forming along their tops (e.g., McNamara and Zhong, 2005). Plumes are predicted to form along the top of upwelling compositional domes in active thermochemical models (e.g., Davaille, 1999). Therefore, our understanding of plume source depends on which hypothesis explains the Earth's mantle. Consequently, using hot spot swell topography to compute plume buoyancy flux to determine core heat loss (e.g., Davies, 1988; Sleep, 1990) is directly affected (e.g., Zhong, 2006).

Discovering the cause of the LLSVPs also directly affects our interpretation of what surface geochemistry tells us about the Earth's interior. The difference in trace element chemistry, particularly incompatible elements and noble gases, between MORBs and OIBs has motivated hypotheses of multiple chemical reservoirs in the Earth's interior including more-primitive mantle material and recycled oceanic crust (e.g., Albarède, 1998; Carlson, 1994; Gonnermann and Mukhopadhyay, 2007, 2009; Hofmann, 1997; Mukhopadhyay, 2012; Tackley, 2000a, 2007; Tolstikhin and Hofmann, 2005; Tolstikhin et al., 2006). Most of these hypotheses rely upon mantle plumes interacting with one or more reservoirs at depth, bringing a small amount of entrained material to surface hot spots as OIBs, whereas divergent boundaries sample depleted background mantle (e.g., Tackley, 2000a). If LLSVPs are indeed caused by compositional reservoirs in the mantle, whether formed by an early differentiation event, the accumulation of oceanic crust, or both, then they are prime candidates to be the geochemical reservoirs hypothesized from geochemical observations.

Finally, compositional reservoirs in the lowermost mantle strongly affects the spatial pattern of heat flux coming out of the core (e.g., Zhang and Zhong, 2011) and could influence the geodynamo (e.g., Driscoll and Olson, 2011; Sreenivasan and Gubbins, 2011).

7.11.4.2.3 Thermal hypotheses

Given that seismic tomography reveals the LLSVPs as having a lower-than-average wave speed, the most obvious hypothesis is that they are caused by hotter-than-average thermal anomalies and are, therefore, megaplumes of the upwelling mantle. However, conventional fluid dynamical calculations at Earth-like convective vigor predict thermal plumes to be much smaller in radius than the LLSVPs (e.g., Olson et al., 1993; Schubert et al., 2004). Thompson and Tackley (1998) found that megaplumes could be formed in axisymmetrical convection models if the temperature dependence of viscosity was sufficiently high (500 kJ mol^{-1} in their case). Their model employed a prescribed initial temperature condition that included a thermal boundary layer at the base of the model. Small-scale instabilities quickly formed within the hot (therefore low-viscosity) lower thermal boundary layer and were swept into a large megaplume along the axis. Given that the experiment was initiated with a prescribed, convection-free (i.e., 1-D) temperature profile, it is unclear whether megaplume formation would regularly repeat over time or if it requires the special case of having an initial boundary layer of uniform thickness. Matyska et al. (1994) suggested that high thermal conductivity in the hottest portions of the D'' layer could also promote the occurrence of large megaplumes, consistent with LLSVP.

Schubert et al. (2004) proposed that the LLSVPs could be caused by poorly imaged clusters of thermal mantle plumes. They provide analytic arguments that demonstrate that megaplumes on the spatial scale of LLSVPs are not dynamically feasible given the rheological and thermal properties of the Earth's mantle. Instead, they hypothesize that numerous smaller plumes form clusters in the large-scale upwelling regions

beneath Africa and the Pacific. This is the result of a highly unstable thermal boundary layer, which nucleates small-scale plume instabilities on timescales short in comparison with the residence time of material at the CMB governed by plate-driven circulation. As viewed by seismic tomography, with its heterogeneous resolution, the clusters of plumes could appear to be grouped together as much larger apparent anomalies.

The plume cluster hypothesis was explored further in McNamara and Zhong (2005), Ritsema et al. (2007), Bull et al. (2009), Schuberth et al. (2009), and Davies et al. (2012). McNamara and Zhong (2005) performed both isochemical and thermochemical convection calculations in 3-D spherical geometry that employed the Earths plate motion history for the past 120 million years as kinematic boundary conditions to guide the historical location of subduction, in a manner similar to Bunge et al. (1998). In the isochemical models, clusters of relatively thin thermal plumes were focused into upwelling regions that formed beneath Africa and the Pacific in response to subduction patterns. In the thermochemical models in which an intrinsically more-dense basal layer was added as an initial condition, subduction history acted to focus the basal layer into piles beneath Africa and the Pacific. Ritsema et al. (2007) converted the temperature fields from these models to variations in shear-wave velocity using a simple linear relationship (e.g., Forte and Mitrovica, 2001). They then applied the seismic resolution operator from tomography model S20RTS (Ritsema et al., 1999, 2004) to the anomalies predicted from the geodynamical models to produce synthetic tomography models. The seismic resolution operator is a measure of how the 'true Earth' is mapped into a seismic tomography model, and when applied to a given distribution of shear-wave velocity anomalies, it shows how the anomalies are distorted by the tomographic inversion. They found that the plume clusters beneath Africa and the Pacific were indeed blurred by the inversion to generate much larger, apparent anomalies. However, these apparent anomalies in the synthetic tomography did not appear as continuous as the LLSVPs observed in actual tomography. Furthermore, the synthetic tomography created from the thermochemical pile models produced a better correlation to actual seismic tomography.

This work was expanded by Bull et al. (2009) who used more thermodynamically consistent conversions from temperature to shear-wave velocity anomaly (e.g., Stixrude and Lithgow-Bertelloni, 2005), explored additional convection parameters, and performed degree-by-degree correlations between synthetic and actual tomography. **Figure 9** displays a representative example of one of the isochemical cases. **Figure 9(a)** displays thermal isosurfaces of the temperature field that highlight the development of plume clusters in the African and Pacific regions. **Figure 9(b)** and **9(c)** shows the temperature field and the

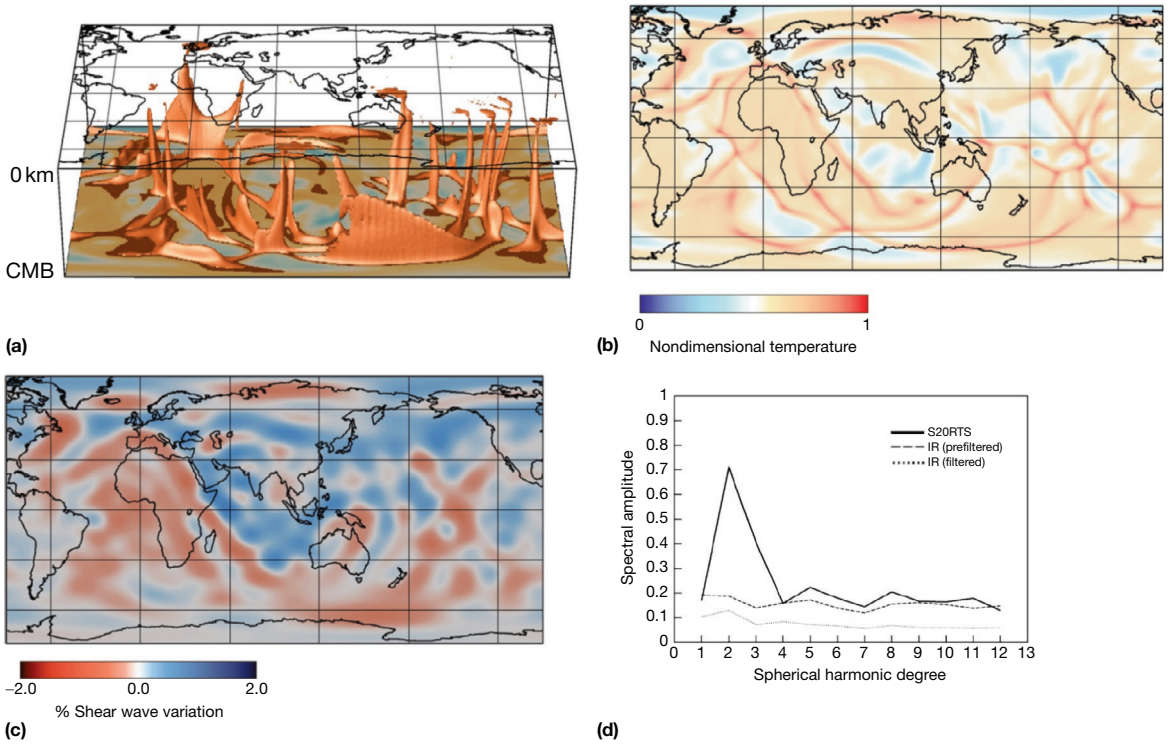

Figure 9 Synthetic shear-wave tomography caused by plume clusters beneath Africa and the Pacific. (a) Plume clusters generated in an isochemical, 3-D spherical convection calculation that utilizes 120 My of plate history as kinematic surface velocity boundary conditions. Results are unwrapped unto a Cartesian box. Isosurfaces of higher-than-average temperature outline the positions of thermal plumes, which form clusters beneath Africa and the Pacific. (b) Map view of the temperature field above the core–mantle boundary (CMB) at 2750 km depth. (c) Map view of synthetic shear-wave tomography generated from the geodynamical model. (d) Amplitude spectra of the spherical harmonic decomposition of the tomographic model S20RTS (Ritsema et al., 1999, 2004) (solid line), temperature field of geodynamical calculation (dark dashed line), and synthetic tomography (light dashed line). Reproduced from Bull AL, McNamara AK, and Ritsema J (2009) Synthetic tomography of plume clusters and thermochemical piles. *Earth and Planetary Science Letters* 278(3–4): 152–162, figures 2, 4, and 5.

resultant synthetic tomography in map view at 2750 km depth. From the figures, it is clear that tomography substantially blurs the thermal anomalies, but not enough to generate continuous anomalies as observed in actual tomography (**Figure 7(b)**). **Figure 9(d)** shows the spectral amplitude as a function of harmonic degree for the actual tomography, the prefiltered thermal field, and the synthetic tomography. The synthetic tomography exhibits a relatively flat spectrum that does not exhibit the large degree-2 and degree-3 amplitudes that are characteristic in the actual tomography.

In contrast, Schuberth et al. (2009) performed a similar analysis on isochemical models, but they found a better agreement with seismic shear-wave tomography, showing that thermal models can explain seismic shear-wave tomography. The discrepancy between the studies may be largely attributed to different rheological properties. Bull et al. (2009) employed a temperature-dependent viscosity (10 000× viscosity contrast due to temperature across the model), whereas Schuberth et al. (2009) employed a radial viscosity. Temperature dependence of viscosity may act to produce more numerous, narrower plumes. Davies et al. (2012) is an expansion upon the earlier Schuberth et al. (2009) work, in which they include a mild temperature dependence of viscosity (100× viscosity contrast due to temperature across the model) and compressibility. Their earlier conclusions that isochemical convection can explain the LLSVPs are unchanged, in addition to further predicting strong seismic velocity gradients along the margins.

In summary, if the LLSVPs are caused by thermal-only anomalies, it is likely that they would be clusters of narrow plumes swept into upwelling regions by subduction that resemble larger anomalies when viewed by tomography. Geodynamics-based tomography prediction studies differ on how well plume clusters can resemble LLSVPs and produce sharp seismic gradients along their margins, and these differences are likely due to different model formulations (rheological description and compressibility). Therefore, it is not clear that thermal-only hypotheses for the cause of LLSVPs can be excluded. However, compositional heterogeneity inferred from the negative correlation of shear-wave and bulk sound velocities still needs to be explained. The possibility of plume clusters may also be restricted to a range of material properties that enter into the effective Rayleigh number, such as viscosity, thermal conductivity, and thermal expansivity.

7.11.4.2.4 Thermochemical hypotheses

7.11.4.2.4.1 Early thermochemical studies and ideas

Some of the earliest geodynamical studies on thermochemical convection were motivated by seismic observations that inferred that the D'' region of the lowermost mantle was characterized by strong heterogeneity in both temperature and composition (e.g., Lay, 1987). Davies and Gurnis (1986) and Hansen and Yuen (1988) showed that mantle flow currents could dynamically shape an intrinsically dense layer into a pile at the base of upwelling regions, leading to a thermally and compositionally heterogeneous lowermost mantle. Dense material could be 'leaked' (i.e., entrained) into the upwelling flow depending on the density contrast between the dense and less-dense components (lower density contrast leads to more entrainment).

A possible source for compositional heterogeneity in the mantle is the subduction and eventual segregation (removal from lithosphere) and accumulation of basaltic oceanic crust in the lowermost mantle (e.g., Coltice and Ricard, 1999; Hofmann and White, 1982). The density of basaltic material varies with pressure (e.g., Ringwood and Irifune, 1988), becoming more dense than the surrounding mantle at lower-mantle depths (e.g., Hirose et al., 1999, 2005). Gurnis (1986) was one of the first to explore this hypothesis by performing geodynamical calculations that included a thin layer of tracers at the top of the model to represent basaltic crust. Kinematic velocity boundary conditions were applied to the surface to ensure subduction of this layer into the mantle. Due to computational limitations at the time, these calculations did not have the mesh resolution to resolve the detailed, small-scale dynamics associated with entrainment and the potential segregation of oceanic crust from its lithosphere, so he examined density contrasts representing end-member cases of either full segregation of the crust from the lithosphere (leading to a maximum density contrast) or no separation (leading to a much lower density contrast because crustal density is partially compensated by lower density of subcrustal lithosphere). He found that if the crust does not segregate, it is unlikely to accumulate. If it does segregate, it may accumulate along the bottom of the mantle for fully internally heated cases and beneath upwelling regions for bottom-heated cases. In all cases, the accumulation of the crust is transient and does not fully survive over geologic timescales.

Olson and Kincaid (1991) performed laboratory tank experiments in 3-D Cartesian geometry. One of their experiments consisted of allowing a stratified slab (including dense 'crustal' layer and lighter subcrustal 'lithosphere' layer) to sink within the background mantle. After descending to the bottom of the tank, the slab buckled and formed a pile that underwent segregation by the lighter lithospheric component forming upwelling instabilities, leaving the dense crustal component behind. The dense crustal material spread out along the bottom of the tank in a spoke-like pattern of ridges, presumably outlining the upwelling currents of the larger-scale flow. Afterward, the ridges of dense material became slowly entrained into upwelling thermal plumes.

Whereas the earlier work of Gurnis (1986) employed an isoviscous rheology, Christensen and Hofmann (1994) performed a similar numerical experiment with temperature-dependent rheology and a layered lithosphere (including basaltic crust over a lighter harzburgite layer). They found that about one-sixth of the basalt that subducted could accumulate in piles in the lowermost mantle; however, this varied with density contrast between the basalt and background mantle, temperature dependence of viscosity, and Rayleigh number. The amount of accumulation increased with increased temperature dependence of viscosity and decreased with increasing Rayleigh number (their crustal thickness was tuned to be one-tenth of the upper thermal boundary layer thickness, which decreases with increasing Rayleigh number). Furthermore, they found that the separation of crust from the lithosphere occurs in the lowermost thermal boundary layer (as shown in the Olson and Kincaid (1991) work).

Kellogg and King (1993) examined the formation of a dense mantle layer resulting from percolation of iron and/or

core–mantle reaction products from the core (treated as an effective chemical diffusion). For chemical diffusivities and other material parameters employed in their study, they found that if the dense component is 3–6% more dense than the background mantle, a high-density layer may survive entrainment into the surrounding mantle and persist for long times.

Tackley (1998) is arguably the first comprehensive numerical study investigating thermochemical convection as the cause of the LLSVPs. His model setup involved inserting a more-dense compositional component into an isochemical system that had reached steady-state conditions. He examined Boussinesq and compressible formulations, 2-D and 3-D Cartesian geometries, depth-dependent thermodynamic parameters, depth- and temperature-dependent viscosity, and internal and basal heating. His study focused on using density contrasts that resulted in long-lived, stable thermochemical structures. These structures would later be regarded as thermochemical piles by the community. He found that the more-dense material was swept away from downwellings and accumulated beneath upwelling regions, forming a spoke-like network of ridges. A small amount of entrainment would occur at the base of mantle plumes located at the intersection of these ridges. The piles would always be hotter than the background mantle, even in cases with only internal heating. This is because heat transport from piles to background mantle is limited to conduction. For a range of density contrasts, the more-dense material could form long-lived, isolated structures with a high degree of topography. The range of density contrasts that led to this behavior was dependent upon material parameters and whether compressibility was implemented. Furthermore, the density contrast required for long-term stability decreased with internal heating and temperature-dependent viscosity.

Davaille (1999) performed laboratory tank experiments to explore thermochemical convection, motivated by the observations of elevated surface topography of the African and South Pacific regions (typically referred to as superswells; e.g., McNutt, 1998), the presence of numerous hot spots in these regions (e.g., Duncan and Richards, 1991), and the presence of LLSVPs in the lowermost mantle beneath them. She varied the thickness, density, and viscosity ratios between two compositional materials, initially stratified and isothermal. Results could be categorized into two dynamical regions: doming and stratified, the division of which was primarily caused by density contrast. The doming regime occurred for cases in which the lower layer was less than 1% more dense than the upper layer and consisted of large compositional plumes or domes that would rise and sink in an oscillatory fashion. This oscillatory motion is caused by the alternation of the dominant buoyancy mechanism (i.e., positive thermal buoyancy versus negative compositional buoyancy). The number of oscillations that the domes could experience before becoming completely stirred with the other material depended strongly on the thickness and viscosity ratios. Thermal plumes formed on the top of domes, entraining some of the dome material into them. For experiments in which the lower layer had a density much greater than 1%, the layers remained stratified with a small amount of entrainment occurring between them. These experiments gave rise to the idea that the LLSVPs could be explained by thermochemical domes, which actively rise and sink within the mantle and are a source for thermal plumes that form atop them and slowly entrain them (e.g., Courtillot et al., 2003). The oscillatory domes exhibited by these experiments are commonly referred to as thermochemical superplumes.

Kellogg et al. (1999) performed a 2-D Cartesian numerical thermochemical convection calculation that contained a thick, higher-density basal layer in the lower mantle. The upper layer contained a single convection cell consisting of a thickened downwelling along one boundary. The basal layer was 4% intrinsically more dense than the upper layer; however, because it heated up to high temperature, the effective density increase was less than 1% due to thermal expansion. The layer exhibited a large degree of topography variation, being suppressed beneath the downwelling and elevated beneath the opposing, upwelling region. They demonstrated that increasing the ratio of perovskite to magnesiowüstite (through Si content) could cause the layer to become more transparent to seismic waves. This work demonstrated that an intrinsically dense layer can exist in the mantle and, at the same time, explain tomographic images of some slabs reaching the lowermost mantle.

These pioneering studies on thermochemical convection, combined with increased seismic observations of the lowermost mantle, have collectively motivated our subsequent conceptual models of the mantle. Most current hypotheses suggest that the LLSVPs are caused by the accumulations of compositional heterogeneity, and current questions center upon their dynamical behavior and how they influence large-scale mantle convection, and thermal and chemical transport. Current conceptual models can be very loosely categorized into the sections in the succeeding text.

7.11.4.2.4.2 Passive thermochemical piles of primordial origin

Conceptually, the simplest thermochemical scenario to study involves starting with a stratified system of two layers, an intrinsically more-dense one underlying one that is less dense. The fundamental scientific assumption associated with this type of model is that at some time in the past (presumably early in Earth's history), an initial stratification developed. This could be due to an early differentiation event or process (e.g., Labrosse et al., 2007; Lee et al., 2010; Nomura et al., 2011) or an early accumulation of subducted crust (e.g., Tolstikhin and Hofmann, 2005; Tolstikhin et al., 2006). More generally, multiple processes may have occurred early in the Earth's history to form a 'basal melange' (Tackley, 2012). In this sense, we can consider this type of model as 'primordial,' with the emphasis that a stratified system formed early enough to justify being used as an initial compositional condition in thermochemical modeling. In addition, if the bottom layer material remains effectively more-dense than the other layer over geologic time, it will remain stable (not undergo wholesale overturn) in the lowermost mantle. This condition requires that the negative buoyancy associated with intrinsic density remains greater than the positive buoyancy associated with thermal expansion. Furthermore, if this material remains in contact with the CMB, it will become and remain significantly hotter than the upper layer material, and if rheology is controlled by temperature dependence, it will be weaker than the upper layer material. This weakness can cause the material to be passively shaped and pushed around by larger-scale mantle convection.

This section deals with work that maintains the following assumptions and properties:

1. At some time in early Earth's history, a less-dense layer was underlain by a more-dense layer.
2. Resultant thermochemical structures formed from the originally more-dense layer remain more-dense than the surrounding mantle through geologic time.
3. Rheology is dominated by temperature dependence, such that the hot, more-dense thermochemical structures are weaker than the surrounding mantle and can be passively shaped by larger-scale mantle convection.

Tackley (2002) performed a numerical convection study to investigate three different thermochemical configurations in 3-D Cartesian geometry. One configuration was simply isochemical convection, with no compositional heterogeneity included. The other two involved different volumes of more-dense material, starting in a layered configuration. Cases starting with a more-dense layer equivalent to 30% mantle thickness led to a continuous lower basal layer, similar to that hypothesized by Kellogg et al. (1999), and cases with a more-dense layer equivalent to 10% mantle thickness led to discontinuous thermochemical piles, similar to those of Tackley (1998). For each of these, both constant temperature and zero heat flux bottom thermal boundary conditions were investigated. He compared each thermochemical configuration to the character of seismic heterogeneity as a function of depth. He found that the continuous basal layer configuration led to strong heterogeneity in the mid-lower mantle that is not observed by seismic tomography, whereas the discontinuous thermochemical piles and isochemical cases did a better job, although not conclusively, to describe seismic heterogeneity in the lowermost mantle.

The thermochemical piles in Tackley (2002) developed morphology with characteristics similar to that observed in the thermochemical laboratory experiments of Olson and Kincaid (1991) and would be consistently observed in later laboratory and numerical studies. The more-dense material accumulated into a ubiquitous network of intersecting ridges at the bottom of the mantle, consistent with (and likely governed by) the larger-scale flow occurring in the more-voluminous, less-dense material. The ridges were located at the base of upwelling regions within the less-dense material and were locally elevated where the ridges intersect. Thermal plumes (forming in the less-dense material) were rooted along the ridge tops, particularly at the elevated ridge intersections. More-dense material was entrained into these thermal plumes, providing a mechanism for material exchange across the different materials. Jellinek and Manga (2002, 2004) also found identical morphological features in their Cartesian thermochemical laboratory experiments that involved much thinner dense layers.

An early concern focused on whether the ubiquitous ridge-like network of thermochemical structures observed in the Cartesian thermochemical studies was consistent with the seismic tomography observations of two LLSVPs beneath Africa and the Pacific, each with a somewhat different shape; the African LLSVP is a relatively linear feature, whereas the Pacific one is more rounded. McNamara and Zhong (2004) performed numerical 3-D spherical thermochemical convection calculations to investigate how the morphology of thermochemical structures would be affected by spherical geometry. Each of their cases originated from an intrinsically more-dense layer underlying an intrinsically less-dense one. Various layer thicknesses and density contrasts were investigated for four rheological types: isoviscous, temperature-dependent, temperature- and depth-dependent, and temperature- and composition-dependent. Here, only cases with density contrasts large enough to generate long-lived, stable structures are described. The isoviscous cases resulted in a basal layer with a jagged interface topography that was symmetrical on each side of the interface (i.e., topography looked the same whether viewed from above or below the interface). However, in the temperature-dependent rheology cases, the more-dense material became much weaker than the less-dense material (due to the higher temperature of the more-dense material). It was, therefore, easily swept around and shaped by larger-scale convection currents within the less-dense material. Interestingly, the resultant thermochemical piles developed a morphology effectively identical to those in the Cartesian studies of Tackley (2002), Jellinek and Manga (2002), and Jellinek and Manga (2004). Like the Cartesian studies, the more-dense material accumulated into ridges along the base of the upwelling regions (within the less-dense material) and was swept away from downwellings (within the less-dense material) (**Figure 10(a)–10(c)**). This was an important conclusion because it meant that geometry alone did not play a governing role in the morphology of thermochemical piles. Furthermore, a temperature- and depth-dependent rheology was explored, which included a 30× viscosity increase from the upper to lower mantle and a linearly increasing viscosity with depth in the lower mantle. The main effect of the depth dependence was to increase the size of the thermochemical piles (**Figure 10(d)**). For all of the cases described here, the magnitude of the interface topography was inversely related to the density contrast between layers (larger for smaller density contrasts), and the lateral scale of topographic features was directly related to the size of larger-scale convection cells. The temperature- and composition-dependent rheology cases produced active, dome-like structures described in a later section here.

The numerical 3-D spherical thermochemical convection study of Oldham and Davies (2004) produced similar results, forming thermochemical piles shaped into a network of ridges. They investigated a wide range of initial more-dense layer thicknesses, intrinsic density contrasts between materials, and heating styles. They found that a 1% intrinsic density contrasts led to unstable piles (i.e., the effective density of the more-dense material is less than that of the less-dense material, due to thermal expansion counteracting the intrinsic density). They also found that bottom heating, as opposed to a zero heat flux bottom boundary, required higher intrinsic density contrasts to provide a stable configuration of piles. Intrinsic density contrasts of 4% led to stable configurations in all cases.

The Cartesian and spherical thermochemical studies described in the preceding text were performed in a fluid dynamical context that did not include the influence of plate tectonics. As a result, downwellings and upwellings were relatively evenly spaced, and convection cells had smaller aspect ratios than we think exist in the Earth. McNamara and Zhong

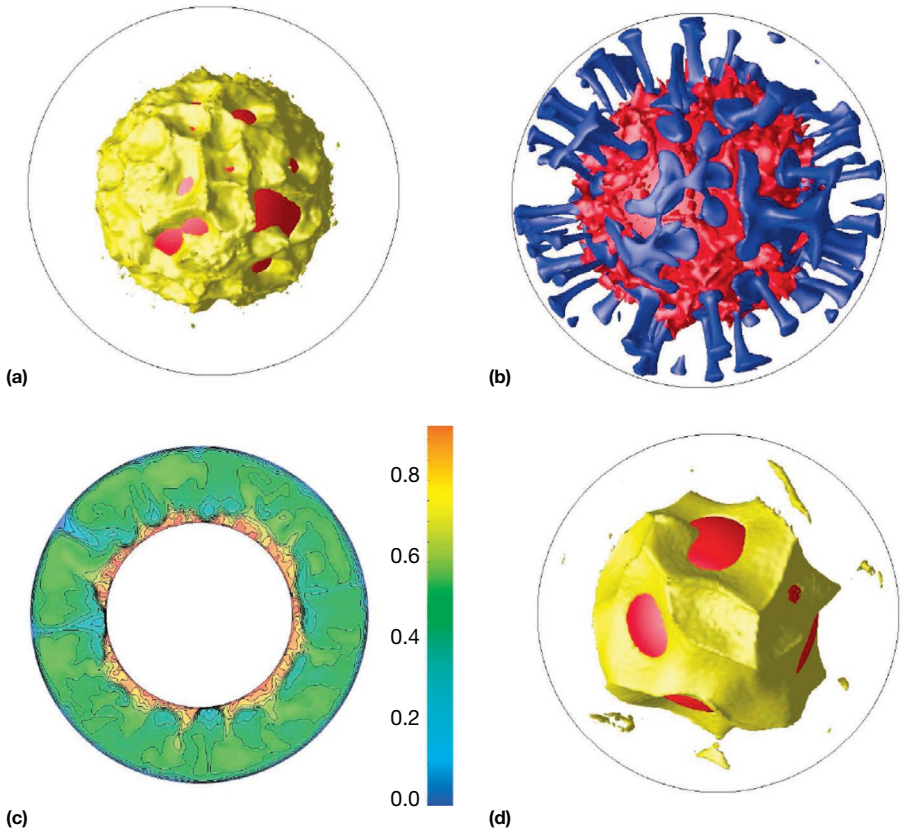

Figure 10 Thermochemical convection calculation in 3-D spherical geometry. The outer black circle represents the equatorial radius (with respect to polar viewpoint). The core is colored red. (a–c) From a calculation that does not have a depth-dependent viscosity. (d) From a calculation that includes a depth-dependent viscosity that includes a viscosity increase into the lower mantle. (a) More-dense material (yellow) accumulates into a ubiquitous network of ridges. (b) Residual temperature isosurfaces that show downwellings (blue) and hotter-than-average material near the CMB (red). (c) Cross section that illustrates the nondimensional temperature field. (d) More-dense material (yellow) for the calculation with depth-dependent viscosity included, in which case the ridges become much larger. Modified from McNamara AK and Zhong S (2004) Thermochemical structures within a spherical mantle: Superplumes or piles? *Journal of Geophysical Research B* 109: B07402, figures 3 and 7.

(2005) hypothesized that convection patterns guided by historical subduction would act to focus the ubiquitous network of ridgelike piles into shapes that better resembled the LLSVPs. They introduced plate history for the past 120 Ma as kinematic velocity boundary conditions to guide the location of subduction, following procedures similar to Bunge et al. (1998) and Lithgow-Bertelloni and Richards (1998). To minimize momentum violation, they had to carefully choose a Rayleigh number that naturally generated convection velocities that were consistent with plate velocities. They found that the more-dense material naturally formed ridgelike morphologies; however, these ridges were focused away from subducting slabs and into regions beneath Africa and the Pacific. Furthermore, the resultant African structure was linear with a NW–SE trend, and the resultant Pacific structure was a superposition of several ridges that combined to form a more rounded structure (Figure 11). Mantle plumes (in the less-dense material) were rooted to the tops of the piles, particularly in regions where ridges intersected. These first-order results that position piles beneath Africa and Pacific and produce a linear NW–SE trend to African structure appear robust; however, morphological details, including the position of plumes, depend highly on material properties used, as demonstrated by other studies (e.g., Bower et al., 2013; Garnero and McNamara, 2008; Zhang et al., 2010). In particular, the depth dependence of viscosity appears to play a large role in controlling the size of the ridges that focused into these regions.

Keeping in mind that the detailed morphology of individual thermochemical structures highly depends upon the material parameters used, Ritsema et al. (2007) and Bull et al. (2009) investigated how thermochemical models with plate history as kinematic velocity boundary conditions compare to actual seismic tomography. **Figure 12(a)** and **12(b)** shows thermochemical piles and the temperature field above the CMB from a calculation with parameters similar to those used in McNamara and Zhong (2005). Assuming a pyrolite composition, Bull et al. (2009) converted temperature and pressure to shear-wave velocity using the thermodynamic methods provided by Stixrude and Lithgow-Bertelloni (2005). Seismic tomography provides a blurred image of actual anomalies due to the heterogeneous distribution of earthquake and seismic station locations, so they applied the resolution operator of the tomography model S20RTS (Ritsema et al., 1999, 2004) to convert the geodynamically predicted shear-wave-velocity field to synthetic tomography (**Figure 12(c)**). **Figure 12(d)** compares the power spectrum of the prefiltered and postfiltered

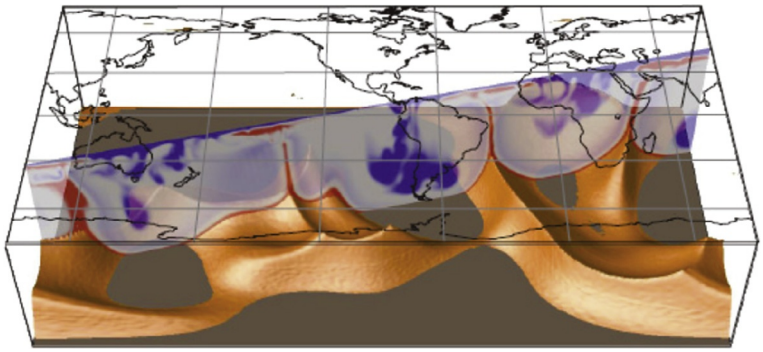

Figure 11 Thermochemical convection calculation in 3-D spherical geometry (unwrapped unto a Cartesian box) that employs 120 My of plate history as kinematic surface velocity boundary conditions. The CMB is colored gray-brown. Thermochemical piles (gold) accumulate into a superposition of ridges beneath Africa and the Pacific. A cross section of the temperature field spans a great-circle plane through the model, illustrating downwellings in subduction regions and thermal plumes that form along pile tops (cold is blue and hot is red). Figure is taken from Garnero and McNamara (2008) and is similar to that performed in McNamara and Zhong (2005).

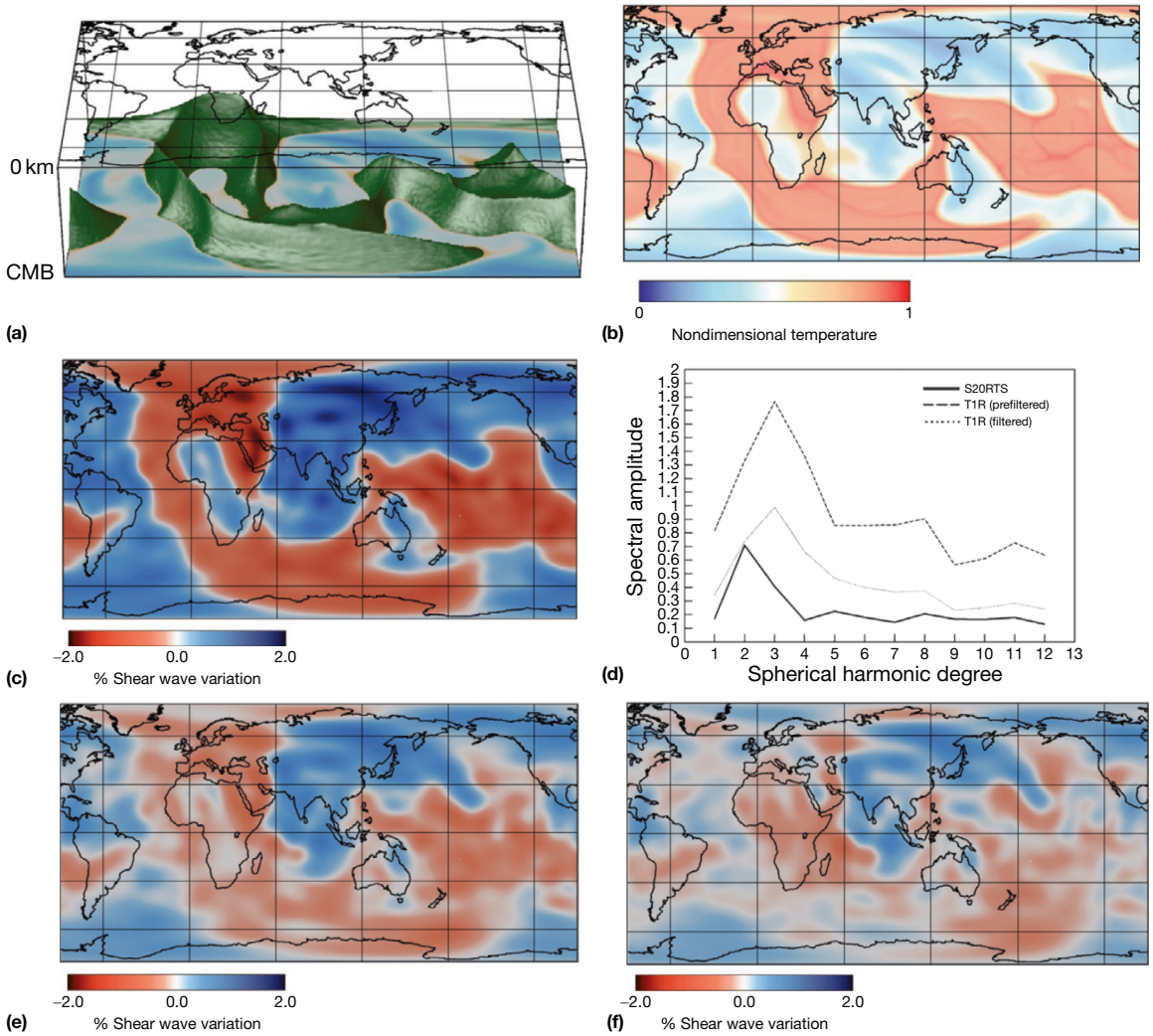

Figure 12 Synthetic tomography created from 3-D spherical geodynamical calculations of thermochemical piles resulting from using 120 My of plate history as kinematic surface velocity boundary conditions. (a) Thermochemical piles (green). (b) Temperature field above the CMB (at 2750 km depth). (c) Synthetic shear-wave tomography produced using the temperature field of the geodynamical calculation. (d) Amplitude spectrum of spherical harmonic decompositions of the tomography model (bold) (Ritsema et al., 1999, 2004), prefiltered temperature field (bold dashed), and synthetic tomography (light dashed). (e, f) Synthetic shear-wave tomography produced using the temperature field of geodynamical calculation and by assuming that thermochemical piles has a 3% and 4% intrinsic increase of shear-wave velocity over background mantle material, respectively. Reproduced from Bull AL, McNamara AK, and Ritsema J (2009) Synthetic tomography of plume clusters and thermochemical piles. *Earth and Planetary Science Letters* 278(3–4): 152–162, figures 2, 4, and 5.

geodynamically predicted shear-wave-velocity fields to that of S20RTS. The tomography model is characterized by large amplitude at degrees 2 and 3 followed by a relatively low-amplitude flat spectrum at higher degrees. The geodynamical model also predicted high amplitudes at degrees 2 and 3; however, unlike the tomography model, it exhibited greater amplitude in degree 3 than in degree 2, and the spectrum at higher degrees was not as flat. By extending plate motions back to 450 Ma, similar calculations of Zhang et al. (2010) were able to reproduce a maximum amplitude in degree 2, even without filtering. The main effects of the tomographic filtering were a reduction in the overall amplitudes and a softening of the variability in the higher-degree spectrum. If thermochemical piles are enriched in silicon, by containing a higher fraction of magnesium silicate perovskite, they could have an increased intrinsic shear-wave velocity (e.g., Kellogg et al., 1999). Bull et al. (2009) found that increasing the intrinsic shear-wave velocity caused the thermochemical piles to appear more diffuse in their predicted seismic tomography (**Figure 12(e)** and **12(f)**).

Deschamps and Tackley (2008, 2009) provided an exhaustive set of numerical thermochemical calculation results aimed at documenting pile morphology, stability, and longevity as a function of rheological properties (temperature dependence, compositional dependence, and depth dependence), viscosity increase from upper to lower mantles, intrinsic density contrast between materials, Rayleigh number, internal heating, Clapeyron slope of the 660 km phase transition, and original layer thicknesses. Furthermore, the spectrum of chemical and thermal heterogeneity as a function of depth is compared to probabilistic tomography models (e.g., Trampert et al., 2004) to assess applicability of each to the actual Earth. They found several key observations. Firstly, they found that the intrinsic density contrast between materials played the largest role, and density contrasts in the range of 90–150 kg m^{-3} led to the formation of thermochemical piles (lower contrasts were unstable and higher contrasts led to stratification). A large temperature dependence of viscosity (greater than 10 000× variation) allowed for the formation of long-lived thermochemical piles that also satisfied probabilistic tomography. The same could be achieved without temperature dependence of viscosity if the intrinsic (i.e., compositional) viscosity ratio between the materials was in the range of 0.1–10. The detailed morphology of piles could be significantly affected by compositional viscosity. The original thickness of the more-dense layer had a second-order influence, and the results were relatively insensitive to internal heating. Interestingly, they found that the negative Clapeyron slope associated with the 660 km phase transition played a significant role toward the stability of thermochemical piles, and they suggested that values in the range −3.0 to −1.5 MPa K^{-1} could lead to compositional heterogeneity that would be satisfied by probabilistic tomography. In Deschamps et al. (2011), they further investigated whether long-lived thermochemical pile models that satisfy probabilistic tomography can also satisfy geochemical observations. Citing that geochemical observations of OIBs provide an upper bound on the amount of primitive material included within OIB source material (to be about 10%), they measure the amount of pile material entrained into thermal plumes that form along pile tops. For the cases they investigate, the thermal plumes contain 2–9% pile material by entrainment, satisfying geochemical constraints. However, it should be noted that constraining the amount of entrainment is difficult in convection models due to the high resolution required.

Nakagawa and Tackley (2004a) investigated how thermochemical models affect cooling of the core. They used numerical mantle convection calculations to provide the thermal boundary conditions (temperature and heat flux) on a core heat balance formulation that included core cooling and inner-core solidification. They investigated three kinds of conceptual mantle models: isochemical, primordial thermochemical piles, and accumulation of subducted crustal material. Starting with an entirely liquid core, they performed calculations that spanned the age of the Earth. As constraints for a successful model, they used present-day values of inner-core radius and surface heat flow and the condition that the CMB heat flux must have been large enough to generate a magnetic field for the last 3 Gy. They found that isochemical models lead to a much larger inner core, indicating that they cooled too quickly. However, both types of thermochemical model acted to partially insulate the core and reduce cooling. They found that a 1.5–2% intrinsic density between materials best satisfied the constraints.

Zhang et al. (2010) performed thermochemical calculations that were a significant advancement over those of McNamara and Zhong (2005) because they employed much longer plate history (450 My) and produced structures that more closely resembled seismic tomography. Their calculations showed that if thermochemical structures are governed by plate motions, then the African structure is expected to be significantly younger than the Pacific structure. They showed that prior to Pangea assembly, the African region was characterized by downwelling, and intrinsically dense material accumulated within the Pacific region. Only after Pangea started to break apart did the African structure begin to form. CMB heat flux was explored in Zhang and Zhong (2011). Their models produce a distribution of seafloor age and surface heat flow consistent with present-day observations. They found CMB heat flux to be greatest in paleosubduction regions where downwellings came into contact with the core. In their thermochemical calculations, piles locally reduced CMB heat flux and acted to insulate the core. Also, they find minimums in equatorial CMB heat flux at times that correspond to the Kiaman and Cretaceous superchrons, hinting that reduced CMB heat flux may be related to geodynamo processes.

Lassak et al. (2007, 2010) attempted to use CMB topography as a constraint to test whether the LLSVPs can be caused by thermochemical piles. Earlier work on isochemical convection showed that downwellings press upon the core, causing downwarped topography, and upwelling plumes pull on the core, causing upwarped topography (e.g., Hager and Richards, 1989; King, 1997). It was unclear how thermochemical piles would affect CMB topography, and it was a common speculation in the community that 'dense piles' would cause down-warped topography because they are 'heavy'. In contrast, Lassak et al. (2007) hypothesized that thermochemical piles would instead cause upwarped CMB topography. They reasoned that in order for downwellings to sweep aside pile material, the downwellings must be more negatively buoyant than the pile material. Furthermore, in order for the pile material to develop large interface topography and accumulate into discontinuous piles

along the CMB, their intrinsic density increase must be significantly reduced by thermal expansion, leading to piles having a near-neutral (but slightly negative) buoyancy. Lassak et al. (2007) performed isochemical and thermochemical numerical convection calculations in a 2-D Cartesian geometry. Note that the magnitude of CMB topography is poorly constrained by modeling because it is directly dependent upon viscosity magnitude (which has large uncertainties), so the focus was to investigate the characteristic pattern of topography in map view, with respect to features such as downwellings, piles, and slabs. They found that CMB topography is strongly sensitive to the temperature dependence of viscosity. Like earlier isochemical studies, they found that isochemical convection leads to downwarped CMB topography beneath downwellings and upwarped CMB topography below upwelling plumes. For thermochemical cases, they found that constant (isoviscous) and weak temperature dependence of viscosity (<1000× viscosity variation) led to downwarped CMB topography beneath piles and upwarped CMB topography beneath downwellings. However, for more realistic, stronger temperature dependence of viscosity, CMB topography beneath downwellings was mostly downwarped, and CMB topography beneath thermochemical piles was mostly flat-shaped (laterally) and slightly positive. They also investigated relative buoyancy within and outside of piles and found that downwelling buoyancy is on par with thermochemical pile buoyancy. In Lassak et al. (2010), they expanded their earlier work to investigate 3-D spherical geometry and include self-gravitation (Zhong et al., 2008). They employed plate history as kinematic surface velocity boundary conditions that resulted in either plume clusters (for isochemical cases) or thermochemical piles (for thermochemical cases) beneath Africa and the Pacific (**Figure 13(a)** and **13(b)**). They demonstrated that the plume cluster hypothesis and the thermochemical pile hypothesis

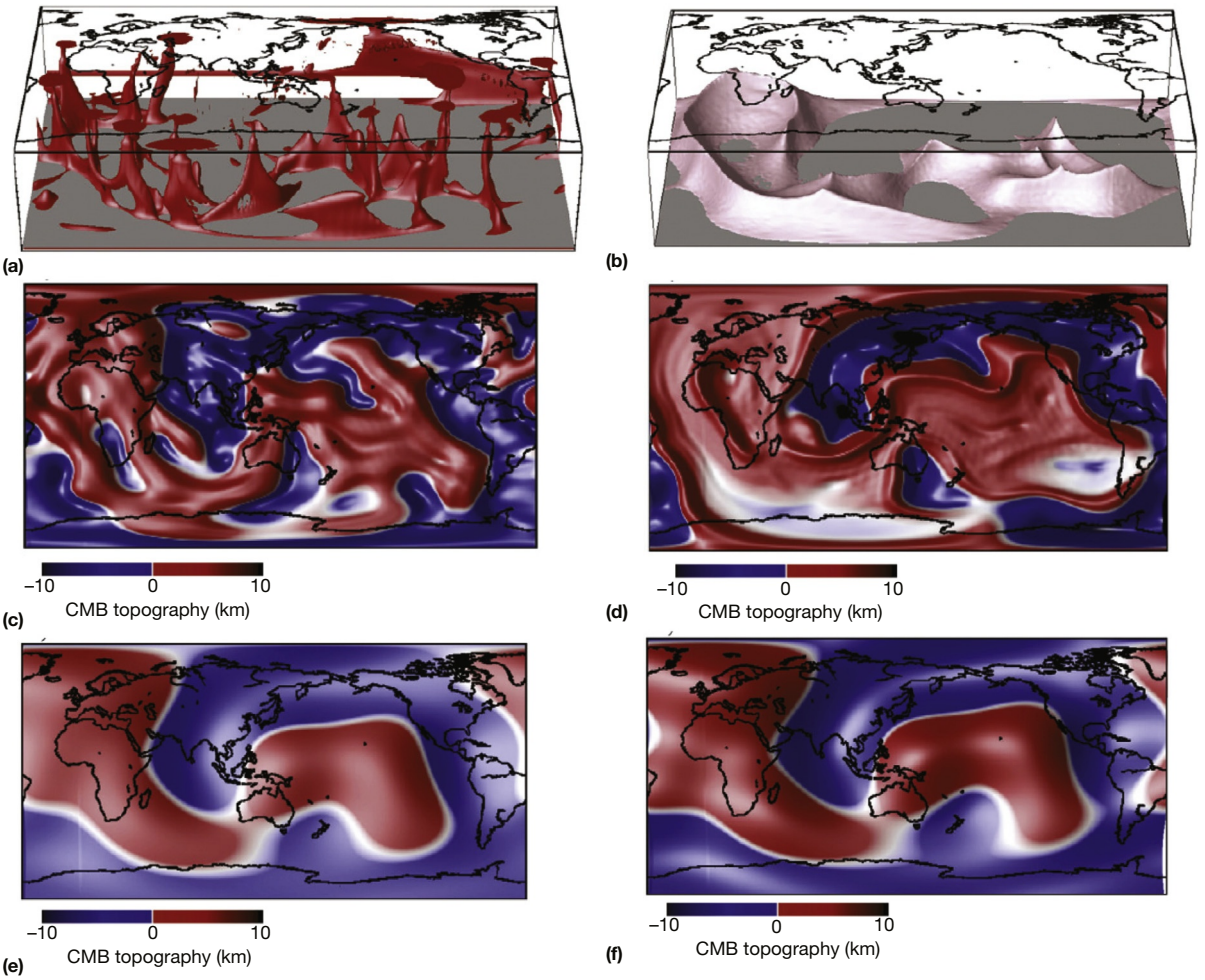

Figure 13 CMB topography predicted for isochemical and thermochemical 3-D spherical convection models. Plate history for the past 120 My was used as kinematic surface velocity boundary conditions. (a) Isosurfaces of higher-than-average temperature, outlining the position of plume clusters. (b) Compositional field illustrating the position of thermochemical piles (pink). (c) CMB topography generated from the isochemical model. (d) CMB topography generated from the thermochemical model. (e) CMB topography generated from the isochemical model, shown only up to degree-4 spherical harmonics. (f) CMB topography generated from thermochemical model, shown only up to degree-4 spherical harmonics. Blue represents downwarped CMB topography and red represents upwarped CMB topography in all cases. Reproduced from Lassak TM, McNamara AK, Garnero EJ, and Zhong SJ (2010) Core–mantle boundary topography as a possible constraint on lower mantle chemistry and dynamics. *Earth and Planetary Science Letters* 289(1–2): 232–241, figures 1, 2, and 5.

each resulted in characteristically different patterns of CMB topography (Figure 13(c) and 13(d)). In both isochemical and thermochemical cases, CMB topography was downwarped beneath downwellings. In the isochemical cases, CMB topography was generally upwarped in plume cluster regions, with a rough relief pattern corresponding to individual plumes (Figure 13(c)). In contrast, the thermochemical cases resulted in relatively flat and slightly upwarped CMB topography beneath piles. In addition, thin ridges of higher topography formed along the perimeters of the piles (Figure 13(d)). This work showed that if LLSVPs are caused by thermochemical piles, CMB topography should form plateau-shaped upwarped topography beneath them, surrounded by a thin rim of locally elevated relief. Seismic observations of CMB topography are not in great agreement between studies, have highly heterogeneous coverage, and are typically represented in low-degree spherical harmonic projections (e.g., Sze and van der Hilst, 2003). Lassak et al. (2010) decomposed and projected their CMB topography results into only low-order spherical harmonics, similar to seismic studies, and found that although plume clusters and thermochemical piles each produce a characteristic pattern of topography, they were virtually identical at long wavelength (Figure 13(e) and 13(f)). Future seismic studies should target the margins of LLSVPs to search for the narrow rim of elevated topography; confirmation of which would support the existence of thermochemical piles.

Yoshida (2008) performed a set of global, instantaneous flow calculations using tomographically derived density distributions to investigate CMB topography. He explored the addition of lateral viscosity variations, the presence of dense thermochemical piles in LLSVP regions, and a viscosity reduction in the lowermost mantle (i.e., representing a D'' layer). He found that each of these additions acted to reduce the amplitude of CMB topography, and one or more of them are required to satisfy seismological constraints of less than 2 km variation.

McNamara et al. (2010) explored whether ultralow-velocity zones (ULVZs) could be used to test whether thermochemical piles exist within LLSVP regions. Under the assumption that the ULVZ is caused by a small volume of high-density compositional heterogeneity, they performed high-resolution, three-component thermochemical calculations in 2-D Cartesian geometry that contained the (a) background mantle, (b) thermochemical piles, and (c) a thin, 5 km thick layer of high-density ULVZ material (Figure 14). They first performed two-component (thermochemical piles within a less-dense, background mantle) calculations until they reached a statistical thermal steady state. They then inserted a 5 km thick layer of ULVZ to investigate where the material would accumulate and what morphology it would develop. The layer of ULVZ material quickly formed multiple accumulations that migrated to the bottom side margins of thermochemical piles due to laterally convergent flow in these locations (e.g., Hernlund and Tackley, 2007). The height and width of accumulated ULVZ largely depend upon density contrast and original volume of material. For the cases studied, typical ULVZ height ranged from 30 to 45 km and ULVZ width ranged from 550 to 1150 km. The calculations were run for the equivalent of several billion years, and during that time, the larger thermochemical piles periodically underwent separations and mergers. If two piles merged, ULVZ material along their margins would be temporarily orphaned within the middle of the new, larger resultant pile before eventually migrating to the margins. Most importantly, it was found that ULVZ accumulations had an asymmetrical thickness, being thicker on the outboard side of the pile and thinner on the inboard side. This is due to differential viscous stress acting on the ULVZ accumulation. Piles are significantly hotter than the background mantle, and temperature-dependent viscosity leads to piles having a much lower viscosity than background mantle. As a result, the inboard pile side of the ULVZ accumulation has a lower viscous stress acting to prop it up than the outboard background mantle side. Future seismic studies should focus on ULVZ shape, and if they observe such an asymmetrical thickness to ULVZ, it would provide strength to the hypothesis that thermochemical piles exist and cause the LLSVPs.

7.11.4.2.4.3 Passive thermochemical piles caused by accumulation of oceanic crust

Another thermochemical hypothesis for the cause of LLSVPs is that they are caused by the accumulation of oceanic crust. Mineral physics experiments indicate that oceanic basaltic crust is expected to become more dense than background mantle at lower-mantle pressures (e.g., Hirose et al., 1999, 2005).

The idea behind this hypothesis is based on the following:

1. Oceanic lithosphere with basaltic crust descends into the lowermost mantle.
2. The oceanic basaltic crust becomes separated from the oceanic lithosphere.
3. The segregated basaltic crust travels to and accumulates at the base of mantle upwelling regions at a rate equal to or greater than the rate at which it is entrained away via mantle plumes.

Geodynamical modeling of this hypothesis is challenging for several reasons. Firstly, the oceanic crust is thin (6 km), which requires high grid resolutions to fully resolve it, particularly as it segregates from the lithosphere. Secondly, with a few exceptions that require special technical innovation (e.g., Crameri et al., 2012), geodynamical models do not self-consistently produce the one-sided, asymmetrical subduction such that occurs on the Earth (see Chapters 7.07 and 7.09, this volume). Instead, geodynamical models typically result in symmetrical, double-sided subduction that leads to a sandwiched layer of oceanic crust between two high-viscosity layers of the lithosphere. It is unclear how the high-viscosity lithosphere envelope surrounding the crust affects its ability to segregate at the base of the mantle. Furthermore, the rheology and strength of subducting slabs in the lower mantle are not well understood, and it is unclear how slabs deform in the lowermost mantle (e.g., buckling and pure shear deformation), and the manner of slab deformation will affect the ability, style, and amount of crustal segregation.

Xie and Tackley (2004a,b) performed 2-D thermochemical calculations that introduced basaltic crust and its complementary harzburgite residuum by melt-induced differentiation to investigate chemical evolution (e.g., U–Pb, Sm–Nd, and He systems). As material exceeded the melting temperature, crust and residue were generated by calculating the amount of melt and placing an equivalent amount of basalt at the surface of the

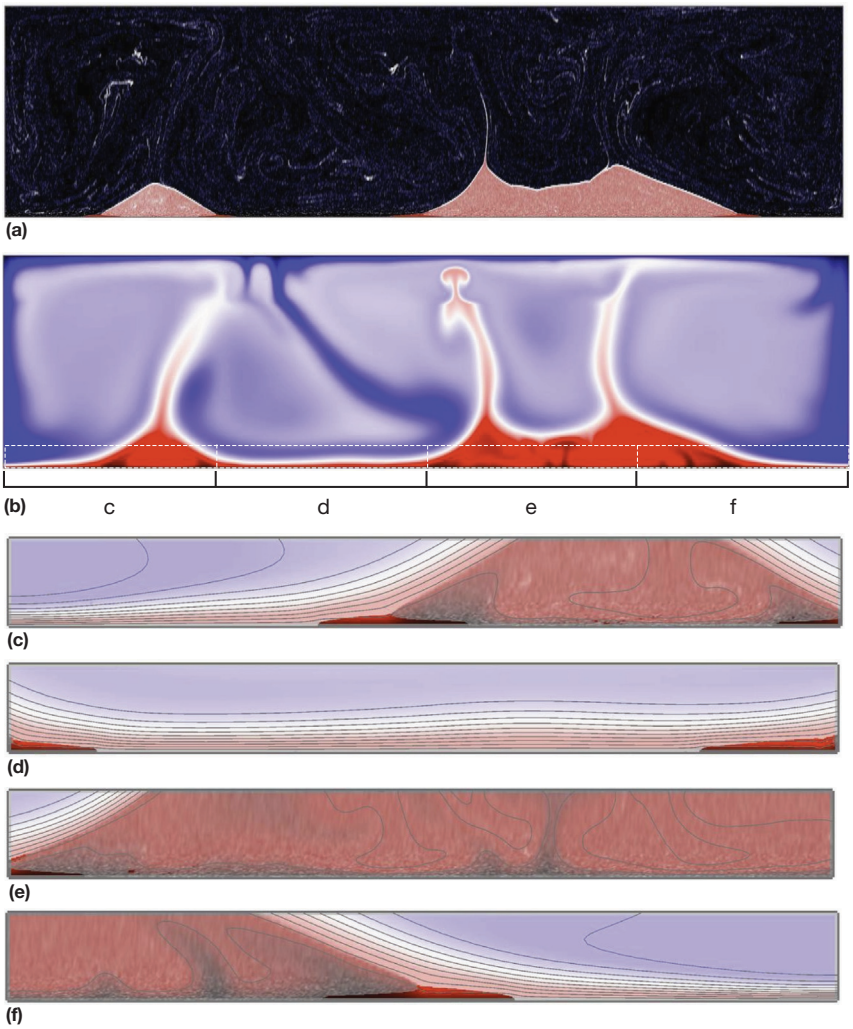

Figure 14 Three-component thermochemical calculation including background mantle, thermochemical piles, and a small volume of high-density ULVZ material. In addition to temperature-dependent viscosity, ULVZ material has an additional 10x intrinsic reduction in viscosity. (a) Compositional field showing background mantle (black), thermochemical piles (red), and ULVZ material (dark red). ULVZ material has accumulated along the CMB at pile margins. (b) Temperature field (red is hot and blue is cold). White boxes at the bottom illustrate the location of zoom panels. (c–f) Zoomed-in panels of the lowermost mantle, illustrating both temperature and compositional fields. ULVZ material accumulates along the margins of thermochemical piles and maintains an asymmetrical shape, being thinner on the side that is in contact with the piles. Reproduced from McNamara AK, Garnero EJ, and Rost S (2010) Tracking deep mantle reservoirs with ultra-low velocity zones. *Earth and Planetary Science Letters* 299 (1–2): 1–9, figure 6.

model. They applied a yield-stress approach to generate subducting slabs (e.g., Tackley, 2000b,c). Starting with a uniform mantle, they found that significant accumulations of more-dense crust could accumulate in the lowermost mantle over geologic time and provide a storage reservoir for heat-producing elements. Characteristic of calculations that involve accumulation of oceanic crust, piles appear quite 'messy,' compared with primordial piles examined in the earlier section, and significant amounts of chemical advection occur across the top interface of piles. This difference is most easily compared in Nakagawa and Tackley (2004b), which examined both primordial piles and accumulation of oceanic crust created by melt-induced differentiation.

Nakagawa and Tackley (2005) performed similar calculations that included the postperovskite phase transition in the lowermost mantle. They found that accumulations of oceanic crust became much hotter than background mantle, likely too hot for the postperovskite phase to occur. Instead, postperovskite mostly occurred at the base of downwelling regions, away from the hot piles. Furthermore, the presence of postperovskite tends to destabilize the accumulations of crustal material because it modifies the lateral density variation at the base of the mantle. Therefore, the presence of postperovskite in the lower mantle requires higher-density contrasts between the basaltic crust and background mantle to form stable, long-lived accumulations.

Nakagawa and Tackley (2006) produced the first 3-D thermochemical calculations involving melt-induced differentiation to generate oceanic crust, in a Cartesian geometry. An important conclusion of this work is that the resultant

accumulations of oceanic crust in their models developed a morphology similar to that in primordial piles, consisting of a network of ridges. Therefore, if seismology better defines the horizontal platform of compositional structures in the lowermost mantle, this cannot be used to discriminate between primordial piles and piles caused by the accumulation of oceanic crust. However, the accumulations of oceanic crust have 'messy' tops compared to primordial piles, so perhaps a careful mapping of LLSVP tops could help differentiate between these scenarios. Nakagawa et al. (2010) greatly expanded this work by employing a 3-D spherical geometry and using self-consistent thermodynamic formulation of mineralogy for a given compositional model (represented by various oxide ratios). They found that the amount of crustal segregation and accumulation was highly sensitive to the compositional model used, each of which provided a different basalt/harzburgite density contrast.

Nakagawa and Tackley (2011) provided an important dynamical observation regarding the role of postperovskite in the amount of crustal segregation. Motivated by mineral physics experiments that indicated that postperovskite may be weaker than perovskite (e.g., Ammann et al., 2010; Hunt et al., 2012), they introduced the postperovskite phase transition and prescribed that phase a lower intrinsic viscosity (1000× lower). As shown in their earlier work, the transition primarily occurred at the base of downwelling regions. This weakening allowed the crust to more easily segregate from the downwelling slab, producing a larger accumulation of crust in the lowermost mantle. The importance of postperovskite weakening was confirmed in the later study of Li and McNamara (2013). Weakening of the slab allows crust to more easily penetrate into the lowermost thermal boundary layer, where it can more easily survive against viscous stirring.

Brandenburg and van Keken (2007a,b) developed 2-D cylindrical models that employed a force-balanced method of plate generation at the surface. Their model provided a greater control of oceanic crust generation and thickness by prescribing a 10 km thick crust (and harzburgite below) within discrete zones located where plates diverge. They recognized an important modeling consideration when doing this kind of work. Model boundaries (or internal symmetry condition in their case) can artificially increase the amount of crustal accumulation, for reasons likely similar to those that allow weakened postperovskite to facilitate more accumulation. The crust that descends with a downwelling along a vertical model boundary is protected from viscous stirring because it is guided, undisturbed, along that boundary. When it arrives in the lowermost mantle, it is directly inserted into the lowermost thermal boundary layer and is therefore not easily stirred by viscous stresses. This was also observed in the preliminary work of Li and McNamara (2013), which was ultimately rectified by removing crustal tracers that entered a thin buffer zone along the vertical boundaries. Brandenburg and van Keken (2007a) found that large accumulations of oceanic crust could form at Earth-like, high Rayleigh numbers only if the intrinsic density between the crust and background mantle was larger than that inferred from mineral physics experiments. Brandenburg et al. (2008) provided a nice culmination of their work, in which they investigated the evolution of several isotopic systems and found that accumulations of crust in the lowermost mantle provide isotopic signatures comparable to the HIMU and EM-1 geochemical components observed in OIBs.

Davies (2008) demonstrated that depth-dependent density contrast between the subducted oceanic crust and background mantle may have led to mantle layering in the early mantle, when it was hotter. Mineral physics experiments indicate that while oceanic crust is expected to be more dense than the background mantle in the upper mantle and most of the lower mantle, it may become less-dense directly below the transition zone, between 660 and 750 km depth. His calculations demonstrated that in an earlier, hotter mantle, this density inversion could cause subducted basalt to be trapped, by what he dubbed a 'basalt barrier mechanism.' The resultant layered convection would lead to a strong temperature contrast between the upper and lower mantles, and layering would episodically break down and avalanching would occur. Eventually, as the mantle cooled, the subducting lithosphere became negatively buoyant enough to penetrate this barrier, and whole mantle convection was established. This transition occurred at about 1.6–1.8 By in his models. An important consideration of this work is that even if oceanic crust is too thin to accumulate in the lower mantle in a steady-state process that is occurring today (e.g., Li and McNamara, 2013), this type of mechanism could facilitate lower-mantle accumulation in the past by flushing large volumes of trapped upper-mantle basalt into the lower mantle.

Tackley (2011) performed 2-D and 3-D thermochemical calculations in which a slab segment (including both basalt and harzburgite) is placed into the mid-mantle and is allowed to descend to the CMB. Under the assumption that slabs thicken as they enter the lower mantle due to a viscosity increase, motivated by Gurnis and Hager (1988), he employed a crustal thickness of 30 km, with a 300 km thick harzburgite layer beneath. The slab segment was inserted at various angles, ranging from shallowly dipping to steeply dipping. He found that the density variation within the slab (dense basalt overlying less-dense harzburgite) caused a torque-induced rotation. For steeply and moderately dipping slabs, this rotation acted to flip the slap upside down such that basalt was on the bottom and harzburgite was on the top. Upon heating at the CMB, the basalt would segregate from the slab, and plumes of harzburgitic material would form plume heads that would entrain some of the basaltic material in the plume tails. For more shallowly dipping slab segments, the slabs landed at the CMB with the basalt side up. In these cases, plumes of harzburgite would escape through the edges of the slab segment and/or form plumes that burst through the basaltic layer.

Li and McNamara (2013) examined whether realistically thin (6 km) oceanic crust could accumulate into large, LLSVP-sized structures within upwelling regions of the lowermost mantle. They performed high-resolution 2-D Cartesian convection calculations, continually introducing a more-dense oceanic crust in the upper 6 km of the model, which was subducted into the lower mantle by downwellings. They explored several buoyancy numbers for the crust, leading to density contrasts ranging from 0% to 3%. Similar to previous studies (e.g., Nakagawa and Tackley, 2011), they found that weakened postperovskite significantly increases the amount of crustal segregation that can occur. In all cases studied, they found that viscous forces exceeded the negative buoyancy

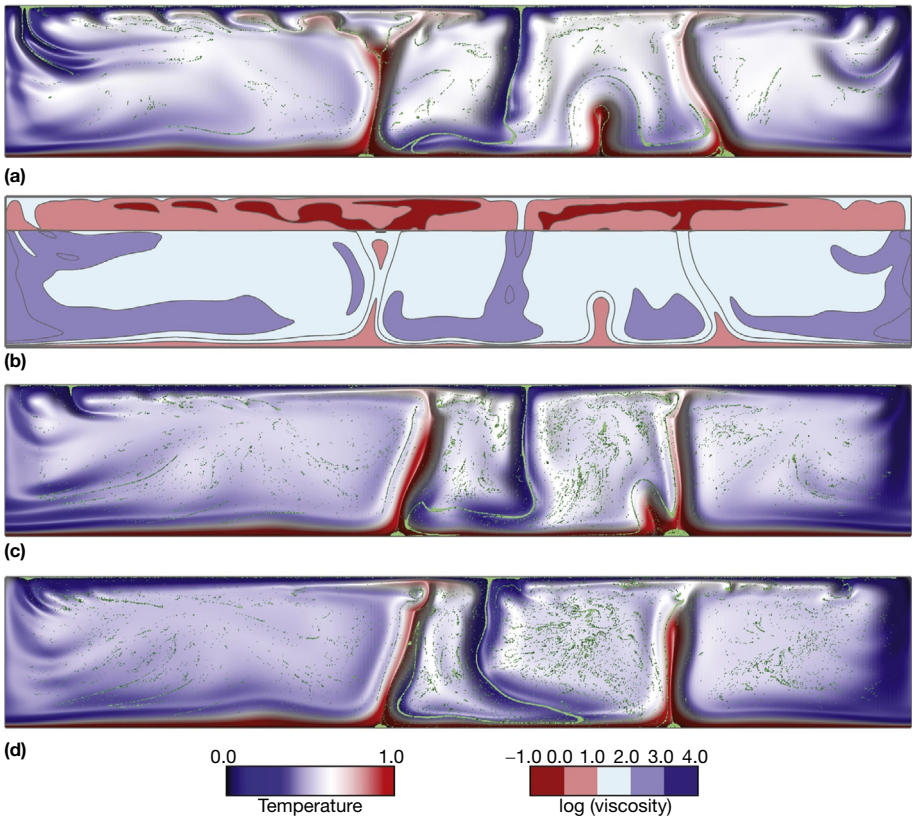

Figure 15 Thermochemical calculation that includes background mantle and a thin, 6 km thick more-dense oceanic crust generated at the surface. (a) Nondimensional temperature field with the oceanic crust (shown in green) superimposed, shown at 1.0 Gy from the start of the calculation. (b) Logarithm of the nondimensional viscosity, shown at 1.0 Gy from the start of the calculation. (c) Nondimensional temperature field with the oceanic crust (shown in green) superimposed, shown at 2.0 Gy from the start of the calculation. (d) Nondimensional temperature field with the oceanic crust (shown in green) superimposed, shown at 2.8 Gy from the start of the calculation. Modified from Li M and McNamara AK (2013) The difficulty for subducted oceanic crust to accumulate at the Earth's core–mantle boundary. *Journal of Geophysical Research*, *Solid Earth* 1–10, figure 1.

forces associated with the more-dense crust and the majority of oceanic crust was easily stirred into the background mantle. A small accumulation (<100 km thick) of crustal material did accumulate at the base of plumes, but the volume did not increase over geologic time due to entrainment into the plumes (**Figure 15**). In conclusion, they found that 6 km thick oceanic crust was too thin to accumulate into large structures on the same spatial scales as LLSVPs. Therefore, if LLSVPs are caused by an accumulation of oceanic crust, they must have formed by thicker accumulations of crust entering the lowermost mantle, which could occur if the oceanic crust was significantly thicker in earlier times and/or if the oceanic crust accumulated in the transition zone before being flushed into the lower mantle (e.g., Davies, 2008).

7.11.4.2.4.4 Combined models: Primordial piles and subducted oceanic crust

If LLSVPs are caused by the accumulation of intrinsically more-dense material, the most general scenario is that they were formed by several processes (e.g., Tackley, 2012), including early differentiation processes and events along with the accumulation of thickened, ancient oceanic crust. Furthermore, the oceanic crust is continually being introduced into the lower mantle through subduction. Therefore, a more appropriate thermochemical model of the Earth's mantle probably should include three components: (1) background mantle that provides the MORB source; (2) an ancient, more-primitive (loosely defined) accumulation of more-dense material; and (3) geologically young oceanic crust being introduced at downwellings (e.g., Tackley, 2000a).

Samuel and Farnetani (2003) and Farnetani and Samuel (2003) were perhaps the first to investigate such three-component thermochemical systems. In Samuel and Farnetani (2003), they performed 2-D Cartesian thermochemical models that included a more-dense basal layer, background mantle, and subducted oceanic lithosphere (that included both the more-dense crust and subcrustal lithosphere without an intrinsic density increase). Their basal layer had a volume equivalent to 25% of mantle volume, and although downwellings could locally depress it, this layer appeared to remain largely continuous throughout the lowermost mantle, as opposed to distinct, isolated piles. Mantle plumes formed along the top of this layer, entraining more-dense material into them. Compositional advection was performed by Lagrangian tracers that also stored the time evolution of U, Th, K, He-3, and He-4. By examining the He ratios in the uppermost mantle beneath divergent regions and within mantle plumes, they constructed histograms that demonstrated that such a

conceptual model predicts that MORBs maintain a narrow range of He-3/He-4 values while OIBs exhibit highly variable ratios, both of which are consistent with geochemical observations. Furthermore, they demonstrated that mantle plumes are expected to entrain multiple compositional components: the more-dense material (i.e., an undegassed, primitive reservoir), oceanic crust, and oceanic lithosphere (i.e., harzburgite).

Nakagawa and Tackley (2004b) employed 2-D cylindrical geometry models, and in their cases, the density of the oceanic crust is significantly higher than the primitive material, both of which are higher than the background mantle. They based the buoyancy number for the primitive material to coincide with estimated density differences from seismic tomography (Forte and Mitrovica, 2001), and they made the buoyancy number for the crustal material large enough to form piles of oceanic crust over geologic time. The primitive material was not dense enough to remain stable, and it formed blobs throughout the mantle, and the crustal material was swept into piles in the lowermost mantle. They found that their resultant compositional structures resembled the depth distribution of seismic heterogeneity (from seismic tomography) and provided a multireservoir model that could satisfy geochemical observations.

Tackley (2011) performed 2-D cylindrical and 3-D spherical calculations of basalt segregation in the presence of a preexisting dense layer residing in the lower 150 km of the mantle (continuation of the work described in the previous section). The initially uniform-thickness dense layer was swept away from the descending slab that included a 30 km thick more-dense oceanic crust. Interestingly, he found that the amount of the lowermost mantle crustal segregation increased as a result of including the preexisting dense layer (compared with identical cases without the preexisting dense layer). In these cases, a fraction of the basalt ended up residing as small subpiles within the preexisting layer. Furthermore, he found that 2-D versus 3-D geometry plays a strong role in the fraction of basalt that segregated from the slab. In 3-D geometry, 50–70% of the crust segregates from the slab in the presence of a preexisting dense layer, compared with only 25–45% in the absence of a preexisting layer. In 2-D, the amount of basalt segregation increases in the presence of a preexisting layer and decreases in its absence.

Li et al. (2014) investigated the evolution of such a three-component thermochemical system over geologic timescales in high-resolution 2-D Cartesian geometry. To generate an initial condition, they first performed a two-component thermochemical calculation that included more-dense material (representing a more-primitive reservoir, loosely defined) and background mantle (representing MORB source) until the system reached a statistically steady thermal state. They employed a buoyancy number ($B = 0.8$) that leads to the formation of distinct, thermochemical piles with thermal plumes rooted along their top cusps. From that initial condition, they performed a series of calculations in which the more-dense oceanic crust was continually introduced into the upper 6 km of the model, which would get transported to the lower mantle via downwellings. The model also included a weakening of postperovskite (which occurred at the base of downwellings), motivated by previous studies that demonstrated its strong role in crustal segregation (e.g., Li and McNamara, 2013; Nakagawa and Tackley, 2011). They varied (1) the density of oceanic crust (ranging from less-dense to more-dense than the more-primitive, thermochemical piles) and (2) the viscosity reduction associated with postperovskite regions. **Figure 16** is a snapshot of their reference case, in which the oceanic crust and more-primitive pile material have the same intrinsic density. In all cases they investigated, they found similar fundamental dynamics characterized by the subducted oceanic crust following one of several pathways in the lower mantle. Oceanic crust that did not reach the lowermost thermal boundary layer right above the CMB did not efficiently segregate from the downwelling slab, and as a result, it was largely stirred directly into the background mantle, forming a 'marble-cake'

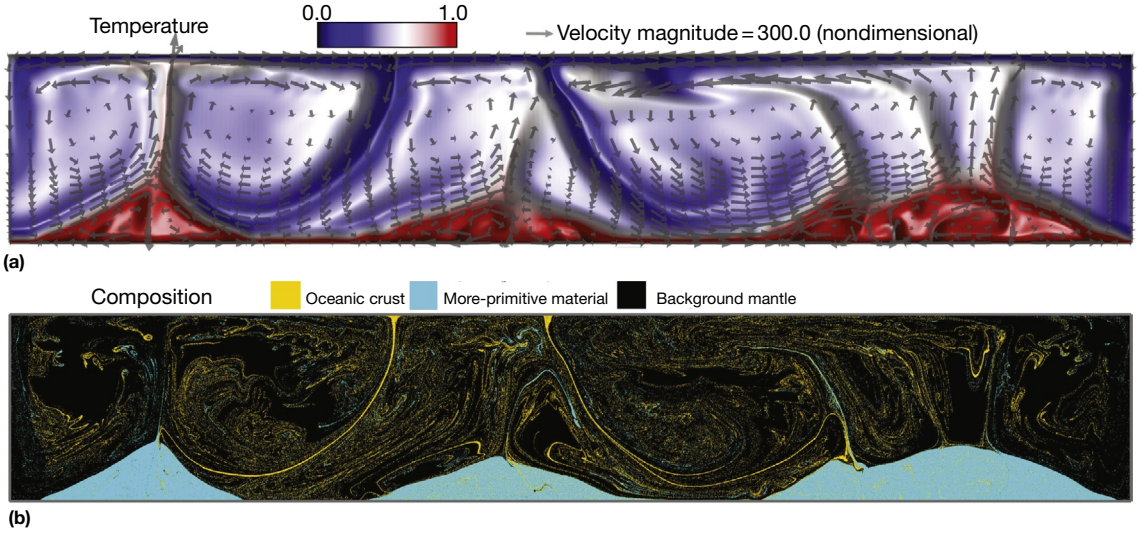

Figure 16 Three-component thermochemical calculation illustrating the interaction of subducted oceanic crust with primordial piles. (a) Nondimensional temperature field with the vectors representing nondimensional viscosity superimposed. (b) Compositional field showing background mantle (black), primordial piles (cyan), and oceanic crust (yellow). Modified from Li M, McNamara AK, and Garnero EJ (2014) Chemical complexity of hotspots caused by cycling oceanic crust through mantle reservoirs. *Nature Geoscience*, http://dx.doi.org/10.1038/ngeo2120.

compositional texture. Oceanic crust that did reach the lowermost thermal boundary layer was then transported laterally toward and up along the top boundaries of the thermochemical piles. Once the oceanic crust reached the top cusp of a thermochemical pile, where thermal plumes are rooted and entrain material from the pile, some fraction of it was entrained directly into the plume. The remainder accumulated at the top of the pile (at the base of the plume) until it was flushed into the pile. Once inside the piles, the oceanic crust was progressively stirred, becoming stretched and thinned with time. Some of this crust would ultimately be entrained, along with the more-primitive pile material, out of the pile and into thermal plumes. This characteristic behavior occurred over the lifetime of the calculations (representing several billion years of geologic time), and as a result, the composition of both thermochemical piles and the background mantle becomes more enriched in the oceanic crust. Assuming that primordial thermochemical piles cause the LLSVPs, this work resulted in the following conclusions:

1. The oceanic crust subducted into the lower mantle is either (a) directly stirred into the background mantle, (b) entrained directly into mantle plumes, or (c) flushed into thermochemical piles (and could be later entrained out into mantle plumes).
2. Mantle plumes are expected to include the following in variable amounts: (a) background mantle, (b) geologically young oceanic crust (which is entrained directly into mantle plumes), and entrained pile material that includes (c) more-primitive material and (d) ancient oceanic crust (that had been flushed into the piles at an earlier time). For the cases studied, mantle plumes contained about 2% more-primitive material and approximately 3% oceanic crust; however, it is important to note that these are likely upper bounds because it is difficult to constrain entrainment in numerical models, even those with high resolution.
3. The fraction of the oceanic crust that gets flushed into piles increases as (a) the density contrast between oceanic crust and more-primitive material increases and (b) the viscosity of postperovskite becomes smaller.

7.11.4.2.4.5 Active (or metastable) thermochemical superplumes

The previous sections highlighted thermochemical scenarios in which the accumulations of more-dense material behaved as long-lived and radially stable, passive structures that are easily swept away from downwellings into upwelling regions. The primary cause for this passive behavior seems to be a combination of their persistent negative buoyancy and weakening due to temperature dependence of viscosity. This section highlights thermochemical work on active structures, which have positive buoyancy and/or a rheology that leads to their having higher viscosity than the surrounding mantle. These types of structures have a rich variability in their morphology and behavior.

Davaille and colleagues had arguably performed the most extensive amount of geodynamical work on active thermochemical structures, performing laboratory tank experiments (e.g., Cadio et al., 2011; Davaille, 1999; Davaille et al., 2002, 2003, 2005; Le Bars and Davaille, 2002, 2004a,b). This collection of work well documents the behavior of both passive and active thermochemical structures as a function of dense layer thickness, viscosity, and intrinsic density. Much of this work is summarized in **Chapter 7.03** of this volume and will not be discussed in detail here. One of the more interesting aspects of that work is that it demonstrates the feasibility that LLSVPs could be caused by thermochemical structures that undergo alternating positive/negative buoyancy through time, resulting in cycles of rising and sinking superplumes. While being intrinsically more dense than the background mantle, as this material heats up at the CMB, thermal expansion causes it to have a net positive buoyancy, forming actively rising superplumes of material. As this material reaches the upper regions of the mantle, it cools and becomes more dense and sinks back down again with negative buoyancy. They demonstrate that this rising/sinking process can occur several times over geologic history before the structures are fully stirred into the mantle and that these structures may explain seismic tomography images (e.g., Davaille et al., 2005). The reader is referred to **Chapter 7.03** of this volume for a more comprehensive description.

McNamara and Zhong (2004) investigated thermochemical convection using both temperature-dependent and composition-dependent viscosities within a 3-D spherical geometry. They performed cases in which the more-dense material had a 100× or 500× intrinsic viscosity increase with respect to the surrounding, background mantle. Combined with temperature-dependent viscosity, this produced unique thermochemical structures consisting of weak interiors and strong 'rinds'. Because the more-dense material maintained a high temperature, the temperature dependence of viscosity had a stronger effect than the compositional dependence within the piles themselves. However, along the margins of the structures, which are cooler than the interior, the compositional dependence dominated, forming the stronger 'rind'. As a result, the more-dense material formed long-lived, rounded domes that maintained a relatively constant height and did not oscillate like the domes of Davaille (1999); however, they migrated laterally around the lower mantle. These domes contained single convection cells, with the upwelling portion located at the center of the dome.

Using seismic tomography to provide density structure, Forte and Mitrovica (2001) computed global flow models that employed radial viscosity profiles (without temperature dependence) constrained by gravity, plate motions, surface topography, and CMB ellipticity. Their results indicated that thermal buoyancy exceeded the negative compositional buoyancy of LLSVP regions and that these regions were actively rising through the mantle. Simmons et al. (2007) advanced this approach, and focusing on the African LLSVP, they concluded that it is best explained as a positively buoyant superplume rising from a negatively buoyant pile residing at the base of the mantle.

Ni et al. (2002) performed 2-D cylindrical thermochemical calculations to investigate the cause of the possible vertical, eastward tilt associated with the African LLSVP, as observed in seismic tomography. They found that conventional Boussinesq calculations failed to produce a tilted thermochemical structure with roughly parallel sides, in the presence of imposed surface plate velocity, unless it had a relatively low buoyancy

number resulting in the structure being unstable. This would imply that if the African LLSVP is caused by a thermochemical pile, it is fortuitously caught in act of overturn, transitioning into an unstable structure. While not impossible, this conclusion is not entirely satisfactory because it implies that we are currently observing a coincidental, transitory event in the African LLSVP. Tan and Gurnis (2005) (concurrently with Samuel and Bercovici, 2006) found a solution to this problem by performing compressible convection calculations in which the more-dense material had a higher bulk modulus than the background mantle, consistent with seismological observations. The higher bulk modulus in the pile material makes it less compressible than the surrounding, background mantle, resulting in a depth-dependent density contrast between the two materials that becomes smaller with depth. This allows for combinations of parameters that produce thermochemical structures that have a height of neutral buoyancy within them, below which pile material becomes less dense than the background mantle and above which pile material becomes more dense than background mantle. The resulting structures are effectively stable overall but have properties of unstable thermochemical structures, particularly in that they have high-standing vertical sides, consistent with seismic tomography observations of the African LLSVP. They refer to these structures as 'metastable superplumes.' Tan and Gurnis (2007) provided an extensive continuation and parameter exploration of this work. In Sun et al. (2007a), they found that such structures can explain various seismic properties of the African LLSVP such as the anticorrelation between bulk and shear-wave velocities and SKS travel times.

Tan et al. (2011) further explored metastable superplumes in 3-D spherical geometry, employing compressibility. As in their earlier 2-D work, the thermochemical structures formed steep-sided dome-like structures. They found that the structures resided away from subduction regions and could survive for billions of years. Furthermore, mantle plume preferentially formed along the margins of the metastable superplume structures, unlike conventional primordial thermochemical piles that typically have plumes rooted along their tops. This is a significant finding given that hot spot locations appear to be statistically situated more along the margins of the LLSVPs than their interiors (e.g., Burke and Torsvik, 2004; Thorne et al., 2004). They also found that metastable superplumes could remain relatively stationary (on a timescale of hundreds of millions of years) if they are located away from subduction; however, changing subduction patterns could cause them to quickly move laterally to maintain their distance from downwellings.

Bower et al. (2013) investigated metastable superplumes in 3-D spherical geometry that employed plate motions for the past 250 million years as kinematic surface velocity boundary conditions. Their plate velocities were distributed into 1 million year intervals, allowing a more continuous and natural development of downwelling structures. This is a significant advance over previous methods (e.g., McNamara and Zhong, 2005) that divided plate motion history into a small number of plate motion configuration stages, each of which lasting for long periods of geologic time and, as a result, generating discontinuous downwelling structures. Furthermore, Bower et al. (2013) recognized that they could generate metastable superplumes using the Boussinesq approximation (which, by definition, neglects compressibility). They achieved this by directly assigning the depth-dependent density contrast between the more-dense material and background mantle that would have self-consistently occurred due to the two materials having different bulk moduli in compressible convection. This is important in two regards. Firstly, it demonstrates that morphological properties of metastable superplumes are physically governed by the depth-dependent density contrast caused by compressibility rather than compressibility itself. Secondly, it demonstrates that such structures can be generated in Boussinesq convection codes. Their study found that plate motions guided the location of metastable superplumes into a ridgelike structure beneath Africa and a rounded structure beneath the Pacific, with plumes forming along the margins of these structures.

7.11.4.3 Long-Term Stability of LLSVPs

Thorne et al. (2004) noted the geographic correlation between the surface locations of the present-day hot spots and the margins of the LLSVPs (defined by the strong gradients in shear-wave tomography that surround the LLSVPs). For hot spots overlying LLSVP regions, they found that hot spots were more than twice as likely to overlie the margins. If one assumes that hot spots are caused by nearly vertical mantle plumes originating in the lowermost mantle, this correlation hints at a physical connection between LLSVP margins and hot spots. In addition to noting this for present-day hot spot locations, Burke and Torsvik (2004), Burke et al. (2008), Torsvik et al. (2008), and Torsvik et al. (2010) found a statistical correlation between the original eruption locations (based on paleomagnetic reconstruction) of LIPs and kimberlites with the margins of the present-day LLSVP locations. The LIP and kimberlite ages extend back to 500 Ma, and it is intriguing that these volcanic features may have originated from these specific locations throughout the Phanerozoic. Assuming a physical connection between these volcanic features and LLSVP margins (based on present-day hot spots), these correlations hint at the possibility that LLSVPs may have remained in the same locations throughout this time.

Conrad et al. (2013) used plate motions since 240 Ma to infer large-scale properties global mantle flow patterns throughout this time. They deconstructed present-day plate velocities into dipole and quadrupole components, which are related to degree-1 and degree-2 convergence and divergence. They found that the African and Pacific regions overlying the LLSVPs are characterized by quadrupole divergence. They perform a similar analysis on the driving forces associated with slab pull and basal tractions on plates, derived from a geodynamical model that uses seismic tomography to infer the density field. There is a general agreement between the dipole and quadrupole locations between the present-day plate motions and the driving forces generated from the geodynamical model, particularly for the quadrupole convergence beneath western Pacific and South America and divergences above the LLSVPs. This agreement provides evidence that plate motions and mantle flow are linked, at least for the present day. They continued this analysis for plate reconstructions extending over the past 240 million years. They found that the

quadrupole divergences remain over the Pacific and Africa throughout, and the quadrupole divergences tend to wander about the margins of the Paleo-Pacific. They used this result to conclude that upwelling has remained stable over the past 240 million years beneath Africa and the Pacific. Furthermore, they speculated that whatever is causing the LLSVPs may be 'stable anchors' that organize mantle convection and maintain upwelling above these regions.

Given our current understanding of thermochemical convection, it is difficult to imagine how thermochemical structures could form 'stable anchors.' From a fluid dynamical standpoint, thermochemical structures appear to be guided by changing subduction patterns, even for active structures. As described earlier, Zhang et al. (2010) carried out spherical thermochemical calculations using 450 My of plate history as surface kinematic boundary conditions. Their calculations showed that while plate motions predict a relatively stationary location for the Pacific structure over that time, it is difficult to reconcile an equally old age for the African structure. Instead, the African structure was created after the breakup of Pangea in their calculations.

7.11.4.4 Summary and Future Work

Over the past 15 years, increased seismic observations of the LLSVPs have motivated numerous geodynamical studies to understand their cause, many of which are briefly described in the preceding text. The first-order question pertains whether the LLSVPs are physical reservoirs of material that are compositionally distinct from the surrounding, background mantle. Although seismic observations increasingly hint at LLSVPs being compositionally distinct, it is unclear whether we can confidently exclude isochemical hypotheses for their cause, particular if such isochemical processes (e.g., plume clusters) may include passive compositional heterogeneity. For example, it is not inconceivable that LLSVPs may be caused by plume clusters that include a focusing of the oceanic crust and lithosphere that is being transported into them through the sides and dispersed through the top. If it is discovered that LLSVPs are indeed caused by distinct compositional reservoirs, then it is important to assess whether they are stable, long-lived structures that have resided at the base of the mantle for most of geologic time or whether they are active structures that rise and sink through the mantle. If they are stable, long-lived structures, it is then important to assess whether they are primordial structures with well-defined edges and tops or whether they are actively being created by the continual accumulation of oceanic crust. Furthermore, it is important to determine whether these structures are actively 'anchoring themselves' to the African and Pacific regions (as speculated due to hot spot and LIP correlations) or whether they are being guided by changing subduction patterns over geologic history.

7.11.5 Ultralow-Velocity Zones (ULVZs)

Ultralow-velocity zones are ~10 km thick regions at the CMB exhibiting seismic velocity decreases of order 10% or more, similar in scale and seismological contrast to the Earth's crust. Much like the crust is a key intermediary between the mantle and surface environment, it is reasonable to expect that ULVZs are also critically important as the frontier between the lowermost mantle and core. Since their discovery less than 2 decades ago (Garnero and Helmberger, 1996), studies of ULVZ have not advanced as far as other areas of deep-Earth science, and there are almost as many models as persons who have ventured to study these enigmatic features (e.g., Hernlund and Tackley, 2007). In the near future, it is hoped that integrated models of the thermal and chemical evolution of the CMB will lead to specific hypothesis tests that help to distinguish between potential origins for ULVZ. It is also important to incorporate ULVZ as a key outcome of processes operating at the CMB, and to explain their relationship to other major features in the deep interior.

7.11.5.1 Seismic Observations

The seismological detection and manifestation of ULVZ are well covered elsewhere (e.g., Lay, 2007); here, we give only a brief overview of the important features. *P*-waves are depressed by ~10% in ULVZ, and *S*-waves may slow by up to ~30%. The tops of ULVZ are relatively sharp, and modeling of the *ScP* phase interacting with ULVZ suggests a density increase of 5% (Reasoner and Revenaugh, 2000) and perhaps as much as 10% (Rost et al., 2005). Furthermore, ULVZ may exhibit internal gradients consistent with an increase in seismic-wave speed with depth (Rost et al., 2006).

ULVZs have been reported in many regions at the CMB, although it is not clear that they always exhibit the same characteristics (Thorne and Garnero, 2004). The Pacific is well oriented between seismic sources and stations for seismic phases turning in the CMB region and has received the most attention in seismological prospecting for ULVZ (Garnero and Helmberger, 1996). Recently, there have been reports of very large 'mega-ULVZ' in the Pacific region. In particular, the presence of an ~900 km wide ULVZ is reported beneath Hawaii (Cottaar and Romanowicz, 2012). An ~800 km wide ULVZ has also been detected inside a proposed gap (He and Wen, 2012) in the center of the mid-Pacific LLSVP (Thorne et al., 2013a). The Coral Sea region in the western Pacific hosts an ~700 km wide ULVZ, and the South China Sea region appears to contain several ~200 km wide ULVZs (Jensen et al., 2013). The northern and northeastern Pacific, on the other hand, does not appear to contain any detectable ULVZ (Rost et al., 2010). ULVZs have also been reported in a variety of other locations, such as Iceland (Helmberger et al., 1998), Africa (Ni and Helmberger, 2001), and the eastern Atlantic (Helmberger et al., 2000).

ULVZs have usually been described as isolated 'islands' of order several hundred kilometer width and 10–30 km thickness, rather than a global layer. Indeed, some portions of the CMB seem to lack any signature of complexity associated with ULVZ-like structures (e.g., Persh et al., 2001; Rost et al., 2010; Vidale and Benz, 1992). Thus, a ULVZ may truly be laterally discontinuous, rather than representing the thicker portions of an otherwise ubiquitous thin layer. However, earthquake sources large enough to be useful are not always impulsive enough to generate very high-frequency waves with ultrafine spatial resolution. Many seismic recordings lose resolving power at length scales under ~1 km at the CMB, such that

they cannot rule out the existence of a very thin (i.e., several 100 m) ULVZ-like layer spanning the entire CMB. Some seismic phases, such as *ScP*, can allow for finer-scale sampling and have been used to argue for the presence of <1 km layering of dense material on the underside of the CMB in some locations (e.g., core-rigidity zones or CRZ; Rost and Revenaugh, 2001), although it is not clear whether these are ubiquitous features of the CMB. Nuclear explosions are highly impulsive sources and also allow one to probe the CMB at fine scales. Ross et al. (2004) used Soviet nuclear test data to show that an ultrathin layer compatible with ULVZ-like properties exists beneath Siberia but is otherwise invisible to ordinary seismic waves. Although their coverage is limited, it is suggestive of an ultrathin layer that could be global in extent. The evidence therefore points to ULVZs as $\sim$10 km thick regions spanning several hundred kilometers in width, while other regions might host a very thin version of a ULVZ (<1 km).

7.11.5.2 Basic Dynamical Principles of a ULVZ Layer

If ULVZs primarily represent compositionally distinct material that is more dense than the overlying mantle, but less dense than the underlying core, then several conclusions may be drawn based on simple fluid mechanical principles. Firstly, in the absence of any external influences, a fluid layer of intermediate density sandwiched between layers of higher and lower density will tend toward a state that minimizes gravitational potential energy (GPE): a layer of uniform thickness. Therefore, lateral heterogeneity in the ULVZ structure at the CMB represents disturbances to this layer that can in principle provide information regarding the dynamical state of the CMB. The velocity of flow v_0 associated with viscous support of topography H_{ULVZ} on a thin compositionally distinct layer exhibiting a net density anomaly $\Delta\rho_{\mathrm{ULVZ}}$ is (e.g., Jellinek and Manga, 2004)

$$v_0 \approx \frac{\Delta\rho_{\mathrm{ULVZ}} g H_{\mathrm{ULVZ}}^2}{\eta_{\mathrm{ULVZ}}} \quad [1]$$

where g is gravitational acceleration and η_{ULVZ} is the dynamical viscosity of the ULVZ. Note that for a layer of distinct composition or phase constitution, η_{ULVZ} is probably different than the viscosity of the overlying mantle. Even if we allow for generous degrees of uncertainty in liquid iron viscosity at CMB conditions, the underlying core is essentially inviscid in comparison with the lower mantle; thus, the primary cause for lateral heterogeneity in ULVZ is expected to be deformation by viscous coupling to overlying mantle convection flows, which leads to thinning of the layer beneath downwelling mantle currents, and thickening of the layer beneath upwelling mantle currents (see **Figure 17**). Thus, the presence of ULVZ as an undulating dense layer at the CMB provides evidence for the presence of ongoing lower-mantle convection, and the distribution of thick and thin regions should reflect the pattern of mantle flow that prevails in the deep mantle (e.g., Sun et al., 2013).

Another important effect to consider is the relative topography generated on the upper and lower surfaces of a thin viscous intermediate layer such as the one described in **Figure 17**. Amplitudes on the upper surface will be greater if the density contrast is relatively small in comparison with the density contrast with the underlying layer. Because the shallow core has almost twice the density of the lower mantle, ULVZ-like structures of order 10% more dense than the overlying mantle should exhibit more dramatic topographic variations on the upper surface (by a factor of $\sim$8 for ULVZ density of 6 kg m^{-3}). Thus, topographic variations of order 10 km on the upper surface of ULVZ will be compensated by order 1 km topographic variations on the underside. In this way, ULVZ should protrude slightly into the core, by an amount that is already similar in magnitude to the longer wavelength amplitude of CMB topography produced by mantle convection processes (Olson et al., 1987). However, previous studies show that CMB topography produced by dense chemical layers is also sensitive to other factors, such as temperature and viscosity variations at a variety of length scales (Lassak et al., 2010).

7.11.5.3 Mechanisms and Hypotheses

Numerous models for ULVZ were proposed in the decade following their discovery and have already been reviewed (e.g., Hernlund and Tackley, 2007). Hypotheses linking ULVZ with mantle plume dynamics and geochemistry have also been reviewed (e.g., Jellinek and Manga, 2004). Here, we only consider the latest work on partial melting and composition anomalies, in addition to evolutionary scenarios that may lead to a combination of both mechanisms. As will be discussed in later sections, if a strong degree of secular cooling

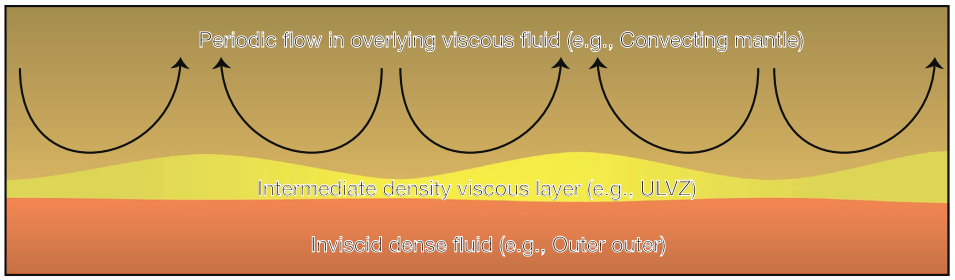

Figure 17 Deformation of a thin layer of intermediate density (i.e., ULVZ) by flows in an overlying viscous medium (i.e., mantle). The underlying inviscid dense fluid (i.e., outer core) does not exert any shear stresses on the layer. In the absence of mantle flow, the topography would relax and flatten into a layer of uniform thickness. The amplitude of topography on the upper and lower surfaces of the layer partly reflects the density contrast between the layers; in this case, the density contrast with the overlying viscous fluid is assumed smaller than the density contrast with the underlying inviscid fluid.

is required at the CMB in order to sustain core convection and the geodynamo to satisfy paleomagnetic evidence, then it is probable that the base of the mantle was extensively molten in the past. The context of cooling of the base of the mantle from an extensively molten state to one that is near the solidus forms the basis of the 'BMO' hypothesis (Labrosse et al., 2007), which we also discuss.

7.11.5.3.1 Partial melt

Partial melting is an oft-cited hypothesis for explaining the properties of ULVZ, particularly the large amplitude and 3:1 ratio of shear-wave and compressional-wave velocity change reported in some seismological studies (Berryman, 2000; Hier-Majumder, 2008; Williams and Garnero, 1996). However, partial melting is a complex phenomenon and is not necessarily straightforward to apply as a mechanism for explaining ULVZ. Relevant questions regarding physical and chemical properties include the melt–solid density contrast (e.g., positive or negative), melt–solid partitioning of major and minor elements, changes in ULVZ viscosity, solidus and liquidus temperatures of material with ULVZ composition, and chemical reaction with the core, among others. All of these have an impact on the plausibility of the partial melt hypothesis. Following is a brief summary of ideas regarding partially molten ULVZ.

It has long been suspected that melts could become more dense than coexisting solid phases in equilibrium at lowermost mantle pressures (e.g., Agee and Walker, 1988; Akins et al., 2004; Hemley and Kubicki, 1991; Ohtani and Maeda, 2001; Rigden et al., 1984; Stolper et al., 1981; Suzuki and Ohtani, 2003; Suzuki et al., 1995). Melt–solid density inversions are well established in a variety of compositions at high P–T (Liu and Bassett, 1986) and in other geologic and planetary contexts (e.g., Agee and Walker, 1988; Warren, 1985). Melt–solid density is affected by two key parameters: (1) the partitioning of major elements with different atomic mass and (2) the volume change of melting. Volume changes upon melting exert an important control on the pressure dependence of melting. In the case of congruent melting, in which the solid produces a melt of identical composition, volume changes alone control the melt–solid density difference. In this case, melting obeys the Clausius–Clapeyron relation:

$$\frac{dT_m}{dP} = \frac{\Delta V}{\Delta S} \quad [2]$$

where T_m is the melting temperature, ΔV is the volume change, and ΔS is the entropy change (upon melting). The dT_m/dP slope is always proportional to the volume change, regardless of melt–solid composition differences, although the magnitude of the slope may differ from the one predicted by eqn [2] in the case of incongruent melting. If the melt has a larger volume, then melting will occur upon isothermal decompression, but if it has smaller volume, then melting is induced by isothermal compression. Although the volume change upon melting is usually positive in the shallow Earth for most mantle silicates, it decreases with pressure owing to the greater compressibility of the melt phase relative to solid phases, yielding a distinct convex shape in most melting curves. Even if the volume change of melting is positive, it is still possible for the melt to become more dense than the coexisting solid phases if enough heavy species preferentially partition into the melt relative to other species in solids. An important example is the relative partitioning of FeO and MgO, which is described by the distribution coefficient,

$$K_D^{Fe-Mg} = \frac{X_{FeO}^{sol} X_{MgO}^{liq}}{X_{FeO}^{liq} X_{MgO}^{sol}} \quad [3]$$

where X_i^j is the mole fraction of component i in phase j. If $K_D^{Fe-Mg} < 1$, then FeO preferentially partitions into the melt phase relative to the solid, and a mole of melt will be heavier than a mole of solid. This effect is likely to be important for melting of the lowermost mantle, for which experiments performed using a variety of compositions find that $K_D^{Fe-Mg} < 1$ (e.g., Andrault et al., 2011; Fiquet et al., 2010), and some have even suggested $K_D^{Fe-Mg} < 0.1$ (Nomura et al., 2011). Relative melt–solid density changes for the reported range of K_D^{Fe-Mg} thus fall in the range ~1–6%. Note that if FeO prefers to enter the melt phase, then the melting temperature of a rock should decrease with addition of FeO.

Partial melting of ordinary mantle material as it circulates through the lowermost mantle thermal boundary layer has been explored in 2-D mantle convection models (Hernlund and Tackley, 2007). When the solidus is less than the CMB temperature, the pattern of convection is modified relative to melt-free thermal convection depending upon the melt–solid density change and the degree of melt percolation from partially molten regions. The largest and thickest partially molten features are correlated with hot upwelling plumes. For a large retained melt fraction, a density decrease upon melting enhances the thermal buoyancy of plumes and tends to produce tall and narrow melt structures along upwelling plume axes. This kind of melt distribution is not consistent with observations of ULVZ. On the other hand, for a density increase upon melting, the partially molten region tends to flatten into thin broad features that are more compatible with seismic inferences of ULVZ. While they showed that ULVZ structures could be produced by dense melting, Hernlund and Tackley, 2007 also found that density anomalies required to produce ULVZ-like structures should drive percolation of melt on timescales that are small in comparison with the residence time of material circulating through the partially molten region. However, the simple percolation model was not able to capture other relevant dynamical effects, such as viscous stirring of ULVZ which may strongly influence melt migration (Hernlund and Jellinek, 2010).

7.11.5.3.2 Composition anomaly

As discussed previously, a partial melt explanation is often favored owing to the relative changes in shear-wave and compressional-wave speeds. However, ULVZs may exhibit a significant density difference relative to the surrounding mantle. If the density change is ~10%, then it is difficult to explain ULVZ as a result of partial melting alone. In the case where the density anomaly is ~10% or more, ULVZs are likely associated with (Fe-enriched) bulk compositions distinct from the mantle. Also, if ULVZs are distinct 'islands' of material without any thinner version of ULVZ between the thicker portions observed seismically, then ULVZs are more likely to represent a composition anomaly. Wicks et al. (2010) proposed that the density and seismic velocities of ULVZ could be explained by the

presence of iron-rich $(Fe_x,Mg_{1-x})O$ magnesiowüstite (with $x \sim 0.9$), a composition predicted by fractional crystallization of a BMO (Nomura et al., 2011) as will be discussed in the next section.

The case of ULVZ as a thin compositionally distinct layer was considered in a 2-D thermochemical mantle convection model (McNamara et al., 2010), which also included larger-scale LLSVP as distinct thermochemical piles. These models showed a tendency for ULVZ to accumulate at the edges of LLSVP (e.g., Hernlund and Tackley, 2007); however, they also showed that LLSVP breakup and merging events could be accompanied by transient behavior that could affect their distribution in any given seismological 'snapshot' of the mantle at present times. For example, merging of two piles would give rise to a transient episode in which the center of the new larger pile is transiently populated by ULVZ inherited from the former edges of the smaller piles, although these would eventually be pushed to the margins of the larger pile as the new flow regime becomes established.

7.11.5.3.3 Partial melting of compositionally distinct material

The simplest way to explain all the properties of ULVZ, as well as some potential variations in their seismic properties from one location to another, is that they represent compositionally distinct material that is at or near the melting temperature relevant for their particular composition. Thus, potential differences in *S*-wave speed anomalies between ULVZs in different locations could be explained by variations in the retained melt fraction inside ULVZs (e.g., Nomura et al., 2011). Since *S*-wave speeds are sensitive to melt fraction, even small differences in partial melt fraction could produce significant heterogeneity in ULVZ populations.

One remaining issue regarding the retention of partial melt inside at least some ULVZs is that even small melt–solid density differences will tend to drive percolation of the fluid through the pore spaces it occupies in the rock matrix. Simple models of ULVZ partial melting that included even a very slight degree of percolation exhibited rapid separation of melt from the solid phase (Hernlund and Tackley, 2007), which is an essential problem for partially molten ULVZ. A neutral melt–solid density difference may prevail; however, it would need to be nearly exact and persist over geologic timescales regardless of secular changes (e.g., CMB cooling, as will be discussed in later sections).

The retention of dense partial melt by viscous stirring of compositionally distinct ULVZ was considered by Hernlund and Jellinek (2010). The model is motivated by the fact that the topography of compositionally distinct ULVZ islands must be supported by viscous stresses arising from flow in the overlying mantle (as discussed earlier), with a stirring velocity v_0 given by eqn [1]. Viscous stirring sets up a dynamical pressure gradient inside the ULVZ that tends to drive melt toward the top of ULVZ, even when the melt is dense and would otherwise drain downward by gravity-driven percolation. The dynamical pressure gradient can become large enough to compete with the driving force for gravity-driven percolation of melt; thus, it must also be considered in the percolation problem. The ratio of the gravity force $\Delta\rho g$ to the dynamical pressure gradient is given by Hernlund and Jellinek (2010)

$$R = \frac{\Delta\rho g H_{\mathrm{ULVZ}}^2}{\eta_{\mathrm{s,\,ULVZ}^{v_0}}} \approx \left(\frac{\Delta\rho}{\Delta\rho_{\mathrm{ULVZ}}}\right)\left(\frac{\eta_{\mathrm{ULVZ}}}{\eta_{\mathrm{s,\,ULVZ}}}\right) \qquad [4]$$

where η_{ULVZ} is the net viscosity of partially molten ULVZ, $\eta_{s,\mathrm{ULVZ}}$ is the viscosity of melt-free ULVZ solids, and eqn [1] has been employed in the approximate expression for R. The value of $\eta_{s,\mathrm{ULVZ}}$ may be very different than the viscosity of the overlying mantle in this scenario because the relevant compositions should be different. Hernlund and Jellinek argued that if $\Delta\rho$ is smaller than $\Delta\rho_{\mathrm{ULVZ}}$ (i.e., ~1% as compared with ~10%) and the viscosity of partially molten ULVZ is less than melt-free ULVZ solids (i.e., $\eta_{\mathrm{ULVZ}} \ll \eta_s$), then stirring-induced dynamical pressure gradients are probably at least 10–100 × stronger than the buoyancy force for gravity-driven percolation (i.e., $R < 0.1$). Their models suggest that for $R < 0.1$, a dense melt is readily driven upward in the ULVZ but that this mechanism also saturates owing to viscosity reduction with increasing melt fraction. A potential observable prediction of this model is that the melt fraction increases with height inside a viscously stirred ULVZ, such that seismic velocity should increase with depth as suggested by Rost et al. (2006). This phenomenon is similar to the focusing of melt migration toward a mid-ocean ridge axis owing to the deviatoric stresses induced by corner-flow (Spiegelman and McKenzie, 1987).

7.11.5.3.4 Basal magma ocean

The models discussed in the preceding text are relevant for the present dynamics and structure of ULVZ, but they do not directly address how ULVZ evolved in the context of the Earth's 4.5 Gy history. As will be discussed in a later section on core–mantle heat exchange, present evidence indicates that the CMB has cooled by more than ~1000 K since the Earth's formation, implying that the base of the early Earth's mantle was at temperatures well above the liquidus for any reasonable mantle composition (e.g., Gomi et al., 2013). Thus, the relevant long-term evolution problem at the CMB is not about melting ostensibly solid silicates to produce ULVZ, but rather involves gradual freezing of an extensively molten lowermost mantle from the early Earth to the present day. The proposal of such a BMO was primarily motivated by secular cooling of the CMB required to sustain a geodynamo since ~3.5 Ga (Labrosse et al., 2007).

Fractional freezing of an ancient BMO since 4.5 Ga provides a possible means for explaining many features of the lowermost mantle, including ULVZ and LLSVP, in addition to establishing a relationship between these features. In the simplest scenario, the BMO is born as a dense iron-rich gravitationally stable liquid layer underlying the solid mantle following the final stages of the Earth's accretion. Assuming that iron oxides depress the melting temperature of deep mantle rocks, fractional crystallization will evolve relatively iron-depleted rocks such that the residual BMO liquid is further enriched in iron. The net effect is that the density of the residual liquid increases and the melting temperature is further depressed. After some degree of Fe enrichment, the solids evolved from a BMO could become sufficiently dense relative to the average mantle that they could resist immediate entrainment into solid mantle flows, hence accumulating to form LLSVP. As fractional crystallization proceeds, the melt would also retain many volatile species whose enrichment would further depress the melting

temperature. With further cooling, the solid fraction of the residual BMO liquid increases to the point where it transitions to a mushy state, for which the solid grains form an interconnected skeleton and residual melt is trapped in the interstitial spaces. The resulting residual mushy mixture would be highly FeO-enriched, with a density anomaly of order ~10% relative to the overlying mantle, and could also remain partially molten as a consequence of fractionation. Thus, residual mush of a BMO may potentially explain all of the primary features of ULVZ.

There are still many questions to be resolved regarding the origin and evolution of a BMO, such as the mechanism of its formation in the early Earth. Several studies have considered the formation of a BMO following crystallization of a completely molten Earth (e.g., following a Moon-forming giant impact) from the mid-mantle, leading to contradictory results and interpretations (e.g., Andrault et al., 2012; Mosenfelder et al., 2009; Nomura et al., 2011; Stixrude et al., 2009; Thomas et al., 2012). While some of the differences between laser-heated DAC studies and shockwave experiments may be reconciled by adopting a revised model for shock heating (Wakabayashi et al., 2014), there is still disagreement on the precise value for equilibrium partitioning of iron between melt and solid (e.g., Andrault et al., 2012; Nomura et al., 2011).

7.11.5.4 Summary

The simplest present explanation for ULVZs is that they represent compositionally distinct material that is probably iron-enriched and this distinct material may or may not be partially molten. This carries important consequences for many processes operating at the CMB in the past and the present and will also play an important role in core–mantle chemical interactions, as will be discussed in a later section. A BMO is suggested by secular cooling constraints at the CMB, and if the required degree of cooling is as large as 1000 K (or greater), then there seems to be no way to avoid such a scenario. Our present challenge is to understand its formation and evolution, and to make predictions that can be further tested against observations. It is not clear that the BMO should have formed by crystallization of a completely molten Earth from mid-mantle depths, and alternative scenarios should also be considered.

7.11.6 Outermost Core Stratification

Much of the outer core exhibits properties that are broadly consistent with convection of a well-mixed isentropic liquid. Seismic models such as PREM (Dziewonski and Anderson, 1981) are able to fit a large volume of normal-mode and other data to an isentropic compression trend with little residual error. However, the data used in such models are not sensitive to departures from the average trend at the top and bottom of the outer core, and subsequent seismological work suggests some kind of anomalous layering at both boundaries. The nature of anomalous material in the outermost core is important because it influences exchange of both heat and matter across the CMB. Furthermore, such structural variations may reflect the consequence of mass transfer across the CMB over geologic timescales and are therefore an essential dynamical component of the CMB region.

7.11.6.1 Seismological Constraints on the Stratified Layer

Seismology is the most direct tool for documenting the presences or absence of outer-core stratification. The outermost core is most effectively sampled by *SmKS* waves (**Figure 2**) and mantle shear (*S*) waves with *SV* particle motion that convert to compressional (*P*) waves upon entering the core, bouncing $m-1$ times from the underside of the CMB and converting back to an *SV*-polarized *S*-wave upon exiting the core. All *SmKS* waves (SKS, *S2KS*, *S3KS*, *S4KS*, etc.) initiate at an epicentral distance corresponding with bottoming depths at the top of the outermost core. This is not the case for *PmKP* (including *PKP*) waves: the *P* velocity reduction going into the core results in *PmKP* waves that do not bottom shallower than the mid-outer core.

A number of seismic studies have used travel-time differences between successive *SmKS* waves to constrain the 1-D velocity gradient in the outer 50–400 km of the core (e.g., Eaton and Kendall, 2006; Garnero and Helmberger, 1995; Garnero et al., 1993a; Hales and Roberts, 1971; Lay and Young, 1990; Souriau and Poupinet, 1991; Tanaka, 2004, 2007; Tanaka and Hamaguchi, 1993). Past work is well summarized by Eaton and Kendall (2006). When compared to the PREM reference model (Dziewonski and Anderson, 1981), most studies provide evidence for velocity reductions between ~0.5% and 1% over the outermost 50–300 km. It is interesting to note that a velocity decrease is not consistent with a simple decrease in density at the top of the outer core without a larger than compensatory change in bulk modulus and appears to contradict Birch's law correlating density and seismic velocity (Birch, 1964). It is also noteworthy that a number of 1-D reference models suggest a distributed velocity reduction relative to PREM, for example, IASP91 of Kennett and Engdahl (1991), SP6 of Morelli and Dziewonski (1993), and AK135 of Kennett et al. (1995). The most recent seismological studies use *SmKS* at higher *m* than previous studies and suggest a velocity reduction distributed over 300 km thickness atop the outer core (e.g., Helffrich and Kaneshima, 2010).

Still, there are many potential errors and residual uncertainties in the seismic characterization of outermost core structure. Hales and Roberts (1971) measured their *SKKS*–*SKS* times without realizing that *SKKS* is 90° phase shifted from *SKS* (indeed, each underside CMB reflection produces an additional 90° phase shift). It was also found that the use of relative *SmKS* times is sensitive to heterogeneous structure at the bottom of the mantle, even if the ray paths are close together (Garnero and Helmberger, 1995; Garnero et al., 1993a; Tanaka, 2007). There is a historical pretext for skepticism about seismically inferred layering in the outer core since it was shown that the original F region of Bullen (1949) was in fact better explained by *D″* scattering (Doornbos and Husebye, 1972). And some of those who previously advocated for some kind of outermost core layering have now changed their opinion upon further examination (Alexandrakis and Eaton, 2010). Thus, it is useful to bear in mind that study of the outermost core layering is complex, and although many workers have

concluded that there is a low-velocity layer, others still disagree about the thickness and magnitude of the velocity contrast.

A sharp seismic reflection arising from liquid–liquid immiscibility such as that which occurs in the Fe–O–S ternary system at atmospheric pressures was sought using PmKP phases, but no compatible signature was found (Helffrich and Kaneshima, 2004). Thus, the variation in light elements in the outermost core probably does not cross a liquid–liquid miscibility gap. In principle, this kind of information can be used to constrain the potential compositions of an outermost core layer, provided that some ranges of composition produce immiscibility at the conditions of the CMB, while others do not. The existence of such immiscibility gaps at core pressures is still controversial, and further experimental work at CMB conditions is probably needed to better constrain thermodynamic models of metal–alloys atop the core.

7.11.6.2 Constraints from Geomagnetism

Geomagnetism also provides constraints on the density profile at the top of the core. In particular, secular variation of the geomagnetic field should be sensitive to the dynamical state of the outermost core. A number of research studies are motivated by the idea of inverting secular variations in the magnetic field for flow in the shallow core via the induction–diffusion equation (cf. Bloxham and Jackson, 1991):

$$\frac{\partial \vec{B}}{\partial t} = \vec{\nabla} \times \vec{v} \times \vec{B} + \frac{1}{\mu_0 \sigma} \nabla^2 \vec{B} \qquad [5]$$

where $\vec{B}$ is the magnetic field, $\vec{\nabla}$ is the gradient vector, $\vec{v}$ is the outer-core flow velocity, is its magnetic permeability, and σ is its electrical conductivity. A limitation of such models is that only the radial component of the magnetic field can be inferred, thus requiring additional simplifications to the flow regime in order to permit inversion for flow velocities. Incompressibility provides one reduction in the degrees of freedom, but one further assumption is also needed. Assumption of a purely toroidal flow, consistent with stratification, has long been thought to correspond to observed features of the secular variation such as stationary field saddle points (Whaler, 1980). Although it is possible to obtain such inversions for purely poloidal convective flow atop the core, opposite to the stratified layer assumption, the results are not easy to explain by physical mechanisms and suggest that the flow is probably toroidal in character (Beggan and Whaler, 2008).

The effects of stratification on dynamo generation and magnetic field characteristics have also been considered in the context of other planetary bodies. For example, models for Mercury's internal evolution yield thermal stratification of the outermost core; however, deep convection driven by the buoyancy evolved due to growth of a solid inner core can generate magnetic fields that are consistent with observations (Christensen, 2006; Wicht et al., 2007). Models for Saturn's interior that satisfy thermal evolution constraints imply the existence of a stably stratified layer that may contribute to the smaller dipole tilt of Saturn's field than is observed in other planets (Stevenson, 1980, 1982). Models that invoke a convecting region overlying a deeper stably stratified region have also been invoked to explain the unusual field morphologies of Uranus and Neptune (Stanley and Bloxham, 2004). Complete suppression of convection owing to stratification inside the cores of Mars, Venus, or other moons that no longer exhibit magnetic fields is also a possibility. Thus, stratification might be considered as a typical phenomenon within the broader context of general planetary evolution and reveals a large variety of potential behaviors. In such a context, the idea that the Earth's outer core may be partly stratified at the boundaries is not exotic or surprising.

Insights into the effects of the outermost core stratification might also be gained from numerical models of the geodynamo. Stanley and Mohammadia (2008) investigated fully 3-D numerical dynamos including a stably stratified outermost layer and homogeneous boundary conditions. They found a tendency for axial thermal winds to develop in cases including a stable layer, which drive a prograde (eastward) flow near the surface of the core in equatorial regions. This might present a problem because some features of the Earth's magnetic field exhibit a retrograde (westward) drift. Their result can be explained by the strong influence of rotation in the liquid outer core, which tends to align flow vorticity parallel to the axis of rotation. In the limit of vanishing viscosity, rotation causes the flow vorticity in the outer core to trend parallel to the rotation axis. While the Earth's core is not inviscid, viscosity is expected to be insignificant in comparison with rotation forces. In particular, the ratio of viscous to rotation forces is measured by the Ekman number ($E = \nu/2\Omega R_0^2$, where ν is the kinematic viscosity, Ω is the rotation rate, and R_0 is the core radius). For the Earth, E is estimated to be of order 10^{-15} or smaller. In this low-Ekman number regime, flows should exhibit a vorticity that is dominantly aligned with the axis of rotation, in which case the radial transfer of heat is greatly enhanced at the equator owing to the radial motions of the fluid at lower latitudes. At the poles, on the other hand, rotation suppresses radial motions and weakens radial advection of heat. This leads to significant differences in heat transfer through equatorial regions relative to the poles, which ultimately gives rise to a large-scale axial prograde thermal wind. The fact that such a wind is opposite in direction to Earth's westward drift, in spite of the evidence for the existence of a chemically stratified layer atop the Earth's core, presents a paradox and is the only finding that is contradictory to the existence of a stratified layer.

On the other hand, recent work on dynamo models with heterogeneous patterns of heat flux imposed at the top of the core suggests that the outermost core stratification may be necessary. These models use seismic tomography models at the bottom of the mantle in an attempt to impose geophysically consistent patterns of heat flux variations at the outer surface of the dynamo model. The resulting models of 'locked' dynamos, for which the velocity and magnetic field become stable, yield generated magnetic fields dominated by four concentrations of flux at high latitudes. These are similar to the present-day geomagnetic field, and their weak time variations also resemble features of the 400-year historical record (Gubbins et al., 2007). However, in order to obtain these kinds of locked solutions it is necessary to increase the influence of thermal conduction at the boundary. One way to produce this effect without artificially increasing the thermal conductivity is to allow for stratification to develop at the top

of the core by a combination of bottom heating and internal heat sinks, which suppresses the radial advection that would otherwise destabilize the high-latitude flux patches (Sreenivasan and Gubbins, 2008). Such dynamics suggest that the top of the Earth's core is only weakly convecting or is density stratified with no vertical motion.

The discrepancy between the aforementioned modeling interpretations might be reconciled in the future by using models that include both a stratified layer and heterogeneously imposed heat flux at the outer surface. It is likely that the influence of rotation on polar–equatorial differences in heat flux will compete with lateral heat flux variations imposed at the CMB by the pattern of deep mantle convection. Indeed, the existence of a westward drift in the Earth's field may offer a compelling constraint on the relative strength of heat flux differences arising from these two distinct mechanisms operating in the Earth's core.

Most dynamo models employ a codensity formulation for the composition and temperature fields (e.g., Braginsky and Roberts, 1995), but this simplifying assumption is not well suited for the physics of this situation, and double-diffusive models will likely be required to capture the relevant behaviors. The dynamics of core convection and the dynamo with a mixture of lateral heat flux variations and strong rotation have only begun to be explored in greater detail. Already dynamo models including a stratified layer atop the outer core are producing interesting results and suggesting new dynamical regimes (e.g., Nakagawa, 2011). Furthermore, generalization of the dynamo process to include fully double-diffusive dynamics involving both heat and composition driving forces while allowing for generalized behavior at the boundaries is still at a very young stage of development, and we look forward to seeing future developments in this field.

It has also been proposed that a stable layer could not be more than about ~100 km thick without being incompatible with the timescale for growth of features in the geomagnetic field that are thought to emerge via magnetic diffusion from the deeper core (Gubbins, 2007). This skin depth constraint may limit the thickness to even smaller thicknesses if the electrical conductivity is as high as indicated by recent mineral physics constraints (e.g., Pozzo et al., 2013). These models are only approximate, and improvements in integrating the spatial and temporal scale of flows atop the core are probably needed to establish a more firm constraint.

7.11.6.3 Stability of the Outermost Core Layers

Since core fluids are expected to exhibit a very small molecular viscosity, viscous entrainment is inefficient and the most effective potential mechanism for mixing a density stratified region at the boundary into the deeper core is by turbulent entrainment. The problem of turbulent entrainment of a layer exhibiting a gravitationally stable density gradient has received a lot of attention in the past owing to its importance in other dynamical settings, such as the shallow ocean. In the ocean problem, the surface is typically warmer than the deep waters, giving rise to a gravitationally stable thermal gradient called the 'thermocline.' Agitation by breaking waves and winds at the surface gives rise to turbulence that mixes the uppermost portions of this stable boundary layer, thus maintaining a dynamical balance that modulates the uppermost boundary layer of the world's oceans. The outermost core problem is more complex in several ways, particularly because Lorentz forces and double-diffusive dynamics also enter the picture. With these caveats in mind, the simpler turbulent entrainment problem may provide a rough guide for assessing the stability of outermost core layers; thus, we consider these arguments in lieu of treating the complete problem.

Entrainment and mixing of a gravitationally stable density gradient implies an increase in GPE that must be balanced. Conservation principles and experiments on turbulent entrainment of a stable layer indicate that the increase in GPE is compensated by a loss in kinetic energy density (KED) in the mixed layer (Turner, 1986), suggesting that the entrainment dynamics can be cast in terms of a nondimensional ratio between GPE and KED:

$$R_i = \frac{N^2}{(u')^2} = \frac{\partial \rho}{\partial z}\frac{g}{\rho (u')^2} \approx \frac{(d \log \rho) g L_M^2}{L_0 u_*^2}, \qquad [6]$$

where Ri is the 'Richardson number,' N is the buoyancy frequency, $\partial\rho/\partial z$ is the stabilizing density gradient, L_M is the thickness of a candidate mixed layer bounding the stratified region, L_0 is the total thickness of the stratified region, and u_* is the 'friction velocity' (typically assumed to be $\sim 10\times$ smaller than the ambient flow velocities in the convecting region).

Stability analysis for turbulent erosion of a density gradient shows that a portion of a density stratified layer adjacent to the convection region of thickness L_M will become mixed if $Ri < 1/4$ (Miles, 1961). For an ~1% density stratification distributed over 100 km atop the core, and a friction velocity of 10^{-5} m s^{-1}, one finds that only the lowermost L_m ~1 mm of the layer is subject to mixing by core flows according to this criteria. However, this length scale is so small that the relevant Reynolds number will also be quite small. For an ambient core flow of $u = 10^{-4}$ m s^{-1}, viscosity of $\mu = 10^{-3}$ Pa s, and density of $\rho = 10^4$ kg m^{-3}, the local Reynolds number ($Re = \rho u L_M/\mu$) is of order unity, which is 2–3 orders of magnitude smaller than values of Re that give rise to turbulent behavior. Unless core viscosity is as small as $\mu = 10^{-5}$ Pa s, then it appears that core flows may be incapable of generating the kind of turbulence at length scales small enough to allow for turbulent entrainment of a significant portion of the stable layer under the stated assumptions. These factors argue for long-term dynamical stability of such a layer against entrainment.

Another way of understanding the stability of the outermost core stratification is to consider that core flows are driven by lateral density perturbations of order 10^{-9} and may therefore be incapable of entraining and mixing material with a stabilizing density contrast which is seismically detectable and therefore significantly greater in magnitude (Stevenson, 1987). The limits of seismically detectable density perturbations are of order 10^{-3}; thus, any seismically detected stratified layer should exhibit six orders of magnitude stronger density contrast than the density perturbations that drive core flows. It is simply unreasonable to suppose that buoyancy forces driving convective flows could overcome opposing buoyancy forces more than a million times stronger in relative magnitude. Thus, any seismically visible stratified layer is likely stable against entrainment into the deeper core.

A more likely mechanism for downward encroachment of a stratified layer into the deeper core is via thermal diffusion of light alloys down the concentration gradient, which may advance the stratified frontier into the deeper core. For half-space diffusion, the frontier would advance downward in proportion to $\sqrt{4D\Delta t}$, where D is the atomic diffusivity and Δt is the elapsed time. For $D \approx 10^{-8}\ \mathrm{m^2\ s^{-1}}$ (Vočadlo et al., 2003), the layer would thus grow downward by ~100 km by half-space diffusion over the age of the Earth. This length scale is similar to what is observed by many seismological studies and suggests that the origin of the layer is caused by core–mantle reactions similar to those proposed by Buffett and Seagle (2010), although it may be too small to account for the much thicker layer inferred by Helffrich and Kaneshima (2010).

7.11.6.4 Composition of the Stratified Layer

One of the peculiar features of the stratified layer is a smaller seismic velocity than the average isentropic trend of the outer core. Clearly, the density must be smaller than the typical core material to provide for gravitational stability. Since the velocity varies as $\sqrt{K/\rho}$, where K is the bulk modulus, the stabilizing reduction in ρ must be more than compensated by a decrease in K in order to produce a negative velocity anomaly. A temperature anomaly is not expected to satisfy this condition, therefore the origin of the layer is likely to be explained by composition variations.

It is important to consider the kinds of general composition variations that could occur in such a layer. Consider the composition of the core fluid to be expressed as a vector as follows:

$$\vec{C} = [C_{\mathrm{Fe}}, C_{\mathrm{Ni}}, C_{\mathrm{O}}, C_{\mathrm{Si}}, C_{\mathrm{S}}, \ldots], \qquad [7]$$

where square brackets denote a vector string and C_{Fe}, C_{Ni}, C_{O}, C_{Si}, C_{s},... are the scalar concentrations of Fe, Ni, O, Si, S, ... The trace of $\vec{C}$ is unity, by definition. Now, we define the composition vector of the well-mixed isentropic convecting part of the core as $\vec{C}_0$ and decompose it into two parts:

$$\vec{C}_0 = \vec{C}_{M,0} + \vec{C}_{A,0}, \qquad [8]$$

where $\vec{C}_{M,0}$ represents the base metal solvent (Fe and Ni) and $\vec{C}_{A,0}$ represents the concentrations of alloying components. Similarly, we can express the concentration in the stratified layer as

$$\vec{C}_{\mathrm{S}} = \vec{C}_{\mathrm{M,S}} + \vec{C}_{\mathrm{A,S}}. \qquad [9]$$

With these definitions, we can be more explicit regarding the kinds of compositional variations that can occur in a stratified layer and how they are related to the origin of the layer itself.

One special case of an outermost core stratified layer is that of a proportional enrichment. A proportional enrichment occurs if the vector $\vec{C}_{\mathrm{A},0}$ is parallel to $\vec{C}_{\mathrm{A,S}}$ (i.e., $\vec{C}_{\mathrm{A},0} \| \vec{C}_{\mathrm{A,S}}$). Assuming that the alloys cause a density decrease in the metal, the gravitational stability condition implies that the magnitude of $\vec{C}_{\mathrm{A,S}}$ is greater than $\vec{C}_{\mathrm{A},0}$ Thus, we can write a proportional enrichment as $\vec{C}_{\mathrm{A,S}} = q\vec{C}_{\mathrm{A},0}$, where $q > 1$ is a scaling factor. A nonproportional enrichment occurs if $\vec{C}_{\mathrm{A},0}$ is *not* parallel to $\vec{C}_{\mathrm{A,S}}$, which is the more general case. Note that if the sound velocity of outermost core fluid is less than the adiabatic trend, as indicated by many seismic studies, then we require that

$$\frac{K_{\mathrm{S}}\left(\vec{C}_{\mathrm{S}}\right)}{K_{\mathrm{S}}\left(\vec{C}_0\right)} < \frac{\rho\left(\vec{C}_{\mathrm{S}}\right)}{\rho\left(\vec{C}_0\right)} < 1, \qquad [10]$$

where K_{S} is the adiabatic bulk modulus, ρ is the density, and the last inequality results from the requirement of gravitational stability.

The condition expressed by [10] may be easier to satisfy in the case of a nonproportional enrichment, since it allows for more degrees of freedom. One of the main issues with proportional enrichment is that a velocity decrease is not usually considered plausible, unless one invokes strongly nonideal mixing (Helffrich, 2012). On the other hand, recent work on mixing of Fe–FeO in the Earth's core suggests that addition of oxygen alone may lower seismic velocity (Komabayashi, 2014). In this case, a proportional enrichment of oxygen could explain a velocity decrease, but such a profile predicts seismic velocities deeper in the outer core that are much slower than observed. Thus, a proportional enrichment alone may be unlikely to explain the usual observations.

7.11.6.4.1 Alloy incompatibility from inner-core growth

If the origin of the outermost core stratified layer is due to incompatible alloys that were expelled by growth of the inner core (e.g., Fearn and Loper, 1981; Helffrich and Kaneshima, 2013), then in the simplest circumstances, we would expect a proportional enrichment in those alloys. A similar situation holds for a stratified layer formed by barodiffusion of light alloys from greater depth and accumulating at the surface of the core (Braginsky, 2007; Gubbins and Davies, 2013). However, another possibility is that $\vec{C}_{\mathrm{A},0}$ contains more than one significant component, one of which is more incompatible than others in the inner core. For example, Alfé et al. (2002) suggested that oxygen is less compatible than sulfur and silicon at inner-core conditions. In such a case, light alloy accumulation may not necessarily give rise to proportional enrichment. Such a mechanism for producing a nonproportional enrichment can in principle be predicted and tested.

A separate problem with light element accumulation due to inner-core crystallization is that the inner-core boundary layer that expels buoyant-incompatible light alloys is expected to be of order 1–10 cm thick (e.g., Deguen et al., 2007), and upwelling currents transporting light alloy-enriched material upward will exhibit a similar length scale. For diffusivities of order $10^{-8}\ \mathrm{m^2\ s^{-1}}$, such an upwelling tendril would have a characteristic diffusion time ranging from several hours to a week, thus becoming quickly diluted. For typical outer core flow velocities ($\sim 1 \times 10^{-4}\ \mathrm{m\,s^{-1}}$) a transit time of order ~1000 years is required to rise from the inner core to the CMB, more than $\sim 10^4$ diffusion times for an upwelling of length scale 10 cm. This estimate is a lower bound because it assumes that such an upwelling current rises directly upward, which is not likely in a convecting fluid subject to the relatively strong influence of rotation. Furthermore, the stretching and mixing by the turbulent environment of outer core convection would

further shorten the timescales over which such structures could remain coherent. Thus, it appears difficult to accumulate buoyant compositionally distinct fluid atop the core.

Another problem is that, while buoyancy sources such as light alloy expulsion from inner-core growth could very well be an important part of driving core convection (Braginsky, 1963), it has already been mentioned that the density fluctuations associated with whatever buoyancy sources are present in the Earth's outer core exhibit lateral density fluctuations of order 10^{-9}, at least six orders of magnitude too small to produce anything that could be seismically detected (Stevenson, 1987). Thus, it is difficult to imagine any driving force for core convection to account for seismological observations of any kind.

7.11.6.4.2 Core–mantle reaction-induced stratification

We discuss core–mantle reactions in greater detail in a later section; thus, we only briefly mention the relevant background for understanding outer-core stratification arising from core–mantle reactions. Many recent experimental and theoretical studies have found that typical mantle compositions will be out of equilibrium with outer-core metal containing a maximum of ~10 wt.% light alloys. The expected direction of the reaction, according to recent studies (Asahara et al., 2007; Frost et al., 2010; Ozawa et al., 2009), is for oxygen to dissolve into the metal. Asahara et al. (2007) initially used this result to argue for iron depletion of the bottom of the mantle, because they did not consider the possibility that the metal reaction products would be gravitationally stable atop the core, thus limiting the extent of the reaction. Indeed, according to seismic observations, the base of the mantle appears Fe-enriched, not Fe-depleted (see ULVZ discussion). Fe enrichment at the base of the mantle should increase the extent of disequilibrium between ambient core fluid and the base of the mantle, requiring even more oxygen atop the core to bring the system closer to equilibrium.

One of the main advantages of core–mantle reactions for explaining seismic observations is that it allows more degrees of freedom to explain the low-velocity anomaly because $\vec{C}_{A,0}$ is *not* parallel to $\vec{C}_{A,S}$. Buffett and Seagle (2010) presented a simple model for a stratified layer produced by core–mantle reactions in the Fe–O system. Their model did not include the diffusion couple on the mantle side, nor did it include a large degree of expected secular cooling of the CMB, and the stratification was consequently weak and subject to significant degrees of entrainment into core flows. Nevertheless, the model exhibits many first-order characteristics that are unlikely to change with more detailed models. As mentioned in the preceding text, diffusivities of up to 10^{-8} m^2 s^{-1} lead to downward encroachment of the layer on the order of ~100 km, a likely outcome of any model employing similar diffusivities. However, one of the main difficulties with this model is that the diffusivities may be too small to account for the much greater thicknesses inferred by Helffrich and Kaneshima (2013), and this difference remains to be explained. Nevertheless, recent thermodynamic models of mixing in the Fe–FeO system (Komabayashi, 2014) provide further support for the Buffett and Seagle mechanism and may provide the simplest explanation for seismological inferences.

7.11.6.5 Summary and Perspective

Both the existence and origin of a stratified layer atop the core are ongoing topics of investigation, and neither should be considered adequately resolved. Highly skilled seismologists have come to completely different conclusions regarding the robustness of inferred layer structures, while mineral physics constraints still exhibit considerable uncertainties. Geomagnetic arguments are confounded by nonuniqueness. The outermost core stratification remains one of the most important first-order problems in deep-Earth geophysics, yet it appears that more work is needed before we can move toward a consensus.

Important clues may still be found and leveraged for the purposes of interpretation. For example, the F layer at the bottom of the outer core also exhibits a negative velocity contrast relative to the adiabatic trend and is probably better resolved than the outermost core stratification (Souriau and Poupinet, 1991; Zou et al., 2008). However, for stability, the F region must exhibit a higher density than the isentropic part of the convecting outer core. If such a layer can be explained by proportional depletion in light alloys (i.e., $\vec{C}_{A,S} = q\vec{C}_{A,0}$ and $q < 1$), then any outermost core stratification that produces a negative density and velocity anomaly likely has an origin distinct from proportional enrichment (Hirose et al., 2013).

7.11.7 Core–Mantle Heat Exchange

CMB heat flow provides a vital link for understanding the fundamental thermal, chemical, and magnetic evolution of Earth's interior. Recent years have witnessed a steady increase in estimates for CMB heat flow, due in part to increased estimates of CMB heat flow based upon hot spot swell buoyancy flux constraints (Labrosse, 2002; Mittelstaedt and Tackley, 2005; Zhong, 2006), in addition to proposed constraints arising from the PPv double-crossing (Hernlund et al., 2005; Wu et al., 2011) and upward revisions in estimates of core thermal conductivity from a combination of several ab initio modeling approaches, laboratory experiments, and recognition of saturation resistivity in the geophysical context (de Koker et al., 2012; Gomi et al., 2013; Pozzo et al., 2012) that place strong constraints on CMB heat flow as far back as ~3.5 Ga. Until these recent developments in understanding CMB heat flow, it was common to think of CMB heat flows of ~5 TW (e.g., Buffett, 2002); however, at the present time, most lines of evidence argue for a CMB heat flow more than 10 TW. This major upward revision in CMB heat flow carries important consequences for the evolution of the Earth's deep interior, requiring ~1000 K of secular cooling at the CMB and extensive melting of the lowermost mantle in the early Earth. In the following sections, we briefly review each of these recent contributions to understanding CMB heat flow.

7.11.7.1 Plume Heat Flow

Volcanic hot spots are associated with topographic swells, or upward deflections of the Earth's surface in the region surrounding the volcanic center. According to models of hot spots involving a deep-seated mantle plume origin, these

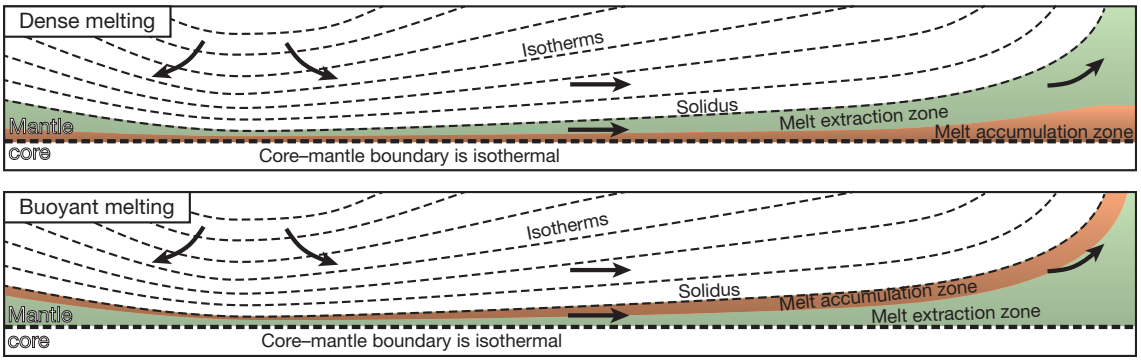

Figure 18 Cartoon of melting scenarios in the lowermost thermal boundary layer, assuming that the CMB is hotter than the mantle solidus. The top and bottom panels show the outcome of scenarios in which the melt is more or less dense than solids, respectively. Arrows represent the mantle flow with downwelling on the left side and upwelling (e.g., a plume) on the right. Melt percolates up or down depending on the melt–solid density difference, leaving melt-depleted rock (green) above or below a melt-enriched layer (orange).

swells are dynamical topography generated in proportion to the upward buoyancy flux of hot material as it rises through the *upper* mantle beneath the lithosphere. Employing this mechanism yields estimates ranging from 41 to 55 Mg s^{-1} buoyancy flux globally (Davies, 1988; Sleep, 1990). If one assigns temperatures and thermal expansivity values to these plumes, such buoyancy fluxes correspond to roughly 2–4 TW advected heat flow carried upward in the *upper* mantle. This order of magnitude of heat flow associated with swells has sometimes been used to argue for a deep, rather than shallow, origin for hot spots (Figure 19).

It has sometimes been assumed that the heat flux carried by plumes in the upper mantle is a reliable estimate of the CMB heat flow, giving rise to broad uncertainties. However, mantle convection studies argue that upper-mantle plume heat flux underestimates the heat flow by a factor of 3–5. While all recent studies agree that upper-mantle plume heat flow is much less than the CMB heat flow, the precise reasons are still debated. Figure 19 gives a brief summary of some arguments. Heat is carried through the mantle by upwellings and downwellings. One view holds that heat flow is dominated by sinking lithospheric slabs in the shallow mantle and by upwelling plumes in the deeper mantle, with the heat carried by hot spot-compatible plumes in a compressible mantle decreasing dramatically upon ascent owing to differential adiabatic cooling, conductive heat loss, and other factors (Zhong, 2006). Another view holds that some plumes may be very weak (Labrosse, 2002), assume the form of transient thermals (Jellinek et al., 2003), or represent passively entrained portions of the lower boundary layer (Romanowicz and Gung, 2002), and in such cases, they may not produce a significant or easily identifiable topographic swell even if they reach the upper mantle.

While a significant underestimation of CMB heat flow by hot spot swells is indicated by many studies, the precise conversion factor between these quantities is not known to a high degree of accuracy. Using plume buoyancy flux in addition to other constraints such as upper-mantle temperatures, calibrated by results from 3-D spherical shell thermochemical convection models, Zhong (2006) proposed CMB heat flow in the range 12.6–14.2 TW. While other studies employ different kinds of models, their results are also consistent with such a large conversion factor between the shallow plume heat flow and CMB heat flow (e.g., Mittelstaedt and Tackley, 2005). Thus, the CMB heat flow in excess of 10 TW is compatible with hot spot swell constraints, and the most detailed models suggest values close to 13 TW.

7.11.7.2 CMB Heat Flow Estimates from *D″* Conductivity and Thermal Gradients

Because radial heat advection vanishes at the CMB, conduction is the only means of passing heat from the top of the core into the very bottom of the mantle. Therefore, one way of estimating CMB heat flux is by direct application of Fourier's law: multiplying the lowermost mantle thermal conductivity by an estimate for the average thermal gradient and using a factor of 1.52×10^{14} m^2 for the CMB area to convert from heat flux to total heat flow. This is in principle a very straightforward procedure, except that both the thermal conductivity and average *D″* geothermal gradient are highly uncertain. Direct determinations of absolute temperature in the deep mantle from seismic velocity variations (e.g., Kawai and Tsuchiya, 2009) are probably ill-posed owing to the accumulation of systematic errors in seismic velocity profile, poorly constrained dependence of seismic velocity upon temperature (and unknown composition), and the influence of independent factors such as variations in elastic anisotropy. The recent discovery of a Pv–PPv phase change has possibly improved our state of knowledge, and when combined with more complete boundary layer and convection models, it may be possible to narrow the range of uncertainty considerably, although the results are model-dependent. While new experimental and theoretical/computational constraints on *D″* thermal conductivity have also emerged, there is still residual uncertainty and thus these estimates should be considered a work in progress. Nevertheless, as we will explain in the succeeding text, the emerging range of CMB heat flow estimates based on recent developments are beginning to converge with other estimates such as plume heat flux (as discussed in the previous section) and core heat flow (discussed in the next section). The mutual consistency of these constraints is a potentially promising development for understanding the dynamics and evolution of the deep Earth.

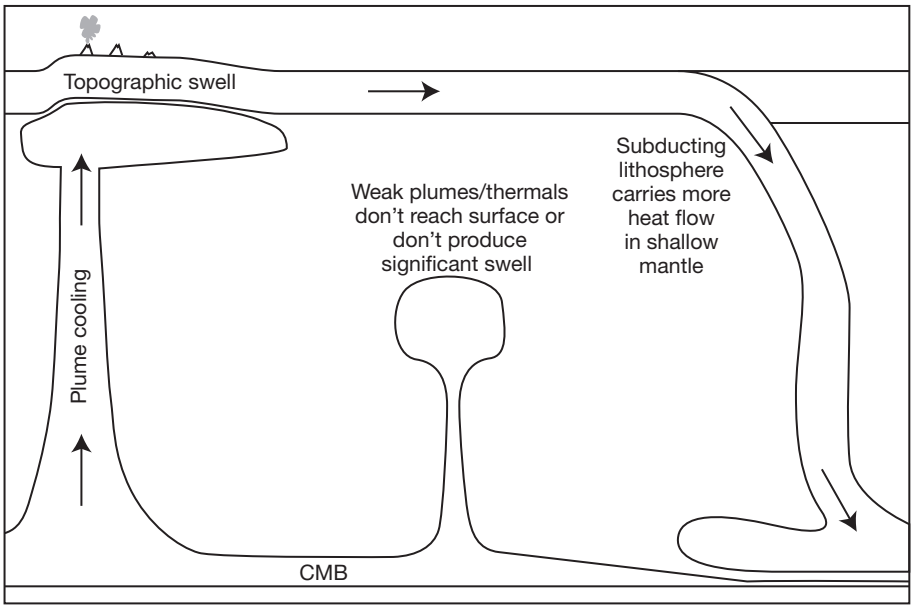

Figure 19 Illustration of some commonly cited reasons that plume heat flux in the upper mantle significantly underestimates CMB heat flow. Plumes may cool more rapidly upon decompression at high temperature than surrounding material in a compressible mantle and lose heat by conduction. Some have proposed weaker plumes or thermals that either do not reach the shallow mantle or do not produce a measurable topographic swell. Some views hold that downwelling slabs carry much of the advected heat flow in the shallow mantle, while plumes carry more heat flow in the deeper mantle.

7.11.7.2.1 Estimates of mantle thermal conductivity

The thermal conductivity of D'' is an important parameter, and is critical for obtaining heat flux estimates from the geothermal gradient. For many years a central value of 10 W m^{-1}K^{-1} was assumed by many workers (e.g., Stacey, 1992), although enough was known to establish at least a factor of 2 uncertainty. By modeling laser heating power versus temperature in the DAC for materials with different conductivities, Manga and Jeanloz (1997) estimated a deep mantle conductivity in the range 5–12 W m^{-1}K^{-1}, with trade-offs in estimates of CMB temperature, similar to models proposed by Goncharov et al. (2007). Recent estimates for Pv-bearing rock fall in this range, including recent experimental measurements and *ab initio* calculations that yield conductivities in the range 9–11 W m^{-1}K^{-1} at the CMB (Manthilake et al., 2011; Ohta et al., 2012). The narrowing in the range of estimates is hopeful; however, these results await further confirmation and a number of other experimental and modeling efforts are currently under way that may yield significantly different values.

The aforementioned estimates are for the lattice thermal conductivity; however, it has also been proposed that radiative effects could be important in the Earth's deep mantle, resulting in a higher effective conductivity (Clark, 1957; Hofmeister, 1999). This radiative conductivity contribution is sensitive to absorption in the near-infrared part of the spectrum, where much of the photon transmitted power lies for mantle temperatures. Early experiments showed that near-infrared absorption increased with pressure, mitigating the effects of increased radiative power at elevated temperatures (Mao and Bell, 1972). Recent measurements of absorption for lower-mantle phases up to CMB pressure are also consistent with a limited radiative effect on lower-mantle conductivity, of order 10% or less compared with the lattice conductivity (Goncharov et al., 2008). Thus, the radiative contribution is usually ignored, since there is little evidence to support a significant effect at depth. However, this still represents another source of uncertainty that must be considered in boundary layer models of the D'' region, and estimates based on lattice conductivity alone must be considered a lower bound.

7.11.7.2.2 Estimates of temperature change and boundary layer thickness

One possible method of obtaining an estimate of the adiabatic temperature drop across the D'' thermal boundary layer ΔT_S is to subtract the extrapolated potential temperatures of the core and mantle at the CMB, anchored by transition zone temperatures from the olivine–spinel transition and freezing temperature estimates for impure iron at the inner-core boundary (Williams, 1998). However, such a procedure yields factor of 2 uncertainties and does not sufficiently constrain the actual quantity of interest: the gradient. An average thermal boundary layer thickness L can additionally be assumed, such that the average gradient is assumed to be $\Delta T_S/L$. However, there are no reliable ways of estimating L, particularly in the presence of complexities such as large-scale chemical heterogeneity, and uncertainties in this parameter also exceed a factor of 2. L may also vary by more than two orders of magnitude in D'' from one region to another, particularly under the influence of thermochemical convection. Thus, the product $\Delta T_S/L$ yields combined uncertainties of a factor of 4 or greater. If one adds an additional factor of 2 uncertainty in thermal conductivity, the uncertainty in heat flow determined by this approach is more than an order of magnitude, which is clearly unacceptable.

7.11.7.2.3 Geothermal gradients and postperovskite

Some phase changes offer reliable determinations of temperature if their depth (pressure) can be tightly constrained by seismological observations of discontinuities caused by changes in elastic properties and density across the transition. Thus, the Pv–PPv transition located in the deep mantle may be seen as quite fortuitous for revealing temperatures in the deep mantle. However, the position of the phase boundary and the Clapeyron slope are still not confidently determined owing to uncertainties in pressure standards used in high-pressure experiments. While ab initio models have improved dramatically in recent years, the interaction potentials used in the calculations are necessarily based upon approximations to full solutions to Schrodinger's equation, and it is not easy to obtain robust error estimates. Therefore, the Pv–PPv phase transition alone exhibits many uncertainties, unless one regards a particular experimental pressure standard as being robust and geophysically consistent, or a specific ab initio technique as being superior to all other constraints.

The Pv–PPv transition may help to constrain ΔT_S, but the procedure is not straightforward. Some attempts have been made to construct a whole mantle geotherm based in part upon the temperature of the Pv–PPv transition at a depth of 2700 km and have been used to estimate the magnitude of the mantle adiabatic gradient (e.g., Ono, 2008). However, as discussed previously, the most straightforward and consistent interpretation of a Pv–PPv origin for the D'' discontinuity is in the circum-Pacific, inside deeply subducted lithosphere that is ~700 K cooler than surrounding mantle (e.g., Hernlund and Labrosse, 2007). Therefore, the temperature at 2700 km given by the Pv–PPv transition more likely refers to the temperature of cold subducted slabs, which is not representative of ambient adiabatic mantle, and therefore significantly underestimates the adiabatic gradient in the mantle.

7.11.7.2.4 Geothermal gradient constrained by a double-crossing

A Pv–PPv double-crossing is only possible if temperature gradients at the CMB exceed the gradient along the Pv–PPv phase boundary, which is given by $\rho g/\Gamma$ (where ρ is the density, g is the acceleration of gravity, and Γ is the Clapeyron slope). The product ρg in D'' is well constrained by seismological models ($\rho g \approx 5.5 \times 10^4$ Pa m^{-1}), while Γ must be greater than about 8 MPa K^{-1} in order for a Pv–PPv double-crossing to be geophysically compatible with other constraints (Hernlund and Labrosse, 2007). Using the range 9–13 MPa K^{-1}, we obtain Pv–PPv phase boundary gradients in the range 4.2–6.1 K km^{-1}.

This constraint is only strictly a lower bound on the geothermal gradient and is only applicable if and where a Pv–PPv double-crossing occurs but may be highly useful because it offers the first direct inference of geothermal gradients just above the CMB in a way that can be constrained directly by laboratory experiments. Furthermore, this constraint is most useful when applied to cold ponded downwellings residing just above the CMB, since these are the locations where most of the heat will be absorbed from the core into the mantle by heat conduction. Denoting the fraction of area of the CMB overlain by a Pv–PPv double-crossing as f_{dc}, a lower bound on total CMB heat flow Q_{cmb} can be written as

$$Q_{cmb} > f_{dc} 4\pi r_{cmb}^2 k \frac{\rho g}{\Gamma}. \quad [11]$$

The challenge in applying this kind of estimate is seismic coverage, which limits our ability to reliably establish an appropriate value for f_{dc}. For reference, if $f_{dc} = 1$ and $k \approx 10$ W m^{-1} K^{-1} (e.g., Manthilake et al., 2011; Ohta et al., 2012; Stacey, 1992), then the aforementioned range of estimates would yield Q_{cmb} >6.4–9.3 TW. Of course, on the basis of seismic observations, we expect that f_{dc} is less than unity, which would reduce this lower bound estimate, but just how much less is not well constrained given insufficient seismic coverage of D''. The actual geothermal gradient could also be much steeper than the phase boundary (see discussion in the succeeding text), corresponding to a larger Q_{cmb}. Therefore, uncertainties exist that would either decrease or increase our estimate of Q_{cmb} based on a Pv–PPv double-crossing, illustrating the trade-offs in utilizing this kind of constraint.

Another complexity in applying the Pv–PPv double-crossing as a constraint on geothermal gradients at the base of the mantle is that material downwelling through a Pv–PPv transition will absorb latent heat, which causes a further steepening of the geothermal gradient above $\rho g/T$ (see Figure 20). Buffett (2007) first estimated this effect for a univariant transition and revised the double-crossing constraint as follows:

$$Q_{cmb} > f_{dc} 4\pi r_{cmb}^2 k \left(\frac{\rho g}{\Gamma} + \frac{v_z L}{\kappa C_p} \right), \quad [12]$$

where v_z is the downwelling velocity through the lower transition, L is the latent heat, κ is the thermal diffusivity, and C_p is the specific heat. $L = T\Delta S$, where ΔS is the entropy change for the transition, and can be estimated from the P–T slope of the Pv–PPv phase boundary and volume change via the Clausius–Clapeyron relation. However, it is difficult to estimate v_z just above the CMB based upon dynamical considerations, as there are many uncertainties in viscosity and other parameters (Buffett, 2007). Another approach is to use solutions to the advection–diffusion equation in the boundary layer to estimate v_z/κ. Assuming a first-order variation in downwelling velocity proportional to height z above the CMB such that $v_z = \dot{\varepsilon} z$ (where $\dot{\varepsilon}$ is the strain-rate), it can be shown (e.g.,

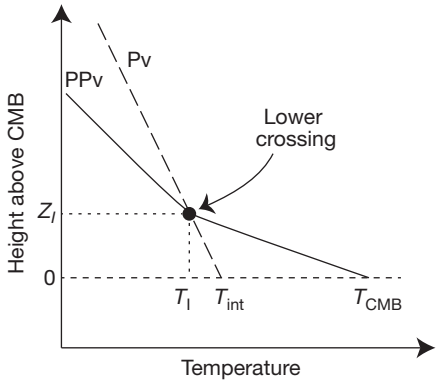

Figure 20 Steepening of the geotherm (solid line) below a lower-crossing of the Pv–PPv phase boundary (dashed line) due to absorption of latent heat.

Hernlund, 2010) that a boundary layer approaches steady conditions such that $\dot{\varepsilon}/\kappa = 2/z_0^2$ over timescales of $1/\dot{\varepsilon}$, where z_0 is a measure of the boundary layer thickness. For the range $z_0 \approx 100$–150 km, compatible with the Pv–PPv double-crossing in a downwelling scenario, one obtains $\dot{\varepsilon}/\kappa \approx 1 \times 10^{-10}\,\mathrm{m}^{-2}$. Thus, ν_z/κ at the height of the lower discontinuity z_l above the CMB is $\dot{\varepsilon} z_l/\kappa \approx z_l \times 10^{-10}\,\mathrm{m}^{-2}$. For $C_p = 1300\ \mathrm{J\ K^{-1}\,kg^{-1}}$ and $L = 100\ \mathrm{kJ\ kg^{-1}}$, the term $\nu_z L/\kappa C_p$ in eqn [12] is $\sim 1\ \mathrm{K\ km^{-1}}$ for $z_l = 10$ km and increases linearly with z_l (although the linear approximation becomes less reliable further above the CMB). For comparison, latent heat release for a PPv → Pv lower-crossing at heights of ~30–50 km above the CMB could steepen the thermal gradient by an amount similar in magnitude to the Pv–PPv phase boundary gradient itself, doubling the implied heat flux bound.

The addition of a two-phase region increases the implied geothermal gradient even further than steepening due to latent heat absorption (Buffett, 2007). However, if the thickness of the Pv–PPv coexistence region is large, then the effects of latent heat become less important in numerical solutions, perhaps due to the distribution of latent heat effects over a larger depth range in addition to the combined effect of latent heat release at the Pv → PPv upper-crossing which tends to exert an opposing influence on the shape of the geotherm (Hernlund, 2010). In any case, when the phase transition thickness is very wide, it is difficult to apply the simpler formulas like eqn [12], and more complete numerical solutions are required to assess the contributions of latent heat.

One method to obtain a direct estimate of the thermal gradient from the double-crossing without requiring any constraints upon the latent heat effect is to assume the position and slope of the Pv–PPv phase boundary, as well as the temperature of the CMB. With this information and an observed depth for the lower-crossing z_l, one can directly calculate the geothermal gradient below the double-crossing by computing $(T_{\mathrm{cmb}} - T_l)/z_l$, where T_l is the temperature at the lower-crossing (see **Figure 20**). This is clearly the most direct approach (van der Hilst et al., 2007); however, it requires accurate knowledge of the phase boundary and CMB temperature, both of which are uncertain by as much as several hundred K; therefore, this constraint is not very reliable at the present time. It is also possible to fit models for the entire geotherm to both the upper-crossing and lower-crossing to obtain an estimate of heat flux using either analytic (Lay et al., 2006) or numerical approaches (Hernlund, 2010). While these solutions exhibit trade-offs with the shape of the geotherm, it is difficult to utilize the additional information as another constraint, and in practice one still encounters similar issues with respect to uncertainties in the phase boundary and CMB temperature.

7.11.7.2.5 CMB heat flux from seismic tomography and boundary layer models

In order to utilize a PPv double-crossing as a constraint upon total CMB heat flow, it is necessary to extrapolate the geothermal gradient from regions where a double-crossing occurs to the remainder of the CMB region. These methods will hopefully yield more relevant constraints on CMB heat flow from considerations of conductivity and thermal gradient variations in the lowermost mantle, and their development is also vital for providing a bridge to other areas of lower-mantle research.

Seismic tomography potentially offers a wealth of information about variations in temperature above the CMB, which could in principle be used to constrain the CMB distribution of heat flux. One possibility is to assume a simple proportionality between seismic-wave speeds in the deepest mantle and CMB heat flux, and this kind of approach is often employed as boundary conditions for dynamo models that seek to relate mantle structure to features of the geomagnetic field (e.g., Aubert et al., 2008; Glatzmaier et al., 1999; Willis et al., 2007). However, this requires assigning a physical value for heat flux to seismic velocity, for example, by defining the upper and lower limits of heat flux using constraints from a Pv–PPv double-crossing, numerical convection models, boundary layer models, or some combination of these.

Here we give a simple illustration of using a tomographic model to extrapolate heat flux to the entire CMB, by assuming a linear dependence between heat flux and seismic velocity. It is important to realize that the minimum heat flux will always be negligible relative to any reasonable maximum heat flux. This is because the lowest heat flux corresponds to the highest temperatures, which will be nearly the same as the CMB temperature (Nakagawa and Tackley, 2008). Therefore, one may build a rough CMB heat flux map by linearly transforming a seismic tomographic model such that the lowest seismic velocities are nil and the highest seismic velocities are unity. The map may then be subsequently scaled by a suitable value for the maximum heat flux, yielding an estimate for CMB heat flux in all locations. The PPv double-crossing is a useful constraint, because it should occur beneath cold downwellings and therefore gives an estimate for the maximum heat flux.

The choice of tomography models is also important. While *S*-wave models have often been used for this purpose, they should be highly sensitive to variations in composition or PPv fraction and are therefore not a good proxy for temperature. In fact, this known sensitivity underlies much of the recent work on D'' discontinuities and LLSVP, as discussed previously. *P*-wave models, on the other hand, should be more sensitive to temperature than to composition or PPv variations and are thus preferred for this purpose (e.g., Trampert et al., 2004). While *P*-wave models are thought to be less reliable owing to relatively poor coverage in the deep mantle (compared with *S*-wave models), the growth in over all data coverage with time and addition of new phases such as P_{diff} indicates that *P*-wave speed models may be more reliable than previously thought (Houser et al., 2008; Manners, 2008). An example of a CMB heat flux map produced in this manner from a *P*-wave speed tomography model is shown in **Figure 21** after assuming a maximum heat flux of 160 mW m^{-2}.

One quantity that can be estimated from these approaches is the relationship between the maximum CMB heat flux q_{max}, and heat flow Q_{cmb}. Any normalized heat flux model can be integrated to yield the proportionality:

$$Q_{\mathrm{cmb}} = A^* q_{\mathrm{max}} \qquad [13]$$

The coefficient A reflects the distribution of heat fluxes obtained from the seismic tomography model, and is unique to every model. For example, in the simple model shown in **Figure 21**, one finds that $A = 81$ (with Q_{cmb} in units of TW and q_{max} in units of W m^{-2}) so that a maximum heat flux of 160 mW m^{-2} would yield a total CMB heat flow of 13 TW,

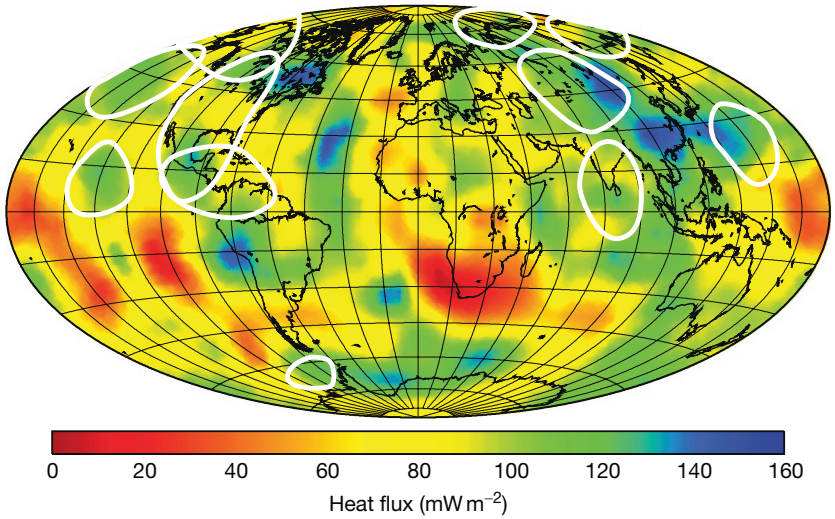

Figure 21 CMB heat flux map produced by assuming a proportionality between temperature and *P*-wave speed velocities using the Scripps *P* model (Houser et al., 2008). In this example, a maximum heat flux of 160 mW m^{-2} is used, corresponding to 13 TW global CMB heat flow. Notice the blue regions of highest heat flux, which can skew the distribution and may be due to features other than heat flux anomalies. Observations of *D″* discontinuities and/or strong seismic anisotropy from **Figure 4** are outlined by thick white lines. In terms of the PPv-double-crossing model described earlier, PPv lenses are predicted to occur in regions with greater than ~80 mW m^{-2} heat flux. This crossover heat flux corresponds to a thermal gradient of ~8 K km^{-1} for a thermal conductivity of 10 W m^{-1} K^{-1}, consistent with Pv–PPv phase boundary gradients of 4.2–6.1 K km^{-1} (for Γ = 9–13 MPa K^{-1}).

consistent with constraints from plume heat flow as discussed previously (and also consistent with core heat flow, as will be discussed in the succeeding text). If one performs the same procedures using a corresponding *S* model (Houser et al., 2008), one obtains $A = 100$; thus, even with the complexities in using *S* discussed earlier, we arrive at a similar result. In general, most models yield similar answers because the dominant distribution of wave speed variations is approximately Gaussian in form (Hernlund and Houser, 2008); thus, the normalized variations have the a similar form and differences in *A* between models are probably more sensitive to the extreme tails of the distribution.

Employing a proportionality between heat flux and seismic-wave speeds, as discussed in the preceding text, is roughly equivalent to assuming that the boundary layer thickness is everywhere the same and that variations in heat flux are mainly due to variations in temperature mapped from seismic-wave speed. However, the boundary layer is expected to be thicker in hotter regions and thinner in colder regions; this effect should amplify differences in implied heat flux for fast and slow regions in seismic tomographic models relative to a simple proportionality. Wu et al. (2011) integrated the heat flux variations using a more dynamically consistent boundary layer model to yield a total heat flow of 13 ± 3 TW, which is probably the most accurate application among all previously proposed techniques for extrapolating heat flux to the entire CMB. Yet, despite the addition of further complexities, the result is similar to prior estimates, converging to ~13 TW.

7.11.7.2.6 Summary of D″ constraints upon CMB heat flow

The discovery of the Pv–PPv phase change and improvements in seismic tomography have revolutionized approaches for estimating CMB heat flow from *D″* structure and have moved beyond rough estimates based on temperature change and boundary layer thickness. While there are still some residual uncertainties in estimating thermal gradients in the deepest mantle, the variation in permissible values is probably within a factor of 2, which is a significant improvement. The convergence of estimates for the lowermost mantle thermal conductivity around ~10 W m^{-1} K^{-1} is also promising, although as noted previously, there may still be some uncertainties, and further research may yet give rise to revisions. The most carefully developed constraints for CMB heat flow (Wu et al., 2011), which rely in part on inferences from the double-crossing model, yield values of CMB heat flow in the range 13 ± 3 TW. CMB heat flow of 13 TW corresponds to a maximum CMB heat flux of around 160 mW m^{-2}, which is more than sufficient to account for a PPv-double-crossing.

7.11.7.3 Heat Flow Constrained by Core Evolution and Dynamics

The most recent major development in core–mantle heat exchange constraints comes from upward revisions in estimates for the conductivity of the Earth's core. Constraints such as plume heat flow and *D″* thermal boundary layer considerations discussed previously can only constrain the Earth's present CMB heat flow, but do not necessarily constrain CMB heat flow in the distant past. Inferences from mantle circulation models depend on plate boundary reconstructions, which themselves are limited to the age of the present seafloor (i.e., several hundred Ma). Constraints involving core conductivity, on the other hand, extend into the Earth's ancient past because they are anchored by the earliest paleomagnetic observations of a geomagnetic field at ~3.5 Ga (Tarduno et al., 2010). Furthermore, while other constraints have some residual

uncertainties and ongoing debates regarding their magnitude and applicability, the recent research on core conductivity, coming from a variety of different approaches, has converged on a surprisingly consistent result. In the following, we give a brief overview of this recent development.

7.11.7.3.1 Heat carried by core conduction and convection

Heat transport in the core differs from that in the mantle in many respects. Sufficiently vigorous convection causes a medium to trend toward a well-mixed isentropic state. Convected heat is carried in the core via radial transport of material exhibiting fluctuations in temperature relative the isentropic value. Even though lateral temperature variations in the core are less than about 10^{-4} K, when coupled with radial flows of order 0.1 mm s^{-1} – consistent with observations of geomagnetic secular variation – it is easy to produce convected heat flows of order ~1 TW (e.g., using $\sim pC_p v_z \Delta T$). Unlike the mantle, the relatively high conductivity and isentropic gradient in core material yield a very large conducted heat flux, which was previously thought by many researchers to be TW at the CMB (e.g., Buffett, 2002; Gubbins et al., 2003; Labrosse et al., 1997) but has recently been upwardly revised to values exceeding 10 TW (de Koker et al., 2012; Gomi et al., 2013; Pozzo et al., 2012). The sum of conducted and convected heat out of the core should be equivalent to the CMB heat flow, and therefore, heat conduction is probably greater than the heat carried by core convection.

There exist a variety of useful equivalent expressions for the isentropic gradient, such as

$$-\left(\frac{dT}{dr}\right)_S = \frac{T\alpha g}{c_p} = \frac{T\gamma g}{\phi} = T\gamma\left(\frac{\partial \log \rho}{\partial r}\right)_S. \qquad [14]$$

where T is temperature, r is radius, S is entropy, α is the thermal expansivity, γ is the Grüneisen parameter, and ϕ is the seismic parameter, which is defined as K_S/ρ (where K_S is the isentropic bulk modulus), or the square of the sound speed in the liquid outer core. Quantities such as ϕ, $(\partial \log \rho/\partial r)_S$, and g are very accurately determined by seismological models that fit a large volume of seismic data to the adiabatic compression trend for the entire outer core (e.g., PREM, Dziewonski and Anderson, 1981), such that they likely contribute less than 1% error to the determination of the large-scale isentropic gradient. Greater uncertainties in estimating $(dT/dr)_S$ arise from the parameter combinations $T\alpha/c_p$ or $T\gamma$. Constraints derived from the PPv double-crossing suggest CMB T to be around 3750 K (Tateno et al., 2009), consistent with an inner-core boundary T of ≈5000 K, although uncertainties at both boundaries probably exceed 10%. The ratio α/c_p not only can be estimated using an experimentally constrained thermal equation of state for iron (e.g., Dewaele et al., 2006) but also likely carry residual uncertainties of at least 10%. While ab initio models should be able to calculate quantities such as γ with relatively high precision, yielding values close to $\gamma = 1.5$ (see Vočadlo et al. (2003) for a review), the errors in this parameter could also be ~10%. Assuming a CMB temperature of 3750 K, with the Dewaele equation of state, one obtains $(dT/dr)_S = 0.89$ K km^{-1}, while using $\gamma = 1.5$ and PREM yields 0.91 K km^{-1}. Thus, these semi-independent estimates yield very similar values, although uncertainties of order 10% still remain. In the following, we will adopt the value 0.9 K km^{-1} for the purpose of estimating conducted heat flux.

The primary uncertainty in estimating the heat conducted along the isentropic gradient has always been the thermal conductivity of impure iron–nickel-alloyed liquid metal at the P–T conditions of the core (i.e., $P > 136$ GPa, $T > 4000$ K). In metals, the thermal conductivity is dominated by transport of heat by electrons, with lattice contributions accounting for ~10% of the total conductivity. The electronic part of the conductivity, k_e, is linearly related to the electrical conductivity σ by the Wiedemann–Franz law:

$$k_e = L_0 \sigma T, \qquad [15]$$

where $L_0 \approx 2.45 \times 10^{-8}$ WΩ K^{-2} is the Lorenz constant. Thus, the dominant contribution to thermal conductivity can be estimated from electrical conductivity from resistivity constraints. However, the measurements cannot be robustly extrapolated across phase transitions and must be performed at very high pressures in the phase stability region of interest.

The first inferences of thermal conductivity at core pressure were derived from shockwave measurements, which yielded values in excess of 100 W m^{-1} K^{-1} for both pure iron (Bi et al., 2002; Keeler and Mitchell, 1969) and iron–silicon alloy (Matassov, 1977). Given concerns regarding the relatively high CMB heat flows implied by these estimates, they were not taken as seriously as lower estimates. Stacey and Anderson (2001) downwardly revised the estimate of k_e to 42 W m^{-1} K^{-1}, and Stacey and Loper (2007) later suggested even lower values for k_e around 30 W m^{-1} K^{-1}, permitting thermal evolution scenarios with low CMB heat flow. More recently, *ab initio* modeling techniques have been developed to study core conductivity and have unanimously found that core conductivity is closer to 100 W m^{-1} K^{-1} atop the core, more compatible with the earlier inferences based upon shock measurements (de Koker et al., 2012; Pozzo et al., 2012). High-pressure ambient-temperature DAC conductivity measurements have exhibited excellent agreement with ab initio calculations on iron and iron–silicon alloys at core pressures, building confidence in the computational model results, although they were only able to directly compare at ambient temperatures owing to experimental limitations (Gomi et al., 2013). However, Gomi et al. (2013) demonstrated that all of the high P–T ab initio results, high-P and ambient-T DAC experimental results, and even the older shockwave measurements are in good agreement with each other if one adopts a resistivity saturation model, which has been well known in the materials science literature for half a century (e.g., Gunnarsson et al., 2003) but was never applied in the geophysical context until now. In fact, saturation resistivity provides a simple theoretical basis for interpreting all of the higher conductivity values derived from every available technique and establishes an absolute theoretical minimum of $k_e \approx 60$ W m^{-1} K^{-1} at the top of the core (Gomi et al., 2013). In summary, very rapid progress in understanding core conductivity has now established estimates for thermal conductivity of $k_e > 90$ W m^{-1} K^{-1} at the CMB, increasing even further with depth in the core below the CMB.

The conducted heat flux implied by a 0.9 K km^{-1} isentropic gradient and thermal conductivity in excess of 90 W m^{-1} K^{-1} is greater than 77 mW m^{-2}, producing a CMB conducted heat

flow greater than 11.6 TW, very close to the values for the CMB heat flow estimated from the mantle constraints discussed previously. Another interesting implication of this result is that the inner core would have begun to crystallize about 0.5 Ga (Gomi et al., 2013) and is therefore only a relatively recent feature of the Earth (approximately Cambrian). This changes very little even if one considers the possible presence of a plausible amount of radioactive potassium in the core (Labrosse, 2003). In the absence of an alternate mechanism for producing the geodynamo, convection in the core prior to the inner core would have been driven solely by thermal buoyancy, requiring a positive convected heat flow in addition to the conducted heat flow. If the heat flow falls below the amount conducted down the adiabatic gradient, then the core would begin to thermally stratify and convection would become impeded. It is unknown precisely how much stratification the Earth's core could tolerate while still producing a geomagnetic field at the surface compatible with paleomagnetic constraints and is a topic that needs to be further investigated. Furthermore, given the fluctuations in CMB heat flow expected over time owing to processes such as periodic assembly and dispersion of continents (i.e., the 'Wilson cycle'), the average CMB heat flow would need to be significantly higher than the lower threshold in order that lower heat flow periods would not shut off the geodynamo (Jaupart et al., 2007). Thus, the conducted heat flow of 11.6 TW likely represents a lower bound on average CMB heat flow during the period 0.5–3.5 Ga prior to the inner core, during the era that the Earth is known to have produced a magnetic field consistent with a geodynamo (Tarduno et al., 2010). Additionally, the conducted heat flow was somewhat higher in the past given the influence of hotter conditions on both the isentropic gradient and thermal conductivity (Gomi et al., 2013).

7.11.7.4 High CMB Heat Flow and Thermal Evolution

Recent estimates for CMB heat flow converge to values of ~13 TW, including plume heat flow, estimates of temperature gradients and thermal conductivity in D'', and a high conducted heat flow down the core isentrope. The possibility for such high heat flow has raised concerns regarding the implied secular cooling of the core and deep mantle. The core has a mass of 2.1×10^{24} kg (Dziewonski and Anderson, 1981) and specific heat of 740 J K^{-1} kg^{-1} (Vočadlo et al., 2003), yielding a total heat capacity of about 1.6×10^{27} J kg^{-1}. Taken over the age of the Earth prior to the formation of an inner core (i.e., before 0.5 Ga), 13 TW heat flow translates to 1.6×10^{30} J, corresponding to ~1000 K average cooling. (For comparison, this is roughly an order of magnitude larger than the rotational kinetic energy of the present-day Earth.) The core has cooled by ~100 K since the birth of the inner core (e.g., Labrosse, 2003); thus, the total secular cooling for 13 TW CMB heat flow is expected to be 1100 K. Keep in mind, however, that this is a lower bound since heat flow is variable and would have been higher, on average, in the past.

There are two major problems with such a large secular cooling of the core. The first is that it is much greater than the secular cooling of the mantle inferred from igneous petrology constraints (e.g., Herzberg et al., 2010), and even with the possibility of chemical layering in the deep mantle, it may be difficult to shield the shallow mantle from plumes rising up from the much hotter deep mantle (e.g., Farnetani, 1997). The second problem is that the temperature of the CMB during the early stages of the Earth's evolution would have been significantly hotter than the liquidus for any reasonable bulk composition (e.g., Andrault et al., 2011; Boehler, 2000; Fiquet et al., 2010; Zerr et al., 1998), and the lowermost mantle should therefore have been molten for an extended period of geologic time (Labrosse et al., 2007). It has been proposed that such a melt would have to be dense enough to remain stable at the bottom of the mantle for the several Gy periods of time prior to temperatures falling to the mantle solidus, since a buoyant melt would otherwise have destabilized the boundary layer, leading to rapid secular cooling to the solidus in the very early Earth, which is incompatible with sustained CMB heat flow of 13 TW or higher. The presence of some kind of long-lived dense BMO is therefore an inescapable outcome of the convergence of CMB heat flow constraints around relatively high values. However, it is not clear that the BMO model can account for such high temperatures in the early Earth, since the implied CMB temperature may exceed the liquidus by an amount greater than predicted in simple models (Labrosse et al., 2007).

7.11.8 Core–Mantle Mass Exchange

It is simplest to think of the Earth's core as a chemically isolated system, having a composition that reflects processes that predate the cessation of the Earth's formation, such as silicate–metal equilibration in a deep magma ocean during the Earth's formation (e.g., Li and Agee, 1996; Wood et al., 2006), and with negligible exchange of matter in the subsequent ~4.4 billion years. On the other hand, it has been hypothesized that some isotopic and chemical signatures may originate from core–mantle mass exchange, such as an elevated Fe/Mn observed in OIBs (Humayun et al., 2004) or Os isotopic fractionation reflecting inner-core growth (Brandon and Walker, 2005). Indeed, recent CMB thermal evolution models (Labrosse et al., 2007), seismic observations (Rost et al., 2005), and inferences from high-P–T experiments (Walker et al., 2002) together highlight the CMB as a potentially highly chemically reactive zone reflecting a large degree of disequilibrium between the average core and mantle at CMB P–T conditions. Understanding the degree of core–mantle mass exchange is important for understanding the long-term evolution of the CMB region, as well as the origin and evolution of its major features.

7.11.8.1 Core Versus Mantle Affinity

Before discussing mass transfer between the mantle and core, it is useful to make a distinction between the material identified as having an affinity for the core and the material that has properties belonging to the mantle. Essential properties of the core matter include a high density (closer to 9900 kg m^{-3}), a high enrichment in iron (e.g., Fe mole fraction $\geq 1/2$), and a metallic character. Essential properties of the mantle matter include a smaller density (closer to 5.5 kg m^{-3}), a high alkali content (i.e., Ca, Na, and Mg), and an ionic character. Some

species, such as O and Si, are equally soluble in the core or mantle matter at CMB conditions and therefore are of little use as a discriminant. Notice that we also avoid using solid versus liquid as a discriminant, since it is not diagnostic of the difference between the core and mantle (both of which contain solids and liquids). The reason for the necessity of establishing this kind of definition is that it is possible for mantle matter to be converted into core matter, and vice versa, such that the properties of 'mantle-ness' and 'core-ness' are not strictly conserved. In this more general view, the CMB is a boundary that may shift through material by transformation of the matter into one form or the other.

There are two distinct ways to transfer material between the mantle and core: (1) by mass transport in which core and mantle materials move relative to one another in opposite directions perpendicular to the CMB and (2) by conversion of the mantle matter into the core matter, or vice versa. In the first case, material of one affinity can be said to be dynamically 'entrained' into the region of matter having the other affinity, but without losing its essential identity. In the second case, the identity of a parcel of matter itself is changed from one kind to the other. Both kinds of mechanisms for core–mantle mass transfer have been proposed in the past.

7.11.8.2 Entrainment and Other Direct Core–Mantle Exchange Processes

Once material has crossed the CMB, the question becomes whether or how it will be transmitted or mixed into the bulk of the mantle or core. However, it is crucially important to recognize that core–mantle mass exchange may be confined – to a greater or lesser degree – to the deepest mantle and/or the topmost outer core by hindrances to radial transport. For example, matter entering the mantle from the core may tend to be inherently dense and exhibit a relatively low viscosity (e.g., due to Fe enrichment), both of which can hinder or slow the viscous entrainment of this material upward to shallower depths. Likewise, matter transmitted from the mantle to the core could be less dense than the underlying core, and downward entrainment in this context is very difficult owing to the virtual absence of viscous forces in the outer-core fluid (although turbulent entrainment might be possible). Still, some degree of entrainment and transport away from the CMB is expected in all cases, though the flux may be limited to a greater or lesser degree depending on a variety of complex factors (e.g., Buffett and Seagle, 2010; Sleep, 1988).

Several kinds of entrainment may occur at the CMB; however, most of the proposed mechanisms involve intrusion of liquid core metal into the base of the mantle rather than the mantle into the core. The latter case is probably ruled out by the very brief Stokes rise time for buoyant mantle material in the core, in addition to the weak ability for core flows to mobilize and/or entrain particles (Solomatov et al., 1993). Percolation of fluid through a solid matrix relies on the ability for the liquid to form an interconnected grain-wetting network within solid crystalline rock via decompaction (von Bargen and Waff, 1986). While the strong surface tension of metals can inhibit wetting, this may be less effective at high temperatures and impurity concentrations. Some experiments at conditions close to CMB P–T support grain wetting between iron and PPv-bearing rocks for liquid metal fractions greater than ~2% (Sakai et al., 2006). Thus, iron may be likely to penetrate into, and flow through, mantle rocks at CMB conditions by decompaction and percolation. However, the strong buoyancy force between metals and silicates/oxides at the CMB acts to drain fluid back into the core. It may be possible to support a limited degree of intrusion by capillary forces; however, this is estimated to accommodate only limited intrusion of order 100 m or less (Poirier et al., 1998). It has also been suggested that poroviscoelastic entrainment of core fluid can occur (Petford et al., 2005); however, it is not clear that the requisite dilatant elastic properties exist for materials at D'' conditions. Kanda and Stevenson (2006) proposed a simple mechanism for obtaining core fluid intrusion into the mantle, which relies upon decompaction and percolation but is driven by downward deflection of the CMB into the core, such as the dynamical topography expected beneath the mantle downwelling currents. In this case, the limiting depth extent of intrusion will be similar to the dynamical topography itself, of order 1 km (e.g., Olson et al., 1987; Tanaka, 2010). Once the mantle material moves away from regions of downward deflection into the core, it will rise upward again and much of the core fluid could be expected to drain back into the core. However, a small residual fraction of order 1% may not completely wet grain boundaries and could therefore become frozen into the rock matrix. Entrainment of iron into mantle rocks, even at small fractions, will affect the bulk density of the rock, and might cause it to become dense enough to resist upward transport into the overlying mantle. However, as discussed previously, in the regime of viscous entrainment that dominates mantle dynamics, such material will gradually be eroded away and mixed into the overlying mantle.

7.11.8.3 Core–Mantle Chemical Reactions

CMB chemical reactions involve the exchange of chemical components between phases belonging to the core and mantle and occur at the atomic scale by interdiffusion of molecular components across the interface between these phases. These chemical reactions occur whenever the *chemical potentials* (μ) of mutually intersoluble components are unequal; thus, CMB disequilibrium is manifested as a discontinuity or gradient in chemical potential(s) across the CMB. (Note: a discontinuity or gradient in *concentration* does *not* imply disequilibrium.) Core–mantle disequilibrium may be an important driving force for the long-term evolution of heterogeneous structures at the CMB, and is probably relevant to ULVZ as the veneer separating the overlying mantle from the top of the core. The top of the core may be chemically distinct from the deeper core, particularly if the stratification inferred by seismology exists, as discussed in Section 6.

It is helpful to clarify the meaning of terminology used in this context. For example, the *solubility* of a given component in a particular phase (e.g., oxygen in iron liquid) is not always a clearly defined concept. In some cases, there may be a *solubility limit* for a given solute in a specific phase, and a concentration at this limit is said to be at *saturation* or to be *saturated*. Concentrations below or above any such limit are *undersaturated* or *oversaturated*, respectively. However, in some cases, there is no solubility limit, and a mixture of 2 components in a phase can

be said to exhibit complete solution series between the pure end-members, in which case they may also be said to be *miscible*. Yet, even if a solubility limit does occur, saturation is not always relevant to the actual concentration(s) of solute(s) expected in a phase (i.e., solvent). In many cases, we are more interested in the *equilibrium concentration*, which is always less than the saturation limit (if one exists) and is instead determined by chemical equilibrium between 2 or more phases (solvents) which are able to freely exchange the component (solute) of interest. A component i, which is soluble in both phase j and phase k, is said to be in chemical equilibrium whenever $\mu_i^j = \mu_i^k$, where μ is the chemical potential and is a function of the bulk chemical composition of the phase in addition to the P–T conditions. This relationship is as fundamental as equality of temperature between two bodies at thermal equilibrium.

In the equilibrium partitioning case, the concentration of a component in one phase also depends on the concentration of that component in the other phase(s), and these concentrations are generally distinct from one another. In the case of a saturated solution, on the other hand, the concentration of the component in the saturated phase does not depend on the concentration of that component in other phases, since it is at the limit of its solubility. Being saturated in a component does not, however, preclude the relevance of equilibrium exchange of that component at subsaturated concentrations. A phase with concentrations of a component above the saturation limit is metastable and said to be *supersaturated*; such a mixture is prone to precipitation of another phase that hosts the excess solute. Supersaturation can occur, for example, as a saturated (or undersaturated) phase cools or rises to lower pressures, in which case the solubility might drop below the existing concentration (as happens in degassing of magmas during ascent). Core–mantle mass exchange processes driven by saturation and/or equilibrium between phases have been proposed in the past, and we discuss various examples in the following.

7.11.8.3.1 Length scales of equilibration

Although there exists large-scale disequilibrium between the core and mantle (discussed in the next section), at sufficiently small scales, it is possible to achieve 'local equilibrium,' although one needs to be careful about how this is defined. If a small parcel of core fluid of length scale L_c is brought into contact with a small parcel of mantle of length scale L_m under conditions of chemical disequilibrium, the exchange of components between them by diffusion offers an opportunity for these to approach equilibrium since net diffusion rates are driven by differences in chemical potential. The timescale for equilibration in such a case is thus limited by the diffusion timescales $\tau_c = L_c^2/D_c$ and $\tau_m = L_m^2/D_m$, where D_c and D_m are the limiting (i.e., slowest) diffusivities of interacting components in the core and mantle matters, respectively. Recognizing a large degree of uncertainty in estimates of the limiting diffusivities, we can obtain rough order of magnitude estimates using values of $D_c \sim 10^{-8}\ m^2\ s^{-1}$ (Vočadlo et al., 2003) and a much larger range of potential variation for relevant mantle materials $D_m \sim 10^{-16}\ m^2\ s^{-1}$–$10^{-14}\ m^2\ s^{-1}$ (Van Orman and Crispin, 2010).

There is one further caveat for local equilibrium that is important to keep in mind. In order to approach equilibrium, the diffusion timescale of locally equilibrating matter must be smaller than the timescales of other processes that are perturbing the equilibrium, such as secular changes in temperature or composition as discussed previously. The timescale for secular shifts in equilibrium at the CMB is typically very slow over geologic timescales (i.e., of order 10^8 years), although it still presents a limit upon the size of regions in the core or mantle that may approach equilibrium.

For a core parcel of scale L_c and a mantle parcel of scale L_m, equating the diffusion timescales gives

$$\frac{L_c}{L_m} = \sqrt{\frac{D_c}{D_m}}. \qquad [16]$$

In words, the size of a core parcel that may equilibrate with a mantle parcel on a given timescale is larger by a factor $\sqrt{D_c/D_m}$. For processes relevant to the Earth's CMB, $\sqrt{D_c/D_m} \sim 10^3 - 10^4$. Therefore, 'local equilibrium' can be approached over significantly larger length scales in the core than in the mantle. Assuming a typical residence time for mantle material convecting along the CMB of 10^8 years, the thickness of the zone that is able to approach equilibrium on the mantle side is only of order 0.1–10 m. Over the history of the Earth, material with this residence time would have been circulated through the CMB region ~45 times, accounting for a total layer thickness of order 10–1000 m at the CMB. Even if one were to account for variable rates of mantle convection through geologic history, core–mantle reactions limited by diffusion length scales alone would only affect a very small fraction of mantle (about 10–100 ppm by volume). The volume of core that would be affected could be much larger, although the influence of reactions on core dynamics may be more severe (e.g., leading to stratification, Buffett and Seagle, 2010).

It is possible to dramatically increase the length scales of mantle reaction zones if core fluid intrudes into the mantle along grain boundaries by decompaction, as discussed previously. It is still required that the metals and oxides are mixed/homogenized to a scale finer than 0.1–10 m (see the preceding text) in order for equilibrium to be approached; thus, in the slowest diffusion case, it may be necessary to mix to length scales approaching the grain size, which is readily satisfied by grain-scale percolation mechanisms. For mantle flow through the CMB region with an average residence time of about 100 My, the dynamical topography-driven mechanism proposed by Kanda and Stevenson (2006) would accommodate interaction with a volume of mantle equivalent to ~50 km thickness at the CMB over the Earth's history. On the other hand, the volume of core matter available for reaction may be significantly smaller if metals become largely isolated from the top of the core by virtue of a complex intergrain geometry and/or stabilizing composition-induced density gradient owing to reactions (e.g., by enrichment of metals in oxygen). Thus, a more significant volume of mantle may be reacted with the core if metal intrudes by decompaction, and as mentioned earlier, some residue of this metal could be trapped inside the rock matrix below a wetting fraction of order 1%. Core fluid reacted with the mantle in this manner will drain back into the

core; however, if it contains even a very small enrichment in light alloys (Si, O, etc.), it may be impossible for the core to downwardly entrain the fluid and mix it into the deeper core.

7.11.8.3.2 Disequilibrium-driven reactions

It is important to recognize that, even in the mildest of circumstances, the CMB should be a chemically reactive zone for much of the Earth's history (Stevenson, 1981). Core–mantle disequilibrium may be an inherent consequence of the manner in which the Earth's core formed and is constantly perturbed by secular changes during the Earth's evolution since formation. It is thought that elemental abundances in the silicate Earth reflect metal–silicate equilibrium during a shallower magma ocean phase in differentiating planetesimals or the proto-Earth (e.g., Wood et al., 2006), which are distinct from the much higher-pressure and higher-temperature conditions that have prevailed at the CMB since formation. Therefore, the average core and mantle should be far from equilibrium at CMB P–T from the very beginning of the Earth's history. Furthermore, equilibrium is generally temperature sensitive, and the CMB undergoes secular cooling over time (perhaps more than 1000 K, as discussed previously). Thus, secular cooling continuously shifts the bulk of the core and mantle away from any equilibrium that may have been established in the past. Finally, secular changes in the composition of the core and/or mantle materials circulating through (or accumulating at) the CMB are expected, causing another perturbation to the disequilibrium between the core and mantle in the CMB region itself. For example, such secular composition changes can arise in the mantle as a result of the accumulation of MORB (e.g., Christensen and Hofmann, 1994) or banded-iron formation (Dobson and Brodholt, 2005) or from fractional crystallization of a BMO (Labrosse et al., 2007), while in the outer core, a secular enrichment in incompatible alloys is expected as the inner core grows by fractional crystallization (Braginsky, 1963).

On the basis of experiments performed up to mid-mantle P–T conditions in the DAC, it has long been suspected that some silicates and oxides may readily dissolve into metallic iron at high P–T (e.g., Dubrovinsky et al., 2004; Knittle and Jeanloz, 1991). Knittle and Jeanloz (1991) combined (Mg, Fe)SiO_3^{Pv} and Fe^M (M = metal) at high P–T in a laser-heated DAC and, upon observing Fe-free Pv, along with FeO and FeSi in the quench products, suggested the reaction

$$(Mg, Fe)SiO_3^{Pv} + Fe^M \rightarrow FeO^M + FeSi^M + MgSiO_3^{Pv} \qquad [17]$$

In the proposed reaction, the $FeSiO_3$ component of Pv decomposes into FeO^M and $FeSi^M$. Such reactions would not be limited to Pv; other oxide phases such as ferropericlase or aluminous phases may also exhibit reactive tendencies with the core (e.g., Dubrovinsky et al., 2004). Some have speculated that FeO^M and $FeSi^M$ reaction products could accumulate in the CMB region as solid phases (Buffett et al., 2000; Kellogg and King, 1993; Manga and Jeanloz, 1996); however, the melting temperature of either species is ~4000 K or less (Fischer and Campbell, 2010; Lord et al., 2010), very similar to estimates of the present CMB temperature. The CMB was much hotter in the first 3 Gy of the Earth's history, ensuring that FeO and/or FeSi would have been molten at the CMB in the past, possibly only reaching the liquidus temperature in recent geologic history. Indeed, recent studies (e.g., Asahara et al., 2007; Frost et al., 2010; Komabayashi, 2014; Ozawa et al., 2009; Tsuno et al., 2013) view core–mantle reactions in the Earth as a coupled dissolution of O (and possibly Si) into the liquid metal core as metallic alloying species, instead of forming stoichiometric solid phases as products.

The Knittle–Jeanloz reaction suggests that the behavior of oxygen exerts an important influence upon CMB reactions. Consider simple dissolution of ferric iron oxide from silicate (*Sil*) into liquid metal (*M*) at equilibrium:

$$FeO^{Sil} \rightleftharpoons O^M + Fe^M. \qquad [18]$$

This equilibrium follows a relation involving a Gibbs free energy change for the reaction ΔG_r according to,

$$K^{M/Sil} = \frac{a_{Fe}^M a_O^M}{a_{FeO}^{Sil}} = \left(\frac{\gamma_{Fe}^M \gamma_O^M}{\gamma_{FeO}^{Sil}}\right)\left(\frac{X_{Fe}^M X_O^M}{X_{FeO}^{Sil}}\right) = \exp\left(\frac{\Delta G_r}{RT}\right), \qquad [19]$$

where K is the (metal–silicate) equilibrium constant, a is the activity of a component (subscript) in a given phase (superscript), γ is the activity coefficient of a component in the designated phase, X is the mole fraction of component in the phase, and R is the gas constant. In the ideal case, at a given pressure, the activity coefficients are unity and the temperature dependence follows the usual Arrhenius relation, with higher temperatures favoring the higher entropy side of the equilibrium (in this case, the metal components). The pressure dependence of the equilibrium, on the other hand, is governed by volume changes of species from the left side to the right side. For example, if the partial molar volume of oxygen in the metal is relatively large in comparison with its partial molar volume in oxides, then reactions involving incorporation of oxygen into the metal will be impeded at elevated pressures. Past debates focused on the possibility of either a diminishing oxygen solubility in metal with increasing pressure (e.g., Rubie et al., 2004) or only a modest change with pressure (e.g., Walker et al., 2002). Some of the early work on this system was performed at relatively low pressures and was not representative of the behavior of the high pressure (hcp) form of iron. However, recent experiments at greater pressures and temperatures (Asahara et al., 2007; Ozawa et al., 2008, 2009; Tsuno et al., 2013) and thermodynamic models (Frost et al., 2010; Komabayashi, 2014) typically yield little or no discernible pressure dependence for the reaction [18]. Thus, the emerging picture is one in which oxygen solubility is only weakly dependent upon pressure but exhibits at least an Arrhenius dependence in temperature. The activity coefficients relevant to this reaction are not well constrained at core conditions, although recent experimental evidence argues for approximately ideal behavior (Komabayashi, 2014). Note that these coefficients can vary with temperature, pressure, and composition; thus, a thorough description of equilibrium is somewhat complex.

The coupled behavior of silicon and oxygen at CMB conditions is also an important consideration, since both species are not mutually soluble in liquid iron at ambient pressures. One way of describing coupled Si and O behavior is to invoke a Si/O exchange equilibrium:

$$SiO_2^{Sil} + 2Fe^M \rightleftharpoons Si^M + 2FeO^{Sil} \qquad [20]$$

Previous experimental work has been divided, with some supporting the incorporation of oxygen and silicon

together Takafuji et al. (2005) and others indicating a limited mutual solubility of oxygen and silicon in metal (e.g., Mann et al., 2009; Ricolleau et al., 2011). A recent model has been proposed that yields a significant enhancement in coupled Si + O solubility in metals at temperatures above ~3000 K (Tsuno et al., 2013). Other recent models consider equilibrium between the volumetrically dominant lower-mantle phases $(Mg,Fe)SiO_3^{Pv}$ and $(Mg,Fe)O^{Pe}$ (Pe = periclase) and (liquid metal) iron, for which the equilibrium can be expressed as

$$FeO^{Pe} \rightleftharpoons Fe^{M} + O^{M}, \quad [21]$$

$$FeSiO_3^{Pv} \rightleftharpoons Fe^{M} + Si^{M} + 3O^{M}, \quad [22]$$

and for closure, one must also add another expression for the iron exchange between Pe and Pv:

$$FeSiO_3^{Pv} + MgO^{Pe} \rightleftharpoons MgSiO_3^{Pv} + FeO^{Pe}. \quad [23]$$

When calibrated with experimental data, this type of model predicts a strong tendency for oxygen to dissolve into the metal at CMB conditions and for typical mantle iron concentrations (e.g., Ozawa et al., 2009). While Si also dissolves into the metal, its tendency to dissolve into the metals is relatively modest. Thus, different models and experiments yield a variety of behaviors, and it is hoped that further work at higher temperatures and pressures will lead to better agreement.

One of the most interesting features of metal–silicate equilibrium models is that an increase in FeO in the silicates is coupled with an increase in oxygen dissolved in metal. For example, in eqn [19], the equilibrium constant is invariant if a_{FeO}^{Sil} increases in proportion to a_O^M. Thus, a higher oxygen content in the metal is associated with a higher iron fraction in the silicate, all else being equal. The recent models and experiments for equilibrium of FeO-bearing components in mantle phases with O dissolved in the core (Asahara et al., 2007; Frost et al., 2010; Ozawa et al., 2008, 2009) suggest that the amount of oxygen that would be present atop the core in equilibrium with typical mantle compositions (e.g., pyrolite, with $Mg\,Mg^{-1} + Fe \approx 90\%$) would exceed the 10 wt% total budget of impurity species in the isentropic convecting region of the outer core by a significant amount (i.e., by several tens of percent). The amount of oxygen in the core liquid is even larger if the base of the mantle is Fe-enriched, consistent with seismic inferences of ULVZ. Thus, these experiments initially seemed to present a kind of paradox, in that the mantle should either be depleted in iron or the core should contain more oxygen. Neither possibility is consistent with seismological constraints.

Asahara et al. (2007) proposed that the base of the mantle is depleted in iron, allowing the equilibrium partitioning to be compatible with the seismologically inferred density of the outer core. However, these models present problems for explaining seismic observations of very dense Fe-rich structures at the CMB (e.g., ULVZ as discussed previously). The models additionally assume that oxygen and/or silicon dissolved into the top of the core following such a reaction would be readily mixed downward into the deeper interior of the outer core. Even if this were to occur, such a process would increase the GPE of the core, thus impeding convection and generation of a geodynamo. For these reasons, a model with a Fe-depleted mantle side in equilibrium with the entire convecting outer core is not satisfactory.

As discussed previously, Buffett and Seagle (2010) proposed an alternative model in which dissolution of oxygen into the top of the core leads to the growth of a buoyant gravitationally stratified layer, since it is likely to be difficult for flows in the outer core to entrain material with a density anomaly of order 1%. In this scenario, the stratified layer encroaches downward into the top of the core from the CMB at a rate controlled by diffusion of oxygen, yielding a layer ~100 km thick over the age of the Earth. The very bottom of the layer could be partly entrained into core flows, presenting an energetic drag upon core convection, but this effect is more limited than the case where all reaction products become entrained into the convecting outer core and is self-regulated by the convective power available for driving convection. Also, since the top of the core is oxygen-enriched, the very bottom of the mantle need not be as depleted in iron. However, the base of the mantle is still depleted in FeO-bearing components in this model, leading to contradictions with seismological observations of very dense (likely Fe-rich) structures at the CMB.

One possibility to resolve all of these issues, while satisfying seismological observations, is that the very bottom of the mantle has been gradually enriched in FeO by processes such as fractional crystallization of liquid over geologic time, as proposed in the BMO model of Labrosse et al. (2007). This would increase the FeO content at the base of the mantle while also increasing the oxygen content at the top of the core. One would still arrive at an oxygen-enriched stratified layer atop the core similar to the Buffett and Seagle model, but in this case, the very base of the mantle would be left Fe-enriched, while the top of the core would contain relatively more oxygen (hence more buoyant and stable).

7.11.8.3.3 Core saturation?

Another possible means of transferring a significant amount of mass between the core and mantle is exsolution, in which a saturated species rises up to the CMB and ostensibly becomes part of the mantle. Precipitation of FeSi and/or FeO solid crystals from the outer core was suggested by Buffett et al. (2000); however, such a mechanism depends on saturation of the core fluid in Si and/or O, which may be unlikely if both are mutually soluble at high temperatures. Another kind of saturation mechanism is often suggested by Stevenson (2012). If some of the metal that formed the Earth's core equilibrated with oxides at very high temperatures during the Earth's formation, then they could possibly have ingested components such as magnesium, which would otherwise be very incompatible in the metal phase. With progressive core cooling, the mixture would become saturated in these components, which would precipitate out of the core and rise up to the CMB, possibly providing a buoyancy source for convection in the early core. A species such as Mg would actually precipitate as MgO, which would then react with the core fluid to form (Mg,Fe)O with a high ratio of FeO/FeO + MgO, thus stripping more oxygen from the core than magnesium and amplifying the buoyancy available for this process. The possibility for this kind of mechanism to occur, and the detailed time evolution of precipitation that would result, remains to be investigated.

7.11.8.4 Summary

Chemical disequilibrium between the core and mantle will give rise to reactions along the CMB, although the direction

of the reactions depends not only upon chemical properties but also on the complex evolution of the CMB region. The extent of such reactions depends critically upon the ability for the core and mantle materials to mix over length scales larger than permitted by diffusion alone. The key to understanding the evolution of core–mantle mass exchange through geologic history is improving our understanding of the chemical and physical properties of the core and mantle materials at CMB conditions. Further experimental and theoretical work to better constrain these properties is needed before we can improve our understanding of how the complex features in the CMB region may be produced by these mechanisms.

7.11.9 Concluding Remarks

The dynamical evolution and state of the Earth's CMB region are a very challenging but increasingly tractable geologic problem. This chapter only touches upon some of the major research topics presently under way; however, the field is very broad and continues to evolve significantly on short timescales. Additionally, new frontiers are presently opening, such as establishing connections between the CMB region and the surface environment, as well as the inner core. Like any geologic environment, the present CMB region represents a convolution of a complex thermal and chemical evolution of the Earth since formation, and the grand challenge is to understand how all of the Earth's systems evolved over time to their present state and how they are linked to one another. We look forward to further advances in our understanding in the coming years and anticipate that a major revision of this chapter will be necessary after several years have elapsed.

Acknowledgments

The authors are grateful to Christine Houser for helping with the manuscript preparation; to Edward J. Garnero for contributing one of the figures; to Stephane Labrosse and David Gubbins for their insightful discussions; and to Shijie Zhong, Gerald Schubert, and David Bercovici for their helpful reviews that improved this chapter.

References

Agee CB and Walker D (1988) Static compression and olivine flotation in ultrabasic silicate liquid. *Journal of Geophysical Research B* 93: 3437–3449.

Akber-Knutson S, Steinle-Neumann G, and Asimow PD (2005) Effect of Al on the sharpness of the MgSiOs perovskite to post-perovskite phase transition. *Geophysical Research Letters* 32: L14303. http://dx.doi.org/10.1029/2005GL023192.

Akins JA, Luo S-N, Asimow PD, and Ahrens TJ (2004) Shock-induced melting of $MgSiO_3$ and implications for melts in Earth's lowermost mantle. *Geophysical Research Letters* 31: L14612.

Albarède F (1998) Time-dependent models of UThHe and KAr evolution and the layering of mantle convection. *Chemical Geology* 145: 413–429.

Alexandrakis C and Eaton DW (2010) Precise seismic-wave velocity atop Earth's core: No evidence for outer-core stratification. *Physics of the Earth and Planetary Interiors* 180: 59–65.

Alfé D, Gillan MJ, and Price GD (2002) Composition and temperature of the Earth's core constrained by combining ab initio calculations and seismic data. *Earth and Planetary Science Letters* 195: 91–98.

Ammann MW, Brodholt JP, Wookey J, and Dobson DP (2010) First-principles constraints on diffusion in lower-mantle minerals and a weak *D″* layer *Nature* 465(7297): 462–465.

Andrault D, Munoz M, Bolfan-Casanova N, Guignot N, Perrillat J-P, Aquilanti G, and Pascarelli S (2010) Experimental evidence for perovskite and post-perovskite coexistence throughout the whole *D″* region *Earth and Planetary Science Letters* 293: 90–96.

Andrault D, Bolfan-Casanova N, Lo Nigro G, Bouhifd MA, Garbarino G, and Mezouar M (2011) Solidus and liquidus profiles of chondritic mantle: Implication for melting of the Earth across its history. *Earth and Planetary Science Letters* 304: 251–259. http://dx.doi.org/10.1016/j.epsl.2011.02.006.

Andrault D, Petitgirard S, Nigro GL, Devidal JL, Veronesi G, Garbarino G, and Mezouar M (2012) Solid–liquid iron partitioning in Earth's deep mantle. *Nature* 487: 354–359.

Antolik M, Gu Y, Ekstrom G, and Dziewonski A (2003) J362D28: A new joint model of compressional and shear velocity in the Earth's mantle. *Geophysical Journal International* 153: 443–466.

Asahara Y, Frost DJ, and Rubie DC (2007) Partitioning of FeO between magnesiowüstite and liquid iron at high pressures and temperatures: Implications for the composition of the Earth's outer core. *Earth and Planetary Science Letters* 257: 435–449. http://dx.doi.org/10.1016/j.epsl.2007.03.006.

Aubert J, Amit H, Hulot G, and Olson P (2008) Thermochemical flows couple the Earth's inner core growth to mantle heterogeneity. *Nature* 454: 758–761. http://dx.doi.org/10.1038/nature07109.

Auzende A-L, Badro J, Ryerson FJ, Weber PK, Fallon SJ, Addad A, Siebert J, and Fiquet G (2008) Element partitioning between magnesium silicate perovskite and ferropericlase: New insights into bulk lower-mantle geochemistry. *Earth and Planetary Science Letters* 269: 164–174. http://dx.doi.org/10.1016/j.epsl.2008.02.001.

Avants M, Lay T, Russell SA, and Garnero EJ (2006) Shear velocity variation within the *D″* region beneath the central Pacific *Journal of Geophysical Research* 111: B05305. http://dx.doi.org/10.1029/2004JB003270.

Badro J, Rueff J-P, Vanko G, Monaco G, Fiquet G, and Guyot F (2004) Electronic transitions in perovskite: Possible nonconvecting layers in the lower mantle. *Science* 305: 383–386.

Beggan C and Whaler K (2008) Core flow modelling assumptions. *Physics of the Earth and Planetary Interiors* 167: 217–222.

Berryman JG (2000) Seismic velocity decrement ratios for regions of partial melt in the lower mantle. *Geophysical Research Letters* 27: 421–424.

Bi Y, Tan H, and Jing F (2002) Electrical conductivity of iron under shock compression up to 200 GPa. *Journal of Physics: Condensed Matter* 14: 10849–10854.

Birch F (1964) Density and composition of the mantle and core. *Journal of Geophysical Research* 69: 4377–4388.

Bloxham J and Jackson A (1991) Fluid flow near the surface of Earth's outer core. *Reviews of Geophysics* 29: 97–120.

Boehler R (2000) High-pressure experiments and the phase diagram of lower mantle and core constituents. *Reviews of Geophysics* 38: 221–245.

Bolton H and Masters G (2001) Travel times of P and S from the global digital seismic networks: Implications for the relative variation of P and S velocity in the mantle. *Journal of Geophysical Research* 106: 13527–13540.

Bower DJ, Gurnis M, and Seton M (2013) Lower mantle structure from paleogeographically constrained dynamic Earth models. *Geochemistry, Geophysics, Geosystems* 14(1): 44–63.

Braginsky SI (1963) Structure of the F layer and reasons for convection in the Earth's core. *Doklady Akademii Nauk SSSR* 149: 8–10.

Braginsky SI (2007) Formation of the stratified ocean of the core: A ternary alloy model. *Earth and Planetary Science Letters* 253: 507–512.

Braginsky SI and Roberts PH (1995) Equations governing convection in Earth's core and the geodynamo. *Geophysical and Astrophysical Fluid Dynamics* 79: 1–97.

Brandenburg JP and van Keken PE (2007a) Deep storage of oceanic crust in a vigorously convecting mantle. *Journal of Geophysical Research-Solid Earth* 112(B6).

Brandenburg JP and van Keken PE (2007b) Methods for thermochemical convection in Earth's mantle with force-balanced plates. *Geochemistry, Geophysics, Geosystems* 8.

Brandenburg JP, Hauri EH, van Keken PE, and Ballentine CJ (2008) A multiple-system study of the geochemical evolution of the mantle with force-balanced plates and thermochemical effects. *Earth and Planetary Science Letters* 276(1–2): 1–13.

Brandon AD and Walker RJ (2005) The debate over core–mantle interaction. *Earth and Planetary Science Letters* 232: 211–225.

Breger L and Romanowicz B (1998) Three-dimensional structure at the base of the mantle beneath the central Pacific. *Science* 282(5389): 718–720.

Buffett BA (2002) Estimates of heat flow in the deep mantle based on the power requirements for the geodynamo. *Geophysical Research Letters* 29, GL014649.
Buffett BA (2007) A bound on heat flow below a double crossing of the perovskite–postperovskite phase transition. *Geophysical Research Letters* 34: L17302. http://dx.doi.org/10.1029/2007GL030930.
Buffett BA and Seagle CT (2010) Stratification of the top of the core due to chemical interactions with the mantle. *Journal of Geophysical Research* 115: B04407. http://dx.doi.org/10.1029/2009JB006751.
Buffett BA, Garnero EJ, and Jeanloz R (2000) Sediments at the top of the Earth's core. *Science* 290: 1338–1342.
Bull AL, McNamara AK, and Ritsema J (2009) Synthetic tomography of plume clusters and thermochemical piles. *Earth and Planetary Science Letters* 278(3–4): 152–162.
Bull AL, McNamara AK, Becker TW, and Ritsema J (2010) Global scale models of the mantle flow field predicted by synthetic tomography models. *Physics of the Earth and Planetary Interiors* 182(3–4): 129–138.
Bullen KE (1949) Compressibility-pressure hypothesis and the Earth's interior. *Monthly Notices of the Royal Astronomical Society Supplement* 5: 355–368.
Bunge H-P, Richards MA, Lithgow-Bertelloni C, Baumgardner JR, Grand SP, and Romanowicz B (1998) Time scales and heterogeneous structure in geodynamic Earth models. *Science* 280(5360): 91–95.
Burke K and Torsvik TH (2004) Derivation of Large Igneous Provinces of the past 200 million years from long-term heterogeneities in the deep mantle. *Earth and Planetary Science Letters* 227(3–4): 531–538.
Burke K, Steinberger B, Torsvik TH, and Smethurst MA (2008) Plume Generation Zones at the margins of large low shear velocity provinces on the core–mantle boundary. *Earth and Planetary Science Letters* 265: 49–60.
Cadio C, Panet I, Davaille A, Diament M, Metivier L, and de Viron O (2011) Pacific geoid anomalies revisited in light of thermochemical oscillating domes in the lower mantle. *Earth and Planetary Science Letters* 306(1–2): 123–135.
Caldeira K and Rampino MR (1991) The mid-Cretaceous super plume, carbon dioxide, and global warming. *Geophysical Research Letters* 18: 987–990. http://dx.doi.org/10.1029/91GL01237.
Carlson RW (1994) Mechanisms of Earth differentiation: Consequences for the chemical structure of the mantle. *Reviews of Geophysics* 32(4): 337–361.
Catalli K, Shim S-H, and Prakapenka V (2009) Thickness and clapeyron slope of the post-perovskite boundary. *Nature* 462: 782–786. http://dx.doi.org/10.1038/nature08598.
Christensen UR (2006) A deep rooted dynamo for Mercury. *Nature* 444: 1056–1058.
Christensen UR and Hofmann AW (1994) Segregation of subducted oceanic crust in the convecting mantle. *Journal of Geophysical Research B* 99: 19867–19884.
Clark SP (1957) Absorption spectra of some silicates in the visible and near infrared. *American Mineralogist* 43: 732–742.
Clement BM (1991) Geographical distribution of transitional VGPs: Evidence for non-zonal equatorial symmetry during the Matuyama-Brunhes geomagnetic reversal. *Earth and Planetary Science Letters* 104: 48–58.
Cobden L and Thomas C (2013) The origin of *D″* reflections: A systematic study of seismic array data sets. *Geophysical Journal International* 194: 1091–1118. http://dx.doi.org/10.1093/gji/ggt152.
Coltice N and Ricard Y (1999) Geochemical observations and one layer mantle convection. *Earth and Planetary Science Letters* 174: 125–137.
Condie KC (2001) *Mantle Plumes and Their Record in Earth History*. Cambridge University Press.
Conrad CP, Steinberger B, and Torsvik TH (2013) Stability of active mantle upwelling revealed by net characteristics of plate tectonics. *Nature* 498(7455): 479–482.
Cormier VF (2000) *D″* as a transition in the heterogeneity spectrum of the lowermost mantle *Journal of Geophysical Research* 105: 16193–16205.
Costin SO and Buffett BA (2004) Preferred reversal paths caused by a heterogeneous conducting layer at the base of the mantle. *Journal of Geophysical Research* 109: B06101. http://dx.doi.org/10.1029/2003JB002853.
Cottaar S and Romanowicz B (2012) An unusually large ULVZ at the base of the mantle near Hawaii. *Earth and Planetary Science Letters* 355–356: 213–222. http://dx.doi.org/10.1016/j.epsl.2012.09.005.
Courtillot V and Olson P (2007) Mantle plumes link magnetic superchrons to phanerozoic mass depletion events. *Earth and Planetary Science Letters* 260: 495–504. http://dx.doi.org/10.1016/j.epsl.2007.06.003.
Courtillot V, Jaeger JJ, Yang Z, Feraud G, and Hofmann C (1996) The influence of continental flood basalts on mass extinctions: Where do we stand? *GSA Special Papers* 307: 513–525. http://dx.doi.org/10.1130/0-8137-2307-8.513.
Courtillot V, Davaille A, Besse J, and Stock J (2003) Three distinct types of hotspots in the Earth's mantle. *Earth and Planetary Science Letters* 205(3–4): 295–308.
Crameri F, Tackley PJ, Meilick I, Gerya TV, and Kaus BJP (2012) A free plate surface and weak oceanic crust produce single-sided subduction on Earth. *Geophysical Research Letters* 39.
Davaille A (1999) Simultaneous generation of hotspots and superswells by convection in a heterogeneous planetary mantle. *Nature* 402: 756–760.
Davaille A, Girard F, and Le Bars M (2002) How to anchor plumes in a convecting mantle? *Earth and Planetary Science Letters* 203: 621–634.
Davaille A, Le Bars M, and Carbonne C (2003) Thermal convection in a heterogeneous mantle. *Comptes Rendus Geoscience* 335: 141–156.
Davaille A, Stutzmann E, Silveira G, Besse J, and Courtillot V (2005) Convective patterns under the Indo-Atlantic box. *Earth and Planetary Science Letters* 239(3–4): 233–252.
Davies DR, Goes S, Davies JH, Schuberth BSA, Bunge H-P, and Ritsema J (2012) Reconciling dynamic and seismic models of Earth's lower mantle: The dominant role of thermal heterogeneity. *Earth and Planetary Science Letters* 353–354: 253–269.
Davies GF (1988) Ocean bathymetry and mantle convection: 1. Large-scale flow and hotspots. *Journal of Geophysical Research* 93: 10467–10480.
Davies GF (2008) Episodic layering of the early mantle by the 'basalt barrier' mechanism. *Earth and Planetary Science Letters* 275(3–4): 382–392.
Davies GF and Gurnis M (1986) Interaction of mantle dregs with convection: Lateral heterogeneity at the core mantle boundary. *Geophysical Research Letters* 13: 1517–1520.
de Koker N, Steinle-Neumann G, and Vlcek V (2012) Electrical resistivity and thermal conductivity of liquid Fe alloys at high P and T, and heat flux in Earth's core. *Proceedings of the National Academy of Sciences* 190: 4070–4073.
de Wijs GA, Kresse G, Vocadlo L, Dobson D, Alfe D, Gillan MJ, and Price GD (1998) The viscosity of liquid iron under Earth's core conditions. *Nature* 392: 805–807.
Deguen R, Alboussiere T, and Brito D (2007) On the existence and structure of a mush at the inner core boundary of the Earth. *Physics of the Earth and Planetary Interiors* 164: 36–49. http://dx.doi.org/10.1016/j.pepi.2007.05.003.
Deschamps F and Tackley PJ (2008) Searching for models of thermo-chemical convection that explain probabilistic tomography. I. Principles and influence of rheological parameters. *Physics of the Earth and Planetary Interiors* 171(1–4): 357–373.
Deschamps F and Tackley PJ (2009) Searching for models of thermo-chemical convection that explain probabilistic tomography. II. Influence of physical and compositional parameters. *Physics of the Earth and Planetary Interiors* 176(1–2): 1–18.
Deschamps F and Trampert J (2003) Mantle tomography and its relation to temperature and composition. *Physics of the Earth and Planetary Interiors* 140(4): 277–291.
Deschamps F, Kaminski E, and Tackley PJ (2011) A deep mantle origin for the primitive signature of ocean island basalt. *Nature Geoscience* 4(12): 879–882.
Deschamps F, Cobden L, and Tackley PJ (2012) The primitive nature of large low shear-wave velocity provinces. *Earth and Planetary Science Letters* 349–350: 198208.
Dewaele A, Loubeyre P, Occelli F, Mezouar M, Dorogokupets PI, and Torrent M (2006) Quasihydrostatic equation of state of iron above 2 mbar. *Physical Review Letters* 97: 215504.
Dobson DP and Brodholt JP (2005) Subducted banded iron formations as a source of ultralow-velocity zones at the core–mantle boundary. *Nature* 434: 371–374.
Dobson DP, Miyajima N, Nestola F, Alvaro M, Casati N, Liebske C, Wood IG, and Walker AM (2013) Inherited textures during the perovskite to post-perovskite transition and seismic anisotropy in *D″* *Nature Geoscience* 6: 575–578.
Doornbos DJ and Husebye ES (1972) Array analysis of PKP phases and their precursors. *Physics of the Earth and Planetary Interiors* 5: 387–399.
Driscoll P and Olson P (2011) Superchron cycles driven by variable core heat flow. *Geophysical Research Letters* 38(9).
Dubrovinsky L, Dubrovinskaia N, and Langenhorst F (2004) Reaction of iron and silica at core–mantle boundary conditions. *Physics of the Earth and Planetary Interiors* 146: 243–247.
Duncan RA and Richards MA (1991) Hotspots, mantle plumes, flood basalts, and true polar wander. *Reviews of Geophysics* 29(1): 31–50.
Dziewonski AM and Anderson DL (1981) Preliminary reference Earth model. *Physics of the Earth and Planetary Interiors* 25: 297–356.
Dziewonski AM, Hager BH, and O'Connell RJ (1977) Large-scale heterogeneities in the lower mantle. *Journal of Geophysical Research* 82: 239–255.
Dziewonski AM, Lekic V, and Romanowicz B (2010) Mantle anchor structure: An argument for bottom up tectonics. *Earth and Planetary Science Letters* 299(1–2): 69–79.
Eaton DW and Kendall J-M (2006) Improving seismic resolution of outermost core structure by multichannel analysis and deconvolution of broadband SmKS phases. *Physics of the Earth and Planetary Interiors* 155: 104–119.
Engdahl ER, van der Hilst RD, and Berrocal J (1995) Imaging of subducted lithosphere beneath South America. *Geophysical Research Letters* 22(16): 2317–2320.
Farnetani CG (1997) Excess temperature of mantle plumes: The role of chemical stratification across *D″* . *Geophysical Research Letters* 24: 1583–1586.

Farnetani CG and Samuel H (2003) Lagrangian structures and stirring in the Earth's mantle. *Earth and Planetary Science Letters* 206(3–4): 335–348.
Fearn DR and Loper DE (1981) Compositional convection and stratification of Earth's core. *Nature* 289: 393–394.
Fiquet G, Auzende AL, Siebert J, Corgne A, Bureau H, Ozawa H, and Garbarino G (2010) Melting of peridotite to 140 Gigapascals. *Science* 329: 1516. http://dx.doi.org/10.1126/science.1192448.
Fischer RA and Campbell AJ (2010) High pressure melting of wüstite. *American Mineralogist* 95: 1473–1477.
Flores C and Lay T (2005) The trouble seeing double. *Geophysical Research Letters* 32, L24305.
Ford SR, Garnero EJ, and McNamara AK (2006a) A strong lateral shear velocity gradient and anisotropy heterogeneity in the lowermost mantle beneath the southern pacific. *Journal of Geophysical Research-Solid Earth* 111(B3).
Ford SR, Garnero EJ, and McNamara AK (2006b) A strong lateral shear velocity gradient and anisotropy heterogeneity in the lowermost mantle beneath the southern Pacific. *Journal of Geophysical Research* 111: B03306. http://dx.doi.org/10.1029/2004JB003574.
Forte AM and Mitrovica JX (2001) Deep-mantle high-viscosity flow and thermochemical structure inferred from seismic and geodynamic data. *Nature* 410: 1049–1056.
Frost DJ, Asahara Y, Rubie DC, Miyajima N, Dubrovinsky LS, Holzapfel C, Ohtani E, Miyahara M, and Sakai T (2010) Partitioning of oxygen between the Earth's mantle and core. *Journal of Geophysical Research* 115: B02202. http://dx.doi.org/10.1029/2009JB006302.
Fukao Y, Obayashi M, Inoue H, and Nenbai M (1992) Subducting slabs stagnant in the mantle transition zone. *Journal of Geophysical Research-Solid Earth* 97(B4): 4809–4822.
Garnero EJ and Helmberger DV (1995) On seismic resolution of lateral heterogeneity in the Earth's outermost core. *Physics of the Earth and Planetary Interiors* 88: 117–130.
Garnero EJ and Helmberger DV (1996) Seismic detection of a thin laterally varying boundary layer at the base of the mantle beneath the central-Pacific. *Geophysical Research Letters* 23: 977–980.
Garnero EJ and McNamara AK (2008) Structure and dynamics of Earth's lower mantle. *Science* 320: 626–628.
Garnero EJ, Helmberger DV, and Grand SP (1993a) Constraining outermost core velocity with SmKS waves. *Geophysical Research Letters* 20: 2463–2466.
Garnero EJ, Helmberger DV, and Grand SP (1993b) Preliminary evidence for a lower mantle shear wave velocity discontinuity beneath the central Pacific. *Physics of the Earth and Planetary Interiors* 79: 335–347.
Glatzmaier GA, Coe RS, Hongre L, and Roberts PH (1999) The role of the Earth's mantle in controlling the frequency of geomagnetic reversals. *Nature* 401: 885–890.
Gomi H, Ohta K, Hirose K, Labrosse S, Caracas R, Verstraete MJ, and Hernlund JW (2013) The high conductivity of iron and thermal evolution of the Earth's core. *Physics of the Earth and Planetary Interiors* 224: 88–103.
Goncharov AF, Beck P, Struzhkin VV, Haugen BD, and Jacobsen SD (2007) Thermal conductivity of lower mantle minerals. *Physics of the Earth and Planetary Interiors*, http://dx.doi.org/10.1016/j.pepi.2008.07.033.
Goncharov AF, Haugen BD, Struzhkin VV, Beck P, and Jacobsen SD (2008) Radiative conductivity in the Earth's lower mantle. *Nature* 456: 231–234.
Gonnermann HM and Mukhopadhyay S (2007) Non-equilibrium degassing and a primordial source for helium in ocean-island volcanism. *Nature* 449(7165): 1037–1040.
Gonnermann HM and Mukhopadhyay S (2009) Preserving noble gases in a convecting mantle. *Nature* 459(7246): 560–563.
Grand SP (1994) Mantle shear structure beneath the Americas and surrounding oceans. *Journal of Geophysical Research* 99: 11591–11621.
Grand SP (2002) Mantle shear-wave tomography and the fate of subducted slabs. *Philosophical Transactions: Mathematical, Physical and Engineering Sciences* 360(1800): 2475–2491.
Grand SP, van der Hilst RD, and Widiyantoro S (1997) Global seismic tomography: A snapshot of convection in the Earth. *GSA Today* 7: 1–7.
Grocholski B, Catalli K, Shim S-H, and Prakapenka V (2012) Mineralogical effects on the detectability of the postperovskite boundary. *Proceedings of the National Academy of Sciences*, http://dx.doi.org/10.1073/pnas.1109204109.
Gu YJ, Dziewonski AM, Su WJ, and Ekstrom G (2001) Models of the mantle shear velocity and discontinuities in the pattern of lateral heterogeneities. *Journal of Geophysical Research, Solid Earth* 106(B6): 11169–11199.
Gubbins D (2007a) Geomagnetic constraints on stratification at the top of the Earth's core. *Earth, Planets and Space* 59: 661–664.
Gubbins D and Davies CJ (2013) The stratified layer at the core–mantle boundary caused by barodiffusion of oxygen, sulphur and silicon. *Physics of the Earth and Planetary Interiors* 215: 21–28.
Gubbins D, Alfe D, Masters G, Price GD, and Gillan MJ (2003) Can the Earth's dynamo run on heat alone? *Geophysical Journal International* 155: 609–622.
Gubbins D, Willis AP, and Sreenivasan B (2007) Correlation of Earth's magnetic field with lower mantle thermal and seismic structure. *Physics of the Earth and Planetary Interiors* 162: 256–260.
Gunnarsson O, Calandra M, and Han JE (2003) Colloquium: Saturation of electrical resistivity. *Reviews of Modern Physics* 75: 1085–1099.
Gurnis M (1986) The effects of chemical density differences on convective mixing in the Earth's mantle. *Journal of Geophysical Research B* 91: 1407–1419.
Gurnis M and Hager BH (1988) Controls of the structure of subducted slabs. *Nature* 335(6188): 317–321.
Hager BH (1984) Subducted slabs and the geoid: Constraints on mantle rheology and flow. *Journal of Geophysical Research* 89: 6003–6015. http://dx.doi.org/10.1029/JB089iB07p06003.
Hager BH and Richards MA (1989) Long-wavelength variations in Earth's geoid: Physical models and dynamical implications. *Philosophical Transactions of the Royal Society A: Mathematical, Physical and Engineering Sciences* 328(1599): 309–327.
Hales AL and Roberts JL (1971) The velocities in the outer core. *Bulletin of the Seismological Society of America* 61: 1051–1059.
Hansen U and Yuen DA (1988) Numerical simulations of thermal-chemical instabilities at the core mantle boundary. *Nature* 334: 237–240.
He Y and Wen LX (2012) Geographic boundary of the Pacific Anomaly and its geometry and transitional structure in the north. *Journal of Geophysical Research* 117: B09308. http://dx.doi.org/10.1029/2012JB009436.
He YM and Wen LX (2009) Structural features and shear-velocity structure of the "pacific anomaly" *Journal of Geophysical Research-Solid Earth* 114.
He YM, Wen LX, and Zheng TY (2006) Geographic boundary and shear wave velocity structure of the "pacific anomaly" near the core–mantle boundary beneath western pacific. *Earth and Planetary Science Letters* 244(1–2): 302–314.
Helffrich G (2012) How light element addition can lower core liquid wave speeds. *Geophysical Journal International* 188: 1065–1070. http://dx.doi.org/10.1111/j.1365-246X.2011.05295.x.
Helffrich G and Kaneshima S (2004) Seismological constraints on core composition from Fe–O–S liquid immiscibility. *Science* 306: 2239–2242.
Helffrich G and Kaneshima S (2010) Outer-core compositional stratification from observed core wave speed profiles. *Nature* 468: 807–810. http://dx.doi.org/10.1038/nature09636.
Helffrich G and Kaneshima S (2013) Causes and consequences of outer core stratification. *Physics of the Earth and Planetary Interiors* 223: 2–7. http://dx.doi.org/10.1016/j.pepi.2013.07.005.
Helmberger D, Ni S, Wen LX, and Ritsema J (2000) Seismic evidence for ultralow-velocity zones beneath Africa and eastern Atlantic. *Journal of Geophysical Research* 105: 23865–23878.
Helmberger DV, Wen L, and Ding X (1998) Seismic evidence that the source of the Iceland hotspot lies at the core–mantle boundary. *Nature* 396: 251–255.
Hemley RJ and Kubicki JD (1991) Deep mantle melting. *Nature* 349: 283–284.
Hernlund J (2013) Mantle fabric unravelled? *Nature Geoscience* 6: 516–518. http://dx.doi.org/10.1038/ngeo1868.
Hernlund JW (2010) On the interaction of the geotherm with a post-perovskite phase transition in the deep mantle. *Physics of the Earth and Planetary Interiors* 180: 222–234.
Hernlund JW and Houser C (2008) On the distribution of seismic velocities in Earth's deep mantle. *Earth and Planetary Science Letters* 265: 423–437. http://dx.doi.org/10.1016/j.epsl.2007.10.042.
Hernlund JW and Jellinek M (2010) Dynamics and structure of a stirred partially molten ultralow-velocity zone. *Earth and Planetary Science Letters* 296: 1–8. http://dx.doi.org/10.1016/j.epsl.2010.04.027.
Hernlund JW and Labrosse S (2007) Geophysically consistent values of the perovskite to post-perovskite transition Clapeyron slope. *Geophysical Research Letters* 34: L05309. http://dx.doi.org/10.1029/2006GL028961.
Hernlund JW and Tackley PJ (2007) Some dynamical consequences of partial melting at the base of Earth's mantle. *Physics of the Earth and Planetary Interiors* 162: 149–163.
Hernlund JW, Thomas C, and Tackley PJ (2005) A doubling of the post-perovskite phase boundary and structure of the Earth's lowermost mantle. *Nature* 434: 882–886. http://dx.doi.org/10.1038/nature03472.
Herzberg C, Condie K, and Korenaga J (2010) Thermal history of the Earth and its petrological expression. *Earth and Planetary Science Letters* 292: 79–88.

Hier-Majumder S (2004) Influence of contiguity on seismic velocities of partially molten aggregates. *Journal of Geophysical Research* 113: B12205, http://dx.doi.org/10.1029/2008JB005662.
Hirose K, Fei YW, Ma YZ, and Mao HK (1999) The fate of subducted basaltic crust in the Earth's lower mantle. *Nature* 397(6714): 53–56.
Hirose K, Takafuji N, Sata N, and Ohishi Y (2005) Phase transition and density of subducted MORB crust in the lower mantle. *Earth and Planetary Science Letters* 237(1–2): 239–251.
Hirose K, Sinmyo R, Sata N, and Ohishi Y (2006) Determination of post-perovskite phase transition in $MgSiO_3$ using Au and MgO pressure standards. *Geophysical Research Letters* 33: L01310.
Hirose K, Labrosse S, and Hernlund J (2013) Composition and state of the core. *Annual Review of Earth and Planetary Sciences* 41: 657–691. http://dx.doi.org/10.1146/annurev-earth-050212-124007.
Hofmann AW (1997) Mantle geochemistry: The message from oceanic volcanism. *Nature* 385: 219–229.
Hofmann AW and White WM (1982) Mantle plumes from ancient oceanic crust. *Earth and Planetary Science Letters* 57: 421–436.
Hofmeister AM (1999) Mantle values of thermal conductivity and the geotherm from phonon lifetimes. *Science* 283: 1699–1706.
Houser C, Masters G, Shearer P, and Laske G (2008) Shear and compressional velocity models of the mantle from cluster analysis of long-period waveforms. *Geophysical Journal International* 174: 195–212. http://dx.doi.org/10.1111/j.1365-246X.2008.03763.x.
Humayun M, Qin L, and Norman MD (2004) Geochemical evidence for excess iron in the mantle beneath hawaii. *Science* 306: 91. http://dx.doi.org/10.1126/science.1101050.
Hunt SA, Weidner DJ, Li L, Wang L, Walte NP, Brodholt JP, and Dobson DP (2009) Weakening of calcium iridate during its transformation from perovskite to post-perovskite. *Nature Geoscience* 2: 794–797. http://dx.doi.org/10.1038/ngeo663.
Hunt SA, Davies DR, Walker AM, McCormack RJ, Wills AS, Dobson DP, and Li L (2012) On the increase in thermal diffusivity caused by the perovskite to post-perovskite phase transition and its implications for mantle dynamics. *Earth and Planetary Science Letters* 319320: 96–103.
Hutko AR, Lay T, Revenaugh J, and Garnero EJ (2008) Anticorrelated seismic velocity anomalies from post-perovskite in the lowermost mantle. *Science* 320: 1070–1074. http://dx.doi.org/10.1126/science.1155822.
Ishii M and Tromp J (1999) Normal-mode and free-air gravity constraints on lateral variations in velocity and density of the Earth's mantle. *Science* 285: 1231–1236.
Ishii M and Tromp J (2001) Even-degree lateral variations in the Earth's mantle constrained by free oscillations and the free-air gravity anomaly. *Geophysical Journal International* 145(1): 77–96.
Ishii M and Tromp J (2004a) Constraining large-scale mantle heterogeneity using mantle and inner-core sensitive normal modes. *Physics of the Earth and Planetary Interiors* 146: 113–124.
Ishii M and Tromp J (2004b) Constraining large-scale mantle heterogeneity using mantle and inner-core sensitive modes. *Physics of the Earth and Planetary Interiors* 146: 113–124.
Jaupart C, Labrosse S, and Mareschal J-C (2007) Temperatures, heat and energy in the mantle of the Earth. In: Bercovici D and Schubert G (eds.) *Treatise on Geophysics*, pp. 253–303. Amsterdam: Elsevier.
Jellinek AM and Manga M (2002) The influence of a chemical boundary layer on the fixity and lifetime of mantle plumes. *Nature* 418: 760–763.
Jellinek AM and Manga M (2004) Links between long-lived hotspots, mantle plumes, *D″*, and plate tectonics *Reviews of Geophysics* 42: RG3002. http://dx.doi.org/10.1029/2003RG000144.
Jellinek AM, Gonnermann HM, and Richards MA (2003) Plume capture by divergent plate motions: Implications for the distribution of hotspots, geochemistry of mid-ocean ridge basalts, and estimates of the heat flux at the core–mantle boundary. *Earth and Planetary Science Letters* 205: 361–378.
Jensen KJ, Thorne MS, and Rost S (2013) SPdKS analysis of ultralow-velocity zones beneath the western Pacific. *Geophysical Research Letters* 40: 1–5. http://dx.doi.org/10.1002/grl.50877.
Kanda RVS and Stevenson DJ (2006) Suction mechanism for iron entrainment into the lower mantle. *Geophysical Research Letters* 33: L02310. http://dx.doi.org/10.1029/2005GL025009.
Kawai K and Tsuchiya T (2009) Temperature profile in the lowermost mantle from seismological and mineral physics joint modeling. *Proceedings of the National Academy of Sciences of the United States of America* 106: 22119–22123. http://dx.doi.org/10.1073/pnas.0905920106.
Kawai K, Geller RJ, and Fuji N (2004a) *D″* beneath the Arctic from inversion of shear waveforms *Geophysical Research Letters* 34: L21305. http://dx.doi.org/10.1029/2007GL031517.
Kawai K, Takeuchi N, Geller RJ, and Fuji N (2007b) Possible evidence for a double crossing phase transition in *D″* beneath Central America from inversion of seismic waveforms *Geophysical Research Letters* 34: L09314. http://dx.doi.org/10.1029/2007GL029642.
Keeler RN and Mitchell AC (1969) Electrical conductivity, demagnetization, and the high-pressure phase transition in shock-compressed iron. *Solid State Communications* 7: 271–274.
Keller G (2005) Biotic effects of late Maastrichtian mantle plume volcanism: Implications for impacts and mass extinctions. *Lithos* 79: 317–341.
Kellogg LH and King SD (1993) Effect of mantle plumes on the growth of *D″* by reaction between the core and mantle *Geophysical Research Letters* 20: 379–382.
Kellogg LH, Hager BH, and van der Hilst RD (1999) Compositional stratification in the deep mantle. *Science* 283(5409): 1881–1884.
Kennett BLN and Engdahl ER (1991) Traveltimes for global earthquake location and phase identification. *Geophysical Journal International* 105: 429–465.
Kennett BLN, Engdahl ER, and Buland R (1995) Constraints on seismic velocities in the Earth from travel times. *Geophysical Journal International* 122: 108–124.
King SD (1997) Geoid and topographic swells over temperature-dependent thermal plumes in spherical-axisymmetric geometry. *Geophysical Research Letters* 24(23): 3093–3096.
Knittle E and Jeanloz R (1991) The Earth's core–mantle boundary: Results of experiments at high pressures and temperatures. *Science* 251: 1438–1443.
Komabayashi T (2014) Thermodynamics of melting relations in the system Fe–FeO: Implications for the oxygen content in the Earth's outer core. *Journal of Geophysical Research* 119: 4164–4177. http://dx.doi.org/10.1002/2014JB010980.
Kuo BY, Garnero EJ, and Lay T (2000) Tomographic inversion of S-SKS times for shear velocity heterogeneity in *D″*: Degree 12 and hybrid models *Journal of Geophysical Research-Solid Earth* 105(B12): 28139–28157.
Labrosse S (2002) Hotspots, mantle plumes and core heat loss. *Earth and Planetary Science Letters* 199: 147–156.
Labrosse S (2003) Thermal and magnetic evolution of the Earth's core. *Physics of the Earth and Planetary Interiors* 140: 127–143.
Labrosse S, Poirier J-P, and Le Mouël J-L (1997) On cooling of the Earth's core. *Physics of the Earth and Planetary Interiors* 99: 1–17.
Labrosse S, Hernlund JW, and Coltice N (2007) A crystallizing dense magma ocean at the base of the Earth's mantle. *Nature* 450: 866–869.
Laj C, Mazaud A, Weeks R, Fuller M, and Herrero-Bervera E (1991) Geomagnetic reversal paths. *Nature* 351: 447.
Larson R (1991) Latest pulse of Earth: Evidence for a mid-Cretaceous superplume. *Geology* 19: 547–550.
Lassak TM, McNamara AK, and Zhong S (2007) Influence of thermochemical piles on topography at Earth's core–mantle boundary. *Earth and Planetary Science Letters* 261(3–4): 443–455.
Lassak TM, McNamara AK, Garnero EJ, and Zhong SJ (2010) Core–mantle boundary topography as a possible constraint on lower mantle chemistry and dynamics. *Earth and Planetary Science Letters* 289(1–2): 232–241.
Lay T (1987) Structure of the Earth: Mantle and core. *Reviews of Geophysics* 25(6): 1161–1167.
Lay T (2007) Deep earth structure-lower mantle and *D″* In: Schubert G (ed.) *Treatise on Geophysics*, pp. 619–654. Elsevier.
Lay T and Garnero EJ (2011) Deep mantle seismic modeling and imaging. *Annual Review of Earth and Planetary Sciences* 39: 91–123.
Lay T and Helmberger DV (1983) A shear velocity discontinuity in the lower mantle. *Geophysical Research Letters* 10: 63–66.
Lay T and Young CJ (1990) The stably-stratified outermost core revisited. *Geophysical Research Letters* 17: 2001–2004.
Lay T, Williams Q, Garnero EJ, Kellogg L, and Wysession ME (1998) Seismic wave anisotropy in the *D″* region and its implications In: Gurnis M, Wysession ME, Knittle E, and Buffett BA (eds.) *The Core–Mantle Boundary Region*. *American Geophysical Union Monograph*, pp. 299–318.
Lay T, Garnero EJ, and Williams Q (2004) Partial melting in a thermo-chemical boundary layer at the base of the mantle. *Physics of the Earth and Planetary Interiors* 146: 441–467.
Lay T, Hernlund J, Garnero EJ, and Thorne MS (2006) A post-perovskite lens and *D″* heat flux beneath the central Pacific *Science* 314: 1272–1276. http://dx.doi.org/10.1126/science.1133280.
Le Bars M and Davaille A (2002) Stability of thermal convection in two superimposed miscible viscous fluids. *Journal of Fluid Mechanics* 471: 339–363.
Le Bars M and Davaille A (2004a) Whole layer convection in a heterogeneous planetary mantle. *Journal of Geophysical Research-Solid Earth* 109(B3).
Le Bars M and Davaille A (2004b) Large interface deformation in two-layer thermal convection of miscible viscous fluids. *Journal of Fluid Mechanics* 499: 75–110.

Lee C-T, Luffi P, Hoink T, Li J, Dasgupta R, and Hernlund JW (2010) Upside-down differentiation and generation of a primordial lower mantle. *Nature* 463: 930–935.
Lekic V, Cottaar S, Dziewonski AM, and Romanowicz B (2012) Cluster analysis of global lower mantle tomography: A new class of structure and implications for chemical heterogeneity. *Earth and Planetary Science Letters* 357–358: 68–77.
Li C, van der Hilst RD, Engdahl ER, and Burdick S (2008) A new global model for P wave speed variations in Earth's mantle. *Geochemistry, Geophysics, Geosystems* 9.
Li J and Agee CB (1996) Geochemistry of mantle–core differentiation at high pressure. *Nature* 381: 686–689. http://dx.doi.org/10.1038/381686a0.
Li M and McNamara AK (2013) The difficulty for subducted oceanic crust to accumulate at the Earth's core–mantle boundary. *Journal of Geophysical Research, Solid Earth* 1–10.
Li M, McNamara AK, and Garnero EJ (2014) Chemical complexity of hotspots caused by cycling oceanic crust through mantle reservoirs. *Nature Geoscience.* http://dx.doi.org/10.1038/ngeo2120.
Li XD and Romanowicz B (1996) Global mantle shear velocity model developed using nonlinear asymptotic coupling theory. *Journal of Geophysical Research-Solid Earth* 101(B10): 22245–22272.
Lithgow-Bertelloni C and Richards MA (1998) The dynamics of Cenozoic and Mesozoic plate motions. *Reviews of Geophysics* 36: 27–78.
Liu L and Bassett WA (1986) *Elements, Oxides, Silicates: High-Pressure Phases with Implications for the Earth's Interior*. Oxford University Press.
Loper DE (1978) Some thermal consequences of a gravitationally powered dynamo. *Journal of Geophysical Research* 83: 5961–5970.
Lord OT, Walter MJ, Dobson DP, Armstrong L, Clark SM, and Kleppe A (2010) The FeSi phase diagram to 150 GPa. *Journal of Geophysical Research* 115: B06208. http://dx.doi.org/10.1029/2009JB006528.
Luo S-N, Ni SD, and Helmberger DV (2001) Evidence for a sharp lateral variation of velocity at the core–mantle boundary from multipathed PKPab. *Earth and Planetary Science Letters* 189: 155–164.
Manga M and Jeanloz R (1996) Implications of a metal-bearing chemical boundary layer in *D″* for mantle dynamics *Geophysical Research Letters* 23: 3091–3094.
Manga M and Jeanloz R (1997) Thermal conductivity of corundum and periclase, implications for the lower mantle. *Journal of Geophysical Research* 102: 2999–3008.
Mann U, Frost DJ, and Rubie DC (2009) Evidence for high-pressure core–mantle differentiation from the metal-silicate partitioning of lithophile and weakly-siderophile elements. *Geochimica et Cosmochimica Acta* 73: 7360–7386.
Manners U (2008) *Investigating the Structure of the Core–Mantle Boundary Using S and P Diffracted Waves*. San Diego: University of California.
Manthilake MAGM, de Koker N, and Frost DJ (2011) Thermal conductivity of $CaGeO_3$ perovskite at high pressure. *Geophysical Research Letters* 38: L08301. http://dx.doi.org/10.1029/2011GL046882.
Mao HK and Bell PM (1972) Electrical conductivity and the red shift of absorption in olivine and spinel at high pressure. *Science* 176: 403–406.
Mao WL, Shen G, Prakapenka VB, Meng Y, Cambell AJ, Heinz D, Shu J, Hemley RJ, and Mao HK (2004) Ferromagnesian postperovskite silicates in the *D″* layer of the Earth *Proceedings of the National Academy of Sciences of the United States of America* 101: 15867–15869.
Mao WL, Mao H-K, Sturhahn W, Zhao J, Prakapenka VB, Shu J, Fei Y, and Hemley RJ (2006) Iron-rich post-perovskite and the origin of ultralow-velocity zones. *Science* 312: 564–565. http://dx.doi.org/10.1126/science.1123442.
Masters G, Johnson S, Laske G, and Bolton H (1996) A shear-velocity model of the mantle. *Philosophical Transactions of the Royal Society A: Mathematical, Physical and Engineering Sciences* 354: 1385–1411.
Masters G, Laske G, Bolton H, and Dziewonski A (2000) The relative behavior of shear velocity, bulk sound speed, and compressional velocity in the mantle: Implications for chemical and thermal structure. In: Karato S-I, Forte A, Liebermann R, Masters G, and Stixrude L (eds.) *Earth's Deep Interior: Mineral Physics and Tomography From the Atomic to Global Scale. American Geophysical Union Monograph*, pp. 63–87. American Geophysical Union.
Matassov G (1977) *The Electrical Conductivity of Iron-Silicon Alloys at High Pressures and the Earth's Core*. Rep UCRL-52322, Lawrence Livermore National Lab.
Matyska C, Moser J, and Yuen DA (1994) The potential influence of radiative heat transfer on the formation of megaplumes in the lower mantle. *Earth and Planetary Science Letters* 125: 255–266.
McCammon C, Kantor I, Narygina O, Rouquette J, Ponkratz U, Sergueev I, Mezouar M, Prakapenka V, and Dubrovinsky L (2008) Stable intermediate-spin ferrous iron in lower-mantle perovskite. *Nature Geoscience* 1: 684–687. http://dx.doi.org/10.1038/ngeo309.
McNamara AK and van Keken PE (2000) Cooling of the Earth: A parameterized convection study of whole versus layered models. *Geochemistry, Geophysics, Geosystems* 1. http://dx.doi.org/10.1029/2000GC000045.
McNamara AK and Zhong S (2004) Thermochemical structures within a spherical mantle: Superplumes or piles? *Journal of Geophysical Research B* 109: B07402.
McNamara AK and Zhong S (2005) Thermochemical structures under Africa and the Pacific Ocean. *Nature* 437: 1136–1139.
McNamara AK, Karato S, and van Keken PE (2001) Localization of dislocation creep in the lower mantle: Implications for the origin of seismic anisotropy. *Earth and Planetary Science Letters* 191: 85–99.
McNamara AK, van Keken PE, and Karato S (2003) Lattice-preferred orientation near the core-mantle boundary; A likely mechanism to produce seismic anisotropy. *Journal of Geophysical Research* 108: 2230. http://dx.doi.org/10.1029/2002JB001970.
McNamara AK, Garnero EJ, and Rost S (2010) Tracking deep mantle reservoirs with ultra-low velocity zones. *Earth and Planetary Science Letters* 299(1–2): 1–9.
McNutt MK (1998) Superswells. *Superswells. Reviews of Geophysics* 36(2): 211–244.
Meade C, Mao HK, and Hu J (1995) High-temperature phase transition and dissociation of (Mg, Fe)SiO_3 perovskite at lower mantle pressures. *Science* 268: 1743–1745. http://dx.doi.org/10.1126/science.268.5248.1743.
Megnin C and Romanowicz B (2000) The three-dimensional shear velocity structure of the mantle from the inversion of body, surface, and higher-mode waveforms. *Geophysical Journal International* 143: 709–728.
Miles JW (1961) On the stability of heterogeneous shear flows. *Journal of Fluid Mechanics* 10: 496508.
Mitchell BJ and Helmberger DV (1973) Shear velocities at the base of the mantle from observations of S and ScS. *Journal of Geophysical Research* 78: 6009–6020.
Mittelstaedt E and Tackley PJ (2005) Plume heat flow is much less than CMB heat flow. *Earth and Planetary Science Letters* 241: 202–210.
Miyagi L, Kanitpanyacharoen W, Stackhouse S, Militzer B, and Wenk HR (2011) The enigma of post-perovskite anisotropy: Deformation versus transformation textures. *Physics and Chemistry of Minerals* 38: 665–678. http://dx.doi.org/10.1029/2002JB001970.
Montelli R, Nolet G, Dahlen FA, Masters G, Engdahl R, and Hung S-H (2004) Finite-frequency tomography reveals a variety of plumes in the mantle. *Science* 303: 338–343. http://dx.doi.org/10.1126/science.1092485.
Morelli A and Dziewonski AM (1993) Body wave travel-times and a spherically symmetric P- and S-wave velocity model. *Geophysical Journal International* 112: 178–194.
Morgan WJ (1971) Convection plumes in the lower mantle. *Nature* 230: 42–43.
Mosenfelder JL, Asimow PD, Frost DJ, Rubie DC, and Ahrens TJ (2009) The $MgSiO_3$ system at high pressure: Thermodynamic properties of perovskite, postperovskite, and melt from global inversion of shock and static compression data. *Journal of Geophysical Research* 114: B01203. http://dx.doi.org/10.1029/2008JB005900.
Mukhopadhyay S (2012) Early differentiation and volatile accretion recorded in deep-mantle neon and xenon. *Nature* 486(7401): 101–104.
Murakami M, Hirose K, Sata N, Ohishi Y, and Kawamura K (2004) Phase transition of $MgSiO_3$ perovskite in the deep lower mantle. *Science* 304: 855–858.
Murakami M, Sinogeikin SV, Bass JD, Sata N, Ohishi Y, and Hirose K (2007) Sound velocity of $MgSiO_3$ post-perovskite phase: A constraint on the *D″* discontinuity *Earth and Planetary Science Letters* 259: 18–23.
Nakagawa T (2011) Effect of a stably stratified layer near the outer boundary in numerical simulations of a magnetohydrodynamic dynamo in a rotating spherical shell and its implications for Earth's core. *Physics of the Earth and Planetary Interiors* 187: 342–352. http://dx.doi.org/10.1016/j.pepi.2011.06.001.
Nakagawa T and Tackley PJ (2004a) Effects of thermo-chemical mantle convection on the thermal evolution of the Earth's core. *Earth and Planetary Science Letters* 220(1–2): 107–119.
Nakagawa T and Tackley PJ (2004b) Thermo-chemical structure in the mantle arising from a three-component convective system and implications for geochemistry. *Physics of the Earth and Planetary Interiors* 146: 125–138.
Nakagawa T and Tackley PJ (2005) The interaction between the post-perovskite phase change and a thermo-chemical boundary layer near the core–mantle boundary. *Earth and Planetary Science Letters* 238: 204–216.
Nakagawa T and Tackley PJ (2006) Three-dimensional structures and dynamics in the deep mantle: Effects of post-perovskite phase change and deep mantle layering. *Geophysical Research Letters* 33: L12S11. http://dx.doi.org/10.1029/2006GL025719.
Nakagawa T and Tackley PJ (2008) Lateral variations in CMB heat flux and deep mantle seismic velocity caused by a thermal-chemical-phase boundary layer in 3D spherical convection. *Earth and Planetary Science Letters* 271: 348–358.
Nakagawa T and Tackley PJ (2011) Effects of low-viscosity post-perovskite on thermo-chemical mantle convection in a 3-D spherical shell. *Geophysical Research Letters* 38.

Nakagawa T, Tackley PJ, Deschamps F, and Connolly JAD (2010) The influence of MORB and harzburgite composition on thermo-chemical mantle convection in a 3-D spherical shell with self-consistently calculated mineral physics. *Earth and Planetary Science Letters* 296(3–4): 403–412.

Ni S and Helmberger DV (2001) Probing an ultra-low velocity zone at the core mantle boundary with P and S waves. *Geophysical Research Letters* 28: 2345–2348.

Ni S, Tan E, Gurnis M, and Helmberger D (2002) Sharp sides to the African superplume. *Science* 296: 1850–1852.

Ni SD and Helmberger DV (2003a) Ridge-like lower mantle structure beneath South Africa. *Journal of Geophysical Research-Solid Earth* 108(B2).

Ni SD and Helmberger DV (2003b) Seismological constraints on the South African superplume; could be the oldest distinct structure on Earth. *Earth and Planetary Science Letters* 206(1–2): 119–131.

Ni SD and Helmberger DV (2003c) Further constraints on the African superplume structure. *Physics of the Earth and Planetary Interiors* 140(1–3): 243–251.

Ni SD, Helmberger DV, and Tromp J (2005) Three-dimensional structure of the African superplume from waveform modelling. *Geophysical Journal International* 161(2): 283–294.

Nomura R, Ozawa H, Tateno S, Hirose K, Hernlund J, Muto S, Ishii H, and Hiraoka N (2011) Spin crossover and iron-rich silicate melt in the Earth's deep mantle. *Nature* 473(7346): 199–202. http://dx.doi.org/10.1038/nature09940.

Nowacki A, Walker A, Wookey J, and Kendall J-M (2013) Evaluating post-perovskite as a cause of *D″* anisotropy in regions of palaeosubduction. *Geophysical Journal International* 192: 1085–1090. http://dx.doi.org/10.1093/gji/ggs068.

Oganov AR and Ono S (2004) Theoretical and experimental evidence for a post-perovskite phase of $MgSiO_3$ in Earth's *D″* layer. *Nature* 430: 445–448.

Oganov AR, Martoak R, Laio A, Raiteri P, and Parrinello M (2005) Anisotropy of Earth's *D″* layer and stacking faults in the $MgSiO_3$ post-perovskite phase. *Nature* 438: 1142–1144. http://dx.doi.org/10.1038/nature04439.

Ohta K, Hirose K, and Hernlund J (2012) Lattice thermal conductivity of $MgSiO_3$ perovskite and post-perovskite at the core–mantle boundary. *Earth and Planetary Science Letters* 349350: 109–115.

Ohtani E and Maeda M (2001) Density of basaltic melt at high pressure and stability of the melt at the base of the lower mantle. *Earth and Planetary Science Letters* 193: 69–75.

Oldham D and Davies JH (2004) Numerical investigation of layered convection in a three-dimensional shell with application to planetary mantles. *Geochemistry, Geophysics, Geosystems* 5.

Olson P and Kincaid C (1991) Experiments on the interaction of thermal-convection and compositional layering at the base of the mantle. *Journal of Geophysical Research B* 96: 4347–4354.

Olson P, Schubert G, and Anderson C (1987) Plume formation in the *D″*-layer and the roughness of the core–mantle boundary. *Nature* 327: 409–413.

Olson P, Schubert G, and Anderson C (1993) Structure of axisymmetric mantle plumes. *Journal of Geophysical Research* 98(B4): 6829–6844.

Ono S (2008) Experimental constraints on the temperature profile in the lower mantle. *Physics of the Earth and Planetary Interiors* 170: 267–273. http://dx.doi.org/10.1016/j.pepi.2008.06.033.

Ono S and Oganov AR (2005) In situ observations of phase transition between perovskite and $CaIrO_3$-type phase in $MgSiO_3$ and pyrolitic mantle composition. *Earth and Planetary Science Letters* 236: 914–932.

Otsuka K and Karato S (2012) Deep penetration of molten iron into the mantle caused by a morphological instability. *Nature* 492: 243–246. http://dx.doi.org/10.1038/nature11663.

Ozawa H, Hirose K, Mitome M, Bando Y, Sata N, and Ohishi Y (2008) Chemical equilibrium between ferropericlase and molten iron to 134 GPa and implications for iron content at the bottom of the mantle. *Geophysical Research Letters* 35: L05308. http://dx.doi.org/10.1029/2007GL032648.

Ozawa H, Hirose K, Mitome M, Bando Y, Sata N, and Ohishi Y (2009) Experimental study of reaction between perovskite and molten iron to 146 GPa and implications for chemical equilibrium at the core–mantle boundary. *Physics and Chemistry of Minerals* 36: 355–363.

Panning M and Romanowicz B (2006) A three-dimensional radially anisotropic model of shear velocity in the whole mantle. *Geophysical Journal International* 167: 361–379. http://dx.doi.org/10.1111/j.1365-246X.2006.03100.x.

Persh SE, Vidale JE, and Earle PS (2001) Absence of short-period ULVZ precursors to PcP and ScP from two regions of the CMB. *Geophysical Research Letters* 28: 859–862.

Petford N, Yuen D, Rushmer T, Brodholt J, and Stackhouse S (2005) Shear-induced material transfer across the core–mantle boundary aided by the post-perovskite phase transition. *Earth, Planets and Space* 57: 459–464.

Poirier JP, Malavergne V, and Le Mouël JL (1998) Is there a thin electrically conducting layer at the base of the mantle? In: Gurnis M, Wysession ME, Knittle E, and Buffett BA (eds.) *The Core–Mantle Boundary Region. American Geophysical Union Monograph*, pp. 131–137.

Pozzo M, Davies C, Gubbins D, and Alfè D (2012) Thermal and electrical conductivity of iron at Earth's core conditions. *Nature* 485: 355–358.

Pozzo M, Davies C, Gubbins D, and Alfe D (2013) Transport properties for liquid silicon-oxygen-iron mixtures at Earth's core conditions. *Physical Review B* 87: 014110.

Reasoner C and Revenaugh J (2000) ScP constraints on ultralow-velocity zone density and gradient thickness beneath the Pacific. *Journal of Geophysical Research B* 105: 173–182.

Resovsky JS and Ritzwoller MH (1999) Regularization uncertainty in density models estimated from normal mode data. *Geophysical Research Letters* 26: 2319–2322.

Ricard Y, Richards M, LithgowBertelloni C, and Le Stunff Y (1993) A geodynamic model of mantle density heterogeneity. *Journal of Geophysical Research* 98: 21895–21909.

Richards MA and Engebretson DC (1992) Large-scale mantle convection and history of subduction. *Nature* 30: 437–440.

Ricolleau A, Fei Y, Corgne A, Siebert J, and Badro J (2011) Oxygen and silicon contents of earth's core from high pressure metal-silicate partitioning experiments. *Earth and Planetary Science Letters* 310: 409–421.

Rigden SM, Ahrens TJ, and Stolper EM (1984) Densities of liquid silicates at high pressures. *Science* 226: 1071–1073.

Ringwood AE and Irifune T (1988) Nature of the 650-km seismic discontinuity: Implications for mantle dynamics and differentiation. *Nature* 331(6152): 131–136.

Ritsema J and van Heijst H (2002) Constraints on the correlation of p- and s-wave velocity heterogeneity in the mantle from p, pp, ppp, and *pkpab* traveltimes. *Geophysical Journal International* 149: 482–489.

Ritsema J, Garnero EJ, and Lay T (1997) A strongly negative shear velocity gradient and lateral variability in the lowermost mantle beneath the Pacific. *Journal of Geophysical Research* 102: 20395–20411.

Ritsema J, van Heijst HJ, and Woodhouse JH (1999) Complex shear wave velocity structure imaged beneath Africa and Iceland. *Science* 286(5446): 1925–1928.

Ritsema J, van Heijst HJ, and Woodhouse JH (2004) Global transition zone tomography. *Journal of Geophysical Research-Solid Earth* 109(B2).

Ritsema J, McNamara AK, and Bull AL (2007) Tomographic filtering of geodynamic models: Implications for model interpretation and large-scale mantle structure. *Journal of Geophysical Research-Solid Earth* 112(B1).

Ritsema J, van Heijst HJ, Deuss A, and Woodhouse JH (2011) S40RTS: A degree-40 shear velocity model for the mantle from new Rayleigh wave dispersion, teleseismic traveltimes, and normal-mode splitting function measurements. *Geophysical Journal International* 184: 1223–1236.

Romanowicz B (2003) Global mantle tomography: Progress status in the last 10 years. *Annual Review of Earth and Planetary Sciences* 31: 303–328.

Romanowicz B and Gung Y (2002) Superplumes from the core–mantle boundary to the lithosphere: Implications for heat flux. *Science* 296: 513–516.

Ross AR, Thybo H, and Solodilov LN (2004) Reflection seismic profiles of the core–mantle boundary. *Journal of Geophysical Research B* 109, B08303.

Rost S and Revenaugh J (2001) Seismic detection of rigid zones at the top of the core. *Science* 294: 1911–1914.

Rost S, Garnero EJ, Williams Q, and Manga M (2005) Seismic constraints on a possible plume root at the core–mantle boundary. *Nature* 435: 666–669.

Rost S, Garnero EJ, and Williams Q (2006) Fine-scale ultralow-velocity zone structure from high-frequency seismic array data. *Journal of Geophysical Research* 111: B09310. http://dx.doi.org/10.1029/2005JB004088.

Rost S, Garnero EJ, Thorne MS, and Hutko AR (2010) On the absence of an ultralow-velocity zone in the North Pacific. *Journal of Geophysical Research* 115: B04312. http://dx.doi.org/10.1029/2009JB006420.

Rubie DC, Gessmann CK, and Frost DJ (2004) Partitioning of oxygen during core formation on the Earth and Mars. *Nature* 429: 58–61.

Sakai T, Kondo T, Ohtani E, Terasaki H, Endo N, Kuba T, Suzuki T, and Kikegawa T (2006) Interaction between iron and post-perovskite at core–mantle boundary and core signature in plume source region. *Geophysical Research Letters* 33: L15317. http://dx.doi.org/10.1029/2006GL026868.

Samuel H and Bercovici D (2006) Oscillating and stagnating plumes in the earth's lower mantle. *Earth and Planetary Science Letters* 248: 90–105.

Samuel H and Farnetani CG (2003) Thermochemical convection and helium concentrations in mantle plumes. *Earth and Planetary Science Letters* 207(1–4): 39–56.

Saxena SK, Dubrovinsky LS, Lazor P, Cerenius Y, Haggkvist P, Hanfland M, and Hu J (1996) Stability of perovskite ($MgSiO_3$) in the earth's mantle. *Science* 274: 1357–1359. http://dx.doi.org/10.1126/science.274.5291.1357.

Schubert G, Masters G, Tackley PJ, and Olson P (2004) Superplumes or plume clusters? *Physics of the Earth and Planetary Interiors* 146: 147–162.

Schuberth BSA, Bunge HP, and Ritsema J (2009) Tomographic filtering of high-resolution mantle circulation models: Can seismic heterogeneity be explained by temperature alone? *Geochemistry, Geophysics, Geosystems* 10.

Schuberth SA, Zaroli C, and Nolet G (2012) Synthetic seismograms for a synthetic Earth: Long- period P- and S-wave traveltime variations can be explained by temperature alone. *Geophysical Journal International* 1–20. http://dx.doi.org/10.1111/j.1365-246X.2011.05333.x.

Sidorin I, Gurnis M, Helmberger DV, and Ding X (1998) Interpreting *D″* seismic structure using synthetic waveforms computed from dynamic models *Earth and Planetary Science Letters* 163: 31–41.

Simmons NA, Forte AM, and Grand SP (2006) Constraining mantle flow with seismic and geodynamic data: A joint approach. *Earth and Planetary Science Letters* 246: 109–124. http://dx.doi.org/10.1029/2006GL028009.

Simmons NA, Forte AM, and Grand SP (2007) Thermochemical structure and dynamics of the African superplume. *Geophysical Research Letters* 34: L02301. http://dx.doi.org/10.1029/2006GL028009.

Sinmyo R, Hirose K, Nishio-Hamane D, Seto Y, Fujino K, Sata N, and Ohishi Y (2008) Partitioning of iron between perovskite/postperovskite and ferropericlase in the lower mantle. *Journal of Geophysical Research* 113: B11. http://dx.doi.org/10.1029/2008JB005730.

Sleep N (1990) Hotspots and mantle plumes: Some phenomenology. *Journal of Geophysical Research* 95: 6715–6736.

Sleep NH (1988) Gradual entrainment of a chemical layer at the base of the mantle by overlying convection. *Geophysical Journal* 95: 437–447.

Solomatov VS, Olson P, and Stevenson DJ (1993) Entrainment from a bed of particles by thermal convection. *Earth and Planetary Science Letters* 120: 387–393.

Souriau A and Poupinet G (1991) A study of the outermost liquid core using differential travel times of SKS, SKKS and S3KS phases. *Physics of the Earth and Planetary Interiors* 68: 183–199.

Spera FJ, Yuen DA, and Giles G (2006) Tradeoffs in chemical and thermal variations in the post-perovskite phase transition: Mixed phase regions in the deep lower mantle? *Physics of the Earth and Planetary Interiors* 159: 234–246. http://dx.doi.org/10.1016/j.pepi.2006.07.007.

Speziale S, Zha C, Duffy TS, Hemley RJ, and Mao HK (2001) Quasi-hydrostatic compression of magnesium oxide to 52 GPa: Implications for the pressure–volume–temperature equation of state. *Journal of Geophysical Research* 106: 515–528.

Spiegelman M and McKenzie D (1987) Simple 2-D models for melt extraction at mid-ocean ridges and island arcs. *Earth and Planetary Science Letters* 83: 137–152.

Sreenivasan B and Gubbins D (2008) Dynamos with weakly convecting outer layers: Implications for core-boundary locking. *Geophysical and Astrophysical Fluid Dynamics* 102: 395–407. http://dx.doi.org/10.1080/03091920801900047.

Sreenivasan B and Gubbins D (2011) On mantle-induced heat flow variations at the inner core boundary. *Physics of the Earth and Planetary Interiors* 187(34): 336–341.

Stacey F (1992) *Physics of the Earth*. Brookfield.

Stacey FD and Anderson OL (2001) Electrical and thermal conductivities of Fe–Ni–Si alloy under core conditions. *Physics of the Earth and Planetary Interiors* 124: 153–162.

Stacey FD and Loper DE (2007) A revised estimate of the conductivity of iron alloy at high pressure and implications for the core energy balance. *Physics of the Earth and Planetary Interiors* 161: 13–18.

Stackhouse S, Brodholt JP, Price GD, Wookey J, and Kendall JM (2005) The effect of temperature on the acoustic anisotropy of the perovskite and post-perovskite polymorphs of $MgSiO_3$. *Earth and Planetary Science Letters* 230: 1–10.

Stackhouse S, Brodholt JP, Dobson DP, and Price GD (2006) Electronic spin transitions and the seismic properties of ferrous iron-bearing $MgSiO_3$ post-perovskite. *Geophysical Research Letters* 33: L12S03.

Stanley S and Bloxham J (2004) Convective-region geometry as the cause of Uranus' and Neptune's unusual magnetic fields. *Nature* 428: 151–153. http://dx.doi.org/10.1038/nature02376.

Stanley S and Mohammadia A (2008) Effects of an outer thin stably stratified layer on planetary dynamos. *Physics of the Earth and Planetary Interiors* 168: 179–190. http://dx.doi.org/10.1016/j.pepi.2008.06.016.

Stevenson DJ (1980) Saturn's luminosity and magnetism. *Science* 208: 746–748.

Stevenson DJ (1981) Models of the Earth's core. *Science* 214: 611–619.

Stevenson DJ (1982) Reducing the non-axisymmetry of a planetary dynamo and an application to Saturn. *Geophysical and Astrophysical Fluid Dynamics* 21: 113–127.

Stevenson DJ (1987) Limits on lateral density and velocity variations in the Earth's outer core. *Geophysical Journal of the Royal Astronomical Society* 88: 311–319.

Stevenson DJ (2012) How to keep a dynamo running in spite of high thermal conductivity. In: *Abstract DI11C-03 presented at 2012 Fall Meeting AGU San Francisco, California 3–7 December*.

Stixrude L (1997) Structure and sharpness of phase transitions and mantle discontinuities. *Journal of Geophysical Research* 102: 14835–14852.

Stixrude L and Lithgow-Bertelloni C (2005) Thermodynamics of mantle minerals: 1. Physical properties. *Geophysical Journal International* 162: 610–632. http://dx.doi.org/10.1111/j.1365-246X.2005.02642.x.

Stixrude L, de Koker N, Sun N, Mookherjee M, and Karki BB (2009) Thermodynamics of silicate liquids in the deep Earth. *Earth and Planetary Science Letters* 278: 226–232. http://dx.doi.org/10.1016/j.epsl.2008.12.006.

Stolper E, Walker D, Hager BH, and Hays JF (1981) Melt segregation from partially molten source regions: the importance of melt density and source region size. *Journal of Geophysical Research* 86: 6261–6271.

Su WJ and Dziewonski AM (1997) Simultaneous inversion for 3-D variations in shear and bulk velocity in the mantle. *Physics of the Earth and Planetary Interiors* 100: 135–156.

Sun D, Song TA, and Helmberger D (2006) Complexity of *D″* in the presence of slab-debris and phase changes *Geophysical Research Letters* 33: 1207. http://dx.doi.org/10.1029/2005GL025384.

Sun D, Tan E, Helmberger D, and Gurnis M (2007a) Seismological support for the metastable superplume model, sharp features, and phase changes within the lower mantle. *Proceedings of the National Academy of Sciences* 104: 9151–9155.

Sun D, Helmberger DV, Jackson JM, Clayton RW, and Bower DJ (2013) Rolling hills on the core–mantle boundary. *Earth and Planetary Science Letters* 361: 333–342. http://dx.doi.org/10.1016/j.epsl.2012.10.027.

Sun DY, Helmberger D, Ni SD, and Bower D (2009) Direct measures of lateral velocity variation in the deep Earth. *Journal of Geophysical Research-Solid Earth* 114.

Sun XL, Song DX, Zheng SH, and Helmberger D (2007b) Evidence for a chemical-thermal structure at base of mantle from sharp lateral P-wave variations beneath Central America. *Proceedings of the National Academy of Sciences of the United States of America* 104(1): 26–30.

Suzuki A and Ohtani E (2003) Density of peridotite melts at high pressure. *Physics and Chemistry of Minerals* 30: 449–456.

Suzuki A, Ohtani E, and Kato T (1995) Flotation of diamond in mantle melt at high pressure. *Science* 269: 216–218.

Sze EKM and van der Hilst RD (2003) Core mantle boundary topography from short period PcP, PKP, and PKKP data. *Physics of the Earth and Planetary Interiors* 135(1): 27–46.

Tackley PJ (1998) Three-dimensional simulations of mantle convection with a thermo-chemical basal boundary layer: *D″*? In: Gurnis M, Wysession ME, Knittle E, and Buffett BA (eds.) *The Core–Mantle Boundary Region*, pp. 231–253. Washington, D.C.: American Geophysical Union.

Tackley PJ (2000a) Mantle convection and plate tectonics: Toward an integrated physical and chemical theory. *Science* 288(5473): 2002–2007.

Tackley PJ (2000b) Self-consistent generation of tectonic plates in time-dependent, three-dimensional mantle convection simulations: 1. Pseudoplastic yielding. *Geochemistry, Geophysics, Geosystems* 1. http://dx.doi.org/10.1029/2000GC000036.

Tackley PJ (2000c) Self-consistent generation of tectonic plates in time-dependent, three-dimensional mantle convection simulations: 2. Strain weakening and asthenosphere. *Geochemistry, Geophysics, Geosystems* 1. http://dx.doi.org/10.1029/2000GC000043.

Tackley PJ (2002) Strong heterogeneity caused by deep mantle layering. *Geochemistry, Geophysics, Geosystems* 3. http://dx.doi.org/10.1029/2001GC000167.

Tackley PJ (2007) *Mantle Geochemical Geodynamics*, pp. 437–505. Elsevier.

Tackley PJ (2011) Living dead slabs in 3-D: The dynamics of compositionally-stratified slabs entering a "slab graveyard" above the core–mantle boundary. *Physics of the Earth and Planetary Interiors* 188(3–4): 150–162.

Tackley PJ (2012) Dynamics and evolution of the deep mantle resulting from thermal, chemical, phase and melting effects. *Earth-Science Reviews* 110: 1–25.

Tackley PJ, Nakagawa T, and Hernlund JW (2007) Influence of the post-perovskite transition on thermal and thermo-chemical mantle convection. In: Lay T, Yuen DA, Hirose K, and Brodholt J (eds.) *The Last Phase Transition: American Geophysical Union Monograph*.

Takafuji N, Hirose V, Mitome M, and Bando Y (2005) Solubilities of O and Si in liquid iron in equilibrium with (Mg, Fe)SiO_3 perovskite and the light elements in the core. *Geophysical Research Letters* 32: L06313. http://dx.doi.org/10.1029/2005GL022773.

Takahashi E, Shimazaki T, Tsuzaki Y, and Yoshida H (1993) Melting study of a peridotite KLB-1 to 6.5 GPa, and the origin of basaltic magmas. *Philosophical Transactions of the Royal Society A: Mathematical, Physical and Engineering Sciences* 342: 105–120.

Takeuchi N (2007) Whole mantle SH velocity model constrained by waveform inversion based on three-dimensional Born kernels. *Geophysical Journal International* 169(3): 1153–1163.

Tan E and Gurnis M (2005) Metastable superplumes and mantle compressibility. *Geophysical Research Letters* 32(20).
Tan E and Gurnis M (2007) Compressible thermochemical convection and application to lower mantle structures. *Journal of Geophysical Research-Solid Earth* 112(B6).
Tan E, Leng W, Zhong S, and Gurnis M (2011) On the location of plumes and lateral movement of thermochemical structures with high bulk modulus in the 3-D compressible mantle. *Geochemistry, Geophysics, Geosystems* 12: Q07005. http://dx.doi.org/10.1029/2011GC003665.
Tanaka S (2004) Seismic detectability of anomalous structure at the top of the Earth's outer core with broadband array analysis of SmKS phases. *Physics of the Earth and Planetary Interiors* 141: 141–152.
Tanaka S (2007) Possibility of a low P-wave velocity layer in the outermost core from global SmKS waveforms. *Earth and Planetary Science Letters* 259: 486–499.
Tanaka S (2010) Constraints on the core–mantle boundary topography from P4KP–PcP differential travel times. *Journal of Geophysical Research* 115: B04310. http://dx.doi.org/10.1029/2009JB006563.
Tanaka S and Hamaguchi H (1993) Velocities and chemical stratification in the outermost core. *Journal of Geomagnetism and Geoelectricity* 45: 1287–1301.
Tarduno JA, Cottrell RD, Watkeys MK, Hofmann A, Doubrovine PV, Mamajek EE, Liu D, Sibeck DG, Neukirch LP, and Usui Y (2010) Geodynamo, solar wind, and magnetopause 3.4 to 3.45 billion years ago. *Science* 327: 1238–1240. http://dx.doi.org/10.1126/science.1183445.
Tateno S, Hirose K, Sata N, and Ohishi Y (2007) Solubility of FeO in (Mg, Fe)SiO_3 perovskite and the post-perovskite phase transition. *Physics of the Earth and Planetary Interiors* 160: 319–325. http://dx.doi.org/10.1016/j.pepi.2006.11.010.
Tateno S, Hirose K, Sata N, and Ohishi Y (2009) Determination of post-perovskite phase transition boundary up to 4400 K and implications for thermal structure in *D″* layer *Earth and Planetary Science Letters* 277: 130–136.
Thomas C, Garnero EJ, and Lay T (2004a) High-resolution imaging of lowermost mantle structure under the Cocos plate. *Journal of Geophysical Research B* 109: B08307.
Thomas C, Kendall J, and Lowman J (2004b) Lower-mantle seismic discontinuities and the thermal morphology of subducted slabs. *Earth and Planetary Science Letters* 225: 105–113.
Thomas C, Wookey J, Brodholt JP, and Fieseler T (2011) Anisotropy as a cause for polarity reversals in d″ reflections *Earth and Planetary Science Letters* 307: 369–376.
Thomas CW, Liu Q, Agee CB, Asimow PD, and Lange RA (2012) Multi-technique equation of state for Fe_2SiO_4 melt and the density of Fe-bearing silicate melts from 0–161 GPa. *Journal of Geophysical Research* 117: B10206. http://dx.doi.org/10.1029/2012JB009403.
Thompson PF and Tackley PJ (1998) Generation of mega-plumes from the core–mantle boundary in a compressible mantle with temperature-dependent viscosity. *Geophysical Research Letters* 25: 1999–2002.
Thorne M, Garnero EJ, and Grand S (2004) Geographic correlation between hot spots and deep mantle lateral shear-wave velocity gradients. *Physics of the Earth and Planetary Interiors* 146: 47–63.
Thorne MS and Garnero EJ (2004) Inferences on ultralow-velocity zone structure from a global analysis of SPdKS waves. *Journal of Geophysical Research* 109: B08301.
Thorne MS, Garnero EJ, Jahnke G, Igel H, and McNamara AK (2013a) Mega ultra low velocity zone and mantle flow. *Earth and Planetary Science Letters* 364: 59–67. http://dx.doi.org/10.1016/j.epsl.2012.12.034.
Thorne MS, Zhang Y, and Ritsema J (2013b) Evaluation of 1-D and 3-D seismic models of the Pacific lower mantle with S, SKS, and SKKS traveltimes and amplitudes. *Journal of Geophysical Research* 118: 50054. http://dx.doi.org/10.1002/jgrb.50054.
To A, Romanowicz B, Capdeville Y, and Takeuchi N (2005) 3d effects of sharp boundaries at the borders of the African and Pacific superplumes: Observation and modeling. *Earth and Planetary Science Letters* 233(1–2): 137–153.
Tolstikhin IN and Hofmann AW (2005) Early crust on top of the Earth's core. *Physics of the Earth and Planetary Interiors* 148: 109–130.
Tolstikhin IN, Kramers JD, and Hofmann AW (2006) A chemical Earth model with whole mantle convection: The importance of a core–mantle boundary layer *D″* and its early formation *Chemical Geology* 226(3–4): 79–99.
Torsvik TH, Smethurst MA, Burke K, and Steinberger B (2006) Large igneous provinces generated from the margins of the large low-velocity provinces in the deep mantle. *Geophysical Journal International* 167: 1447–1460. http://dx.doi.org/10.1111/j.1365-246X.2006.03158.x.
Torsvik TH, Smethurst MA, Burke K, and Steinberger B (2008) Long term stability in deep mantle structure: Evidence from the ca. 300 Ma Skagerrak-Centered Large Igneous Province (the SCLIP). *Earth and Planetary Science Letters* 267(3–4): 444–452.
Torsvik TH, Burke K, Steinberger B, Webb SJ, and Ashwal LD (2010) Diamonds sampled by plumes from the core–mantle boundary. *Nature* 466(7304): 352–355.
Trampert J, Vacher P, and Vlaar N (2001) Sensitivities of seismic velocities to temperature, pressure and composition in the lower mantle. *Physics of the Earth and Planetary Interiors* 124(3–4): 255–267.
Trampert J, Deschamps F, Resovsky J, and Yuen DA (2004) Probabilistic tomography maps chemical heterogenities throughout the mantle. *Science* 306: 853–856.
Tsuchiya T (2003) First-principles prediction of the *P–V–T* equation of gold and the 660-km discontinuity in Earth's mantle. *Journal of Geophysical Research* 108: 2462. http://dx.doi.org/10.1029/2003JB002446.
Tsuchiya T, Tsuchiya J, Umemoto K, and Wentzcovitch RM (2004) Phase transition in $MgSiO_3$ perovskite in the Earth's lower mantle. *Earth and Planetary Science Letters* 224: 241–248.
Tsuno K, Frost DJ, and Rubie DC (2013) Simultaneous partitioning of silicon and oxygen into the earth's core during early earth differentiation. *Geophysical Research Letters* 40: 66–71. http://dx.doi.org/10.1029/2012GL054116.
Turner JS (1986) Turbulent entrainment: the development of the entrainment assumption, and its application to geophysical flows. *Journal of Fluid Mechanics* 173: 431–471.
van der Hilst RD and Karason H (1999) Compositional heterogeneity in the bottom 1000 kilometers of Earth's mantle: Toward a hybrid convection model. *Science* 283(5409): 1885–1888.
van der Hilst RD, Widiyantoro S, and Engdahl ER (1997) Evidence for deep mantle circulation from global tomography. *Nature* 386(6625): 578–584.
van der Hilst RD, de Hoop MV, Wang P, Shim S-H, Ma P, and Tenorio L (2007) Seismostratigraphy and thermal structure of Earth's core–mantle boundary region. *Science* 30: 1813–1817. http://dx.doi.org/10.1126/science.1137867.
Van Orman JA and Crispin KL (2010) Diffusion in oxides. *Reviews in Mineralogy and Geochemistry* 72: 757–825.
Vidale JE and Benz HM (1992) A sharp and flat section of the core–mantle boundary. *Nature* 359: 627–629.
von Bargen N and Waff HS (1986) Permeabilities, interfacial areas and curvatures of partially molten systems: Results of numerical computations of equilibrium microstructures. *Journal of Geophysical Research* 91: 9261–9276.
Vočadlo L, Alfe D, Gillan MJ, and Price GD (2003) The properties of iron under core conditions from first principles calculations. *Physics of the Earth and Planetary Interiors* 140: 101–125.
Wakabayashi D, Funamori N, Sato T, and Sekine T (2014) Equation of state for silicate melts: A comparison between static and shock compression. *Geophysical Research Letters* 41: 50–54. http://dx.doi.org/10.1002/2013GL058328.
Walker A, Forte AM, Wookey J, Nowacki A, and Kendall J-M (2011) Elastic anisotropy of *D″* predicted from global models of mantle flow *Geochemistry, Geophysics, Geosystems* 12: Q10006. http://dx.doi.org/10.1029/2011GC003732.
Walker D, Clark SM, and Cranswick LMD (2002) O_2 volumes at high pressure from $KClO_4$ decomposition: *D″* as a siderophile element pump instead of a lid on the core *Geochemistry, Geophysics, Geosystems* 3: 1070.
Wang Y and Wen LX (2004) Mapping the geometry and geographic distribution of a very low velocity province at the base of the Earth's mantle. *Journal of Geophysical Research* 109: B10305.
Wang Y and Wen LX (2007) Geometry and P and S velocity structure of the "African Anomaly" *Journal of Geophysical Research-Solid Earth* 112(B5).
Warren PH (1985) The magma ocean concept and lunar evolution. *Annual Review of Earth and Planetary Sciences* 13: 201–240. http://dx.doi.org/10.1146/annurev.ea.13.050185.001221.
Wen LX (2001) Seismic evidence for a rapidly-varying compositional anomaly at the base of the Earth's mantle beneath the Indian Ocean. *Earth and Planetary Science Letters* 194: 83–95.
Wen LX (2002) An SH hybrid method and shear velocity structures in the lowermost mantle beneath the central Pacific and South Atlantic Oceans. *Journal of Geophysical Research-Solid Earth* 107(B3).
Wen LX, Silver P, James D, and Kuehnel R (2001) Seismic evidence for a thermo-chemical boundary at the base of the Earth's mantle. *Earth and Planetary Science Letters* 189(3–4): 141–153.
Whaler KA (1980) Does the whole of the Earth's core convect? *Nature* 287: 528–530.
Wicht J, Mandea M, Takahashi F, Christensen UR, Matsushima M, and Langlais B (2007) The origin of Mercury's internal magnetic field. *Space Science Reviews* 132: 261–290. http://dx.doi.org/10.1007/s11214-007-9280-5.
Wicks JK, Jackson JM, and Sturhahn W (2010) Very low sound velocities in iron-rich (Mg, Fe)O: Implications for the core–mantle boundary region. *Geophysical Research Letters* 37: L15304. http://dx.doi.org/10.1029/2010GL043689.

Williams Q (1998) The temperature contrast across *D″* In: Gurnis M, Wysession ME, Knittle E, and Buffett BA (eds.) *The Core–Mantle Boundary Region. American Geophysical Union Monograph*, pp. 73–81.

Williams Q and Garnero EJ (1996) Seismic evidence for partial melt at the base of the Earth's mantle. *Science* 273: 1528–1530.

Williams Q, Revenaugh JS, and Garnero EJ (1998) A correlation between ultra-low basal velocities in the mantle and hot spots. *Science* 281: 546–549.

Willis AP, Gubbins D, and Sreenivasan B (2007) Thermal core–mantle interaction: Exploring regimes for 'locked' dynamo action. *Physics of the Earth and Planetary Interiors* 165: 83–92.

Wood BJ, Walter MJ, and Wade J (2006) Accretion of the Earth and segregation of its core. *Nature* 441: 825–833. http://dx.doi.org/10.1038/nature04763.

Wookey J, Stackhouse S, Kendall J-M, Brodholt J, and Price GD (2005) Efficacy of the post-perovskite phase as an explanation of lowermost mantle seismic properties. *Nature* 438: 1004–1008.

Wright C, Muirhead KJ, and Dixon AE (1985) The P wave velocity structure near the base of the mantle. *Journal of Geophysical Research* 90: 623–634.

Wu B, Driscoll P, and Olson P (2011) A statistical boundary layer model for the mantle *D″* region *Journal of Geophysical Research* 116: B12112. http://dx.doi.org/10.1029/2011JB008511.

Wysession ME, Lay T, Revenaugh J, Williams Q, Garnero EJ, Jeanloz R, and Kellogg LH (1998) The *D″* discontinuity and its implications In: Gurnis M, Wysession ME, Knittle E, and Buffett BA (eds.) *The Core–Mantle Boundary Region. American Geophysical Union Monograph*, pp. 273–297.

Xie S and Tackley PJ (2004a) Evolution of helium and argon isotopes in a convecting mantle. *Physics of the Earth and Planetary Interiors* 146: 417–439.

Xie S and Tackley PJ (2004b) Evolution of U–Pb and Sm–Nd systems in numerical models of mantle convection. *Journal of Geophysical Research B* 109, B11204.

Yoshida M (2008) Core–mantle boundary topography estimated from numerical simulations of instantaneous mantle flow. *Geochemistry, Geophysics, Geosystems* 9.

Zerr A, Diegeler A, and Boehler R (1998) Solidus of the Earth's deep mantle. *Science* 281: 243–245.

Zhang N and Zhong SJ (2011) Heat fluxes at the Earth's surface and core–mantle boundary since Pangea formation and their implications for the geomagnetic superchrons. *Earth and Planetary Science Letters* 306(3–4): 205–216.

Zhang N, Zhong S, Leng W, and Li Z-X (2010) A model for the evolution of the earth's mantle structure since the early paleozoic. *Journal of Geophysical Research* 115.

Zhao DP (2004) Global tomographic images of mantle plumes and subducting slabs: Insight into deep Earth dynamics. *Physics of the Earth and Planetary Interiors* 146(1–2): 3–34.

Zhong S (2006) Constraints on thermochemical convection of the mantle from plume heat flux, plume excess temperature, and upper mantle temperature. *Journal of Geophysical Research* 111: B04409. http://dx.doi.org/10.1029/2005JB003972.

Zhong S, Zuber MT, Moresi L, and Gurnis M (2000) Role of temperature-dependent viscosity and surface plates in spherical shell models of mantle convection. *Journal of Geophysical Research* 105: 11063–11082.

Zhong SJ, McNamara AK, Tan E, Moresi L, and Gurnis M (2008) A benchmark study on mantle convection in a 3-D spherical shell using CitcomS. *Geochemistry, Geophysics, Geosystems* 9.

Zhou M-F, Malpas J, Song X-Y, Robinson PT, Sun M, Kennedy AK, Lesher CM, and Keays RR (2002) *Earth and Planetary Science Letters* 196: 113122.

Zou Z, Koper K, and Cormier VF (2008) The structure of the base of the outer core inferred from seismic waves diffracted around the inner core. *Journal of Geophysical Research* 113. http://dx.doi.org/10.1029/2007JB005316.